Alma Mater Studiorum – Università di Bologna

DOTTORATO DI RICERCA

SCIENZE CHIMICHE

Ciclo XX

Settore/i scientifico disciplinari di afferenza: CHIM/06 CHIMICA ORGANICA

TITOLO TESI

SYNTHESIS, MULTISCALE- MULTIPHASE CHARACTERIZATION AND APPLICATIONS OF THIOPHENE-BASED BIOHYBRIDS

Presentata da: SILVIA ALESI

Coordinatore Dottorato:

Prof. V. Balzani

Relatore:

Prof. A. Bongini

Co-Relatore:

Dr.ssa G. Barbarella

Esame finale anno 2008

*'L'uomo razionale è colui che vuole comprendere
e non colui che vuole avere sempre ragione'*

K. Popper

Table of contents

Chapter 1

Introduction

Abstract

The last decade has highlighted the enormous potential of the convergence of nanoscale electronics and material chemistry with the biological world. 'Nanobiotechnology' is emerging as a novel field in which biological concepts, mechanisms, functions and design features are employed as starting points to create innovative materials with advanced functions. In this chapter, an overview of the studies on bio-organic hybrid materials and their applications in nanobiotechnology is given.

1.1 Biohybrid materials

Nanobiotechnology [1] represents a rapidly growing field of interest. The last decade has highlighted the wide-ranging potential of applying techniques at the molecular and atomic levels to understand and transform biosystems, and of using biological principles and materials to create new devices at the nanoscale.[2]

The fascinating concept of the possibility to communicate with the biological world by means of manmade tools calls for biohybrid materials,[3] constituted of an active biological component and a synthetic component compatible with this biological function and that retains its specific properties in a biological (aqueous) medium.

In this direction bio-inorganic or organic hybrid compounds have been developed as a tool aiming at: a) detecting and monitoring biospecific interactions or biological functions, b) transferring the self-assembly modalities of biomolecules to inorganic-organic functional materials.

Despite the numerous studies devoted to the synthesis and properties of bio–inorganic hybrids systems (biomolecule-nanoparticles, Au-CdSe based) as well as on their organization in functional devices,[4] and the only few examples reported so far on biomolecules linked to organic materials, π-conjugated materials represent most appealing systems with respect to metal nanoparticles for *in vivo* application due to their higher biocompatibility.

In this direction, conjugated polymers such as polythiophene and polypyrrole have been used to couple analyte/receptor interactions, as well as non-specific interactions, into observable responses. [5]

Moreover, the possibility to predict and program the supramolecular structure of the biomolecules, is an attractive tool for directing and governing the assembling of π-conjugated materials in tailored bio-hybrid micro- and nanosystems with (opto)electronic functionalities.[6] In fact, all biomolecules interact and self-organize to form well-defined and complex nano- and micro-scale structures. They naturally form hierarchical arrangements (helices, hairpins, ribbons, fibrils and so on) by means of weak but numerous molecular interactions (van der Waals forces, hydrogen bonds, electrostatic interactions etc.) that can be programmed by a structure-specific design.[7] Therefore, transferring the organization principles of biomolecules into new self-assembling and functional bio-organic hybrid materials is of great interest, in order to

pre-program the supramolecular aggregation modalities and functions of the new biohybrid materials synthesized.

1.2 Sensors and bio-hybrid compounds based on conjugated polymers and oligomers

Among the most interesting examples of organic materials based sensing systems, electrochemical and optical DNA sensors have been reported, containing a fluorescent and/or electroactive conjugated moiety which is able to transduce the hybridization event into a fluorescence and/or electrical signal. A variety of optical and electrochemical DNA hybridization sensors have been proposed and their selectivity, to sense single-nucleotide polymorphisms (SNPs), as well as their sensitivity, to detect a small number of molecules of DNA, have been tested.

G. C. Bazan[8] and co-workers synthesized cationic conjugated polyelectrolytes in order to determine the concentration of a double-stranded DNA. Their structures contain a π-delocalized backbone composed of phenylenefluorene (PF) segments copolymerized with 2,1,3-benzothiadiazole (BT) units and charged pendant groups, that allow excellent solubility in water. Analysis of photoluminescence spectra revealed that dsDNA addition gave rise to more efficient fluorescence resonance energy transfer (FRET), from blue emitting segments to the BT sites, an increase in the BT emission quantum yield, and partial quenching of the phenylene-fluorene segments. Moreover, studies carried out to maximize the range of determination of the dsDNA concentration allowed to generate calibration curves, that respond with a difference in dsDNA concentration of over 7 orders of magnitude, proving the high sensitivity in determining dsDNA concentration of this optical sensing system.
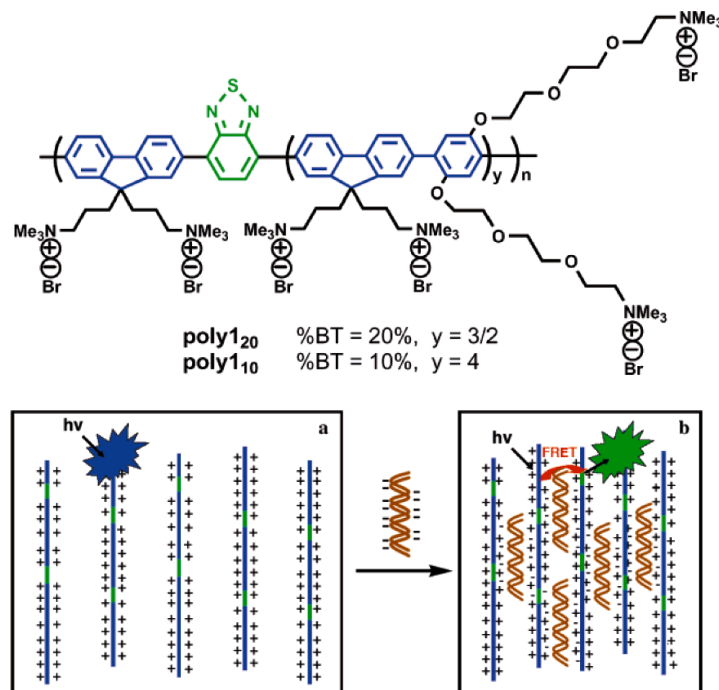
Figure 1.1 *Molecular structure of cationic conjugated polyelectrolytes. Schematic representation of optical changes induced by complexation of dsDNA. (a) Isolated chains of polymers emit blue light in the absence of DNA. (b) Aggregation with negatively charged dsDNA induces interchain energy transfer to BT sites and changes emission colour to green.*

Although most studied detection systems use fluorescence spectroscopy, some electrochemically based sensing methods have been reported in recent years. The interest in electrochemical detection stems from the simplicity of the required voltammetric instrumentation as well as its potential for miniaturization and use in point-of-care assays.

In this direction, the syntheses of several norbornene block copolymers containing oligonucleotide and ferrocenyl side chains and their use in the electrochemical detection of DNA have been reported by C. A. Mirkin and S. T. Nguyen.[9]

The authors synthesized two kinds of DNA-containing block copolymers with either ferrocenyl or dibromoferrocenyl groups via ring-opening metathesis polymerization (ROMP) and demonstrated the possibility of using them to identify a DNA target by using the electrochemical properties of the ferrocenyl moieties.
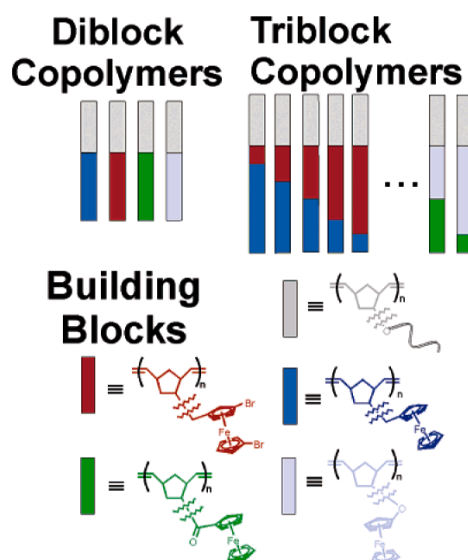
Figure 1.2 *Schematic illustration of the diblock and triblock copolymer labeling strategy used by Mirkin and Nguyen.*

The used polymer-DNA hybrids exhibited predictable and tailorable electrochemical properties, but also unusual and unanticipated DNA hybridization properties. In particular, they showed stronger binding enthalpies and sharper melting profiles than the oligonucleotides from which they were made. These properties allowed an electrochemical detection system to be developed with better target differentiation capabilities than those observed for single-oligonucleotide probes, leading to a higher selectivity in detection of a single-base mismatch.
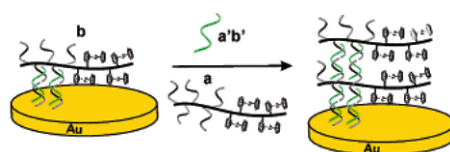
Figure 1.3 *Signal amplification using polymer-DNA probes. Scheme illustrating the addition of multiple layers to the electrode surface controlled by the recognition properties of DNA.*

In nanobiotechnology, synthesis of biohybrid compounds of π-conjugates oligomers are especially directed to get control on the organic moieties self-assembly properties by the judicious choice of bio-substituents.

For example Kato [10] and co-workers reported the formation of supramolecular chiral columnar liquid crystals through the self-assembly of pyrene-containing oligopeptides. Although pyrene has already been incorporated into self-assembled systems, only a limited number of pyrene-containing liquid crystals have been reported.[11]

In this direction, based on the previously demonstrated self-assembling behaviour and hierarchical molecular chirality of the liquid-crystalline dendritic oligo(glutamic acid)s, the authors synthesized pyrene-containing oligo(glutamic acid)s derivatives and demonstrated the presence of thermotropic chiral columnar LC phases for these biohybrid oligomers. Using this kind of material design, they highlighted the properties of the functional moieties such as luminescence, electron conductivity and ferroelectricity, which could be tuned by supramolecular structures formed through bio assisted self-assembly.
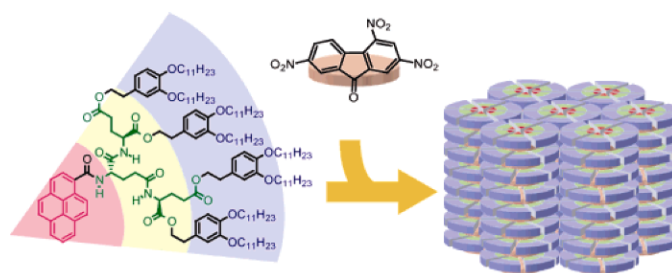
Figure 1.4 *Molecular structures of one of oligo(glutamic acid)s derivatives having pyrene moieties and schematic illustration of its chiral self-assembly modalities.*

Such capability of biomolecules to retain their self-assembly properties, independently of the hybridization with the conjugated materials, is of crucial importance for the pre-programmability of supramolecular structures and functions.

In this direction, E. W. Meijer's group[12] synthesized the thymidylic acid-appended oligo(*p*-phenylenevinylene) (OPV) derivative and examined its molecular recognition-driven self-assembling properties with complementary oligoadenylic acid in aqueous solution. AFM microscopy observations revealed formation of right-handed helical stack structures deriving from the interactions of the thymine moieties of the biohybrid derivative with the complementary single-stranded 20-meric oligodeoxyadenylic acid, acting as tamplate. Moreover, CD spectroscopy showed that the complementary T-A

base pairs formed were able to induce helical stack of the oligo(p-phenylenevinylene)s moieties.

In contrast, self-assembly of the single-component thymine functionalized OPV and its binary self-assembly with the non-complementary 20-meric oligothymidylic acid produced no remarkable formation of fibrous structures like helical stacks.

This paper represents a nice example of bio-driven self assembly, by using an oligonucleotide as a template to induce helical stacking of π-conjugated moieties in aqueous solution.
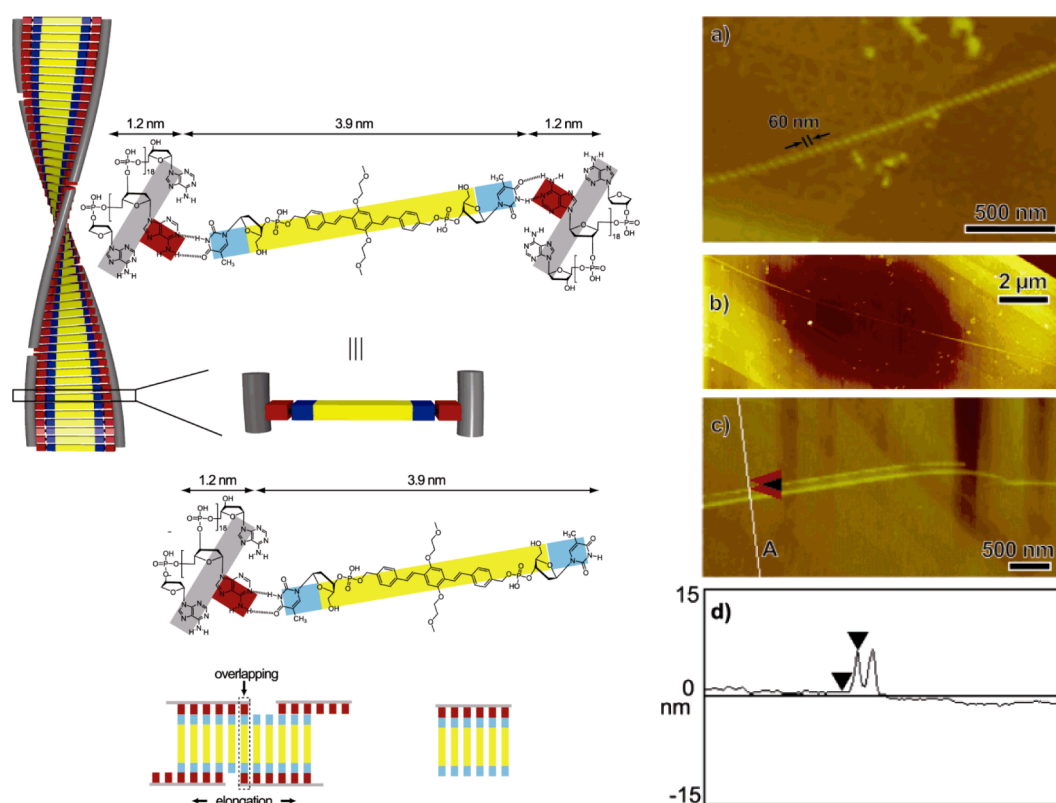
Figure 1.5 *Proposed structure and possible elongation mechanism for the binary self-assembly of thymine functionalized OPV and the single-stranded 20-meric oligodeoxyadenylic acid. AFM images for the binary self-assembly of thymine functionalized OPV and oligodeoxyadenylic acid (T:A) 1:1, 1.8 * 10^{-2} M/1.8 * 10^{-3} M). d) Section profiles along the A axis in Figure c).*

1.3 Sensing systems and bio-hybrids of thiophene-based materials

Only a few examples have been reported concerning the functionalization of thiophene-based compounds with biomolecules, despite the fact that oligo- and polythiophenes are

among the most versatile organic materials. Depending on their chemical structure, oligo- and polythiophenes self-organize in the solid state to form nano- and microstructures associated with semiconducting, light emitting or photoactive properties[13] which are useful for the fabrication of devices such as field effect transistors (FET),[14] light emitting diodes (LED)[15] or photovoltaic devices (OPV).[16]

As in the case of bio-hybrid derivatives of π-conjugated polymers, polythiophenes have been mainly used for the optical amplification of a biological event in solution, through the formation of a complex between the polythiophene and the biomolecule, generally based on weak interactions. As a result of this interaction, the conformation and aggregation state of the polymer change, with a consequent modification of the (opto)electronic output.

For example, polythiophenes with charged pendant groups making them soluble in water, have been described and used as optical transducers in biosensors for the detection of DNA mismatches in pathological samples. The use of water soluble conjugated polyelectrolytes, offer many opportunities to reveal chemical and biochemical events through changes in absorption or photoluminescence signals, electrical conductivity or redox potentials, leading to a very sensitive and specific transduction method.

As far as oligothiophene biohybrid derivatives are concerned, they have been especially designed and synthesized in order to study their self-assembly modalities. In fact, despite the great structural stability and flexibility of thiophene-based materials, it is still difficult to predict and govern their self-organization *in thin films*. Therefore, the design of molecular structures that predictably self-assemble into targeted three-dimensional supramolecular arrangements are of crucial interest.

1.3.1 Polythiophene based sensing systems

O. Inganas and co-workers[17] reported in 2003 a fluorometric DNA hybridization detection method, based on non-covalent coupling of DNA to a water-soluble zwitterionic polythiophene derivative, poly (3-[(S)-5-amino-5-carboxyl-3-oxapentyl]-2,5- thiophenylene hydrochloride (POWT).

The authors showed that the introduction of a single-stranded oligonucleotide, in aqueous solution of POWT was able to induce a planar conformation of the polymer chains and their aggregation. To explain these phenomena, they suggested that the

negatively charged phosphate backbone of ssDNA interacts electrostatically with the positive amino groups of a polymer chain. In this way the polymer internal interactions, between the amino and carboxyl group are disrupted, leading to its planarization. The bases of the DNA strand are subsequently able to form hydrogen bonds with the amino and carboxyl groups of a nearby polymer chain, leading to the aggregation of polymer chains.

Moreover, the authors observed that, on addition of a complementary oligonucleotide, the intensity of the emitted light was increased and blue-shifted. Because the complementary bases form hydrogen bonds with each other, the hydrogen bonding between the polymer chains and the ssDNA chains were disrupted and a new complex was formed, where the polymer chains interact electrostatically with the phosphate backbone and the bases of the doubled-stranded DNA (dsDNA), leading to a separation of the polymer chains and a less planar backbone.
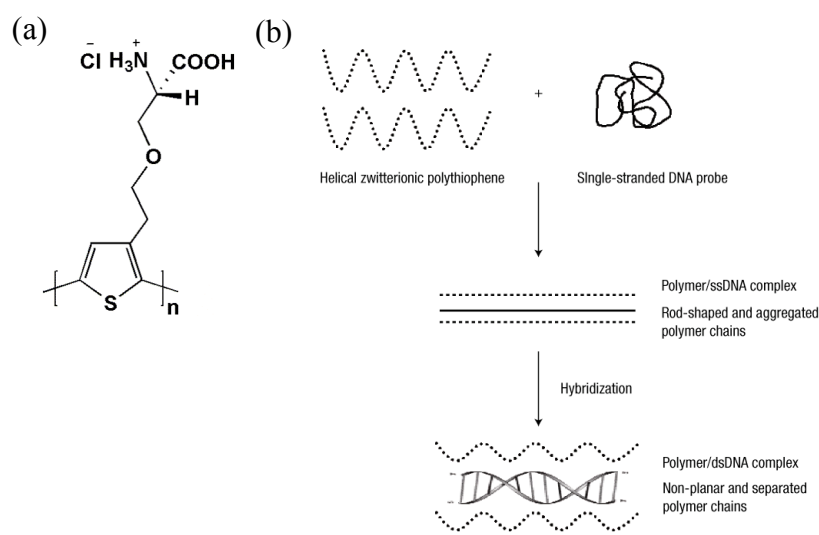
Figure 1.6 *(a) Molecular structure of POWT. (b) Scheme of the formation of zwitterionic polythiophene/DNA complexes. Geometrical changes of polymer (dotted lines) on addition of ssDNA (solid lines) and dsDNA (helical structure).*

Therefore, the polymer backbone could be seen as a coil that is more or less elongated depending on the interaction with DNA (see Figure 1.6). ssDNA forces the coil to become stretched, while the formation of the dsDNA helix on hybridization allowes the

coil to become less extended. In turn the degree of elongation affects the emission processes of the polymer chains through both intra- and inter-chain events.

POWT represents the first example of a polyampholytic conjugated polythiophene which is able to detect biospecific interactions. Moreover, the interaction between the zwitterionic polythiophene and the DNA, as well as the optical phenomena, persist when the polymer is deposited and patterned on a surface, opening a novel way to create DNA chips without using covalent attachment of the receptor or labelling of the analyte. In 2004, the same group[18] reported the formation of a chiral, well ordered supermolecule with the three-dimensional ordered structure of a biomolecule and the electronic properties of a conjugated polymer, by the self-assembly of a negatively charged conjugated polythiophene derivative and a positively charged synthetic peptide. The complexation of the polythiophene and the synthetic peptide (Figure 1.7) cause a change from random-coil to a helical structure of the synthetic peptide and forces the polymer backbone to adopt a non planar conformation.

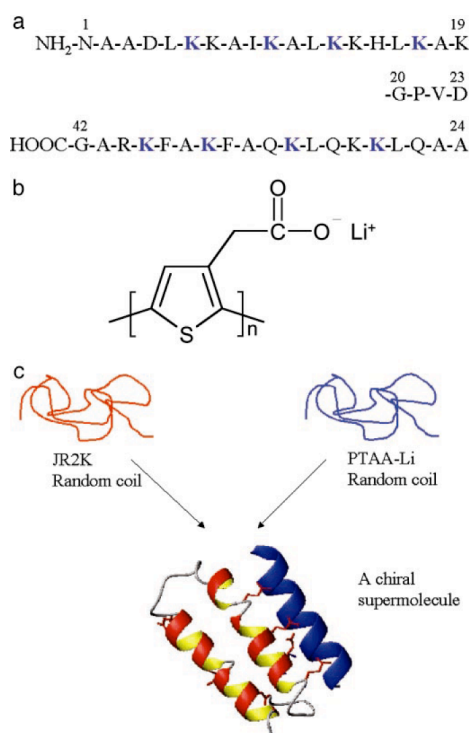**Figure 1.7** *Structural data for peptide JR2K and poly(thiophene acetic acid) PTAA-Li. (a) Amino acid sequence for JR2K. (b) Chemical structure of the repeating unit of PTAA-Li. (c) Schematic drawing of the conformational changes and the supramolecular*

assembly of the synthetic peptide JR2K and PTAA-Li. JR2K does not form homodimers because of electrostatic repulsion.

Although the induction of a main-chain chirality in optically inactive polythiophene in presence of a chiral biomolecule had already been observed, this is the first time the phenomenon has been seen to occur between an optically inactive polymer and a random coil biomolecule. As remarked by the authors, these results could pave the way to a wide range of applications such as biomolecular devices, artificial enzymes and biosensors.

In the same year, M. Leclerc's group reported the specific detection of a few hundred molecules of genetic material using a fluorescent polythiophene biosensor.[19] Such recognition was based on simple electrostatic interactions between a cationic polymeric optical transducer and the negatively charged nucleic acid target. This very sensitive optical detection system allows to achieve a zeptomolar limit of detection (10^{-18} M) and to detect the perfect match between a nucleic acid target and its complementary sequence or the presence of single nucleotide polymorphisms (SNPs). Moreover, as the authors suggested, the possibility to follow hybridization reactions in real time at such low concentrations, could open interesting applications for kinetic and thermodynamic studies of nucleic acids in various biological systems. In addition to its fluorescence, this polythiophene possesses electroactive properties which may serve for detection purposes or to generate structures such as conducting nanowires wrapped around nucleic acid scaffolds.
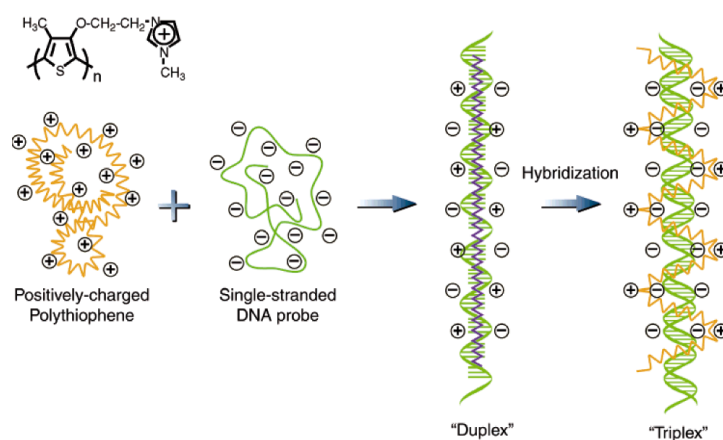
Figure 1.8 *Schematic description of the formation of the polythiophene/single-stranded nucleic acid duplex and the polythiophene/hybridized nucleic acid triplex.*

In 2005, the same authors reported the use of a cationic polythiophene transducer, for the fluorometric detection of hybridization on microarrays,[20] based on the use of surface-bound peptide nucleic acids (PNA) as probes able to hybridize a complementary oligonucleotide.

Since PNA do not have a charged backbone, the cationic polymer does not bind to unhybridized neutral PNA capture probes, but strongly interacts with the negatively-charged backbone of the complementary oligonucleotides bound to PNA probes, allowing transduction of hybridization into a fluorescence signal.

By using PNA as capture probes, the authors provided a simple and sensitive electrostatic approach on solid support, which enables the direct detection and specific identification of unlabelled target nucleic acid analyte with a standard microarray scanner. The sensitivity of the described detection method in solid state is approximately five orders of magnitude more sensitive than the zwitterionic polythiophene used to detect a oligonucleotide within a hydrogel matrix by Nilsson and Inganäs. [16]

Figure 1.9 *A) Scheme of the interaction between cationic polymers and a) ssDNA, b) dsDNA, c) ssPNA and d) PNA-DNA duplex. B) Experimental results for fluorometric detection on microarray when cationic polythiophene transducer is reacted with and a) ssDNA, b) dsDNA, c) ssPNA and d) PNA-DNA duplex. Results are shown in triplicate.*

C) Graphs showing the fluorescence intensity with standard deviation for each triplicate shown in B.

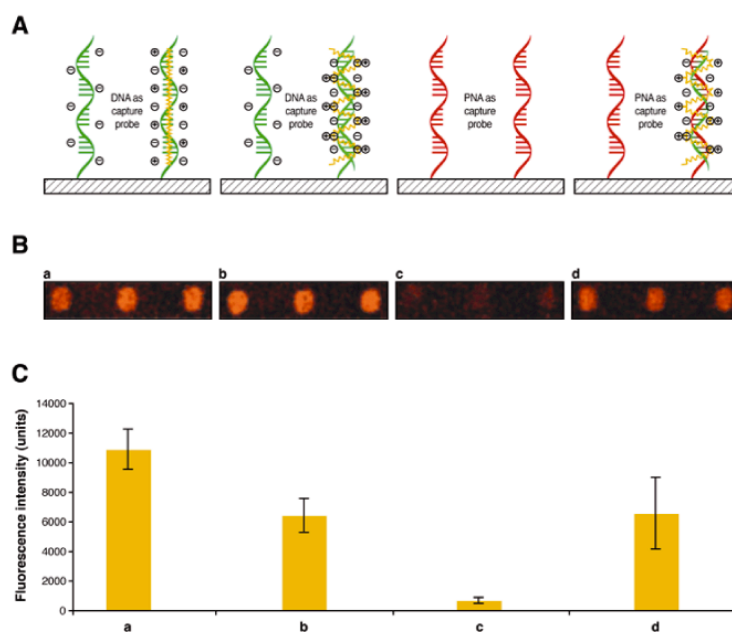For all above mentioned polythiophene based sensing systems, the interactions between the polyelectrolyte and the biomolecule involve electrostatic effects, for example between a positive charged polymer backbone and a negative charged oligonucleotide. Often, these biosensors suffer from the possibility of non-specific polymer-analyte interactions that may reduce their sensitivity or selectivity. For these reasons, the development of biohybrid derivatives with the organic moiety covalently linked to the biomolecule is becoming of great interest. For example, in 2006 S. Wang and co-workers reported [21] a reversible and highly selective chemosensor for mercury(II), based on a polythiophene containing thymine moieties, covalently linked to the side chain of the polymer. In the absence of Hg^{2+} ions, the polythiophene chains remain separated from each other and the polymer exhibits strong fluorescence emission, while upon adding Hg^{2+} ions, a specific thymine–Hg–thymine interaction induces the formation of interpolymer π-stacking aggregation, and results in the fluorescence quenching of the conjugate polymer.

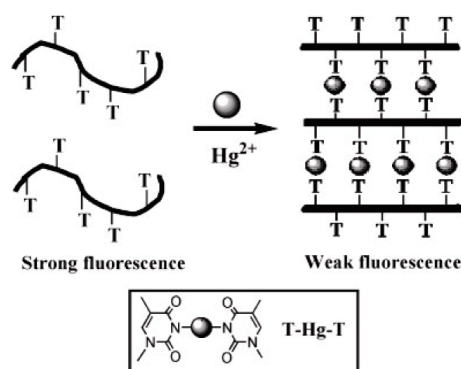**Figure 1.10** *Schematic representation of the transduction mechanism based on Hg^{2+-} mediated interpolymer π-stacking aggregation, which results in the fluorescence self-quenching of the biohybrid polythiophene.*

1.3.2 Bio-hybrid oligothiophenes

The recent finding that polythiophenes can work as optical and electrical sensors to detect DNA modifications necessitates the development of theoretical and experimental

tools to understand and control the interactions of thiophene derivatives with nucleobases. Information on this point is also of crucial interest for the rational production of controlled, bio-driven, self-organizing devices based on semiconducting thiophene oligomers and polymers ('bottom-up manufacturing'). In this direction the conjugation of well-defined 'bio' moieties with synthetic oligomers represent an attractive strategy that allows enhanced structural control at the nanometer level and a deeper understanding of the interactions of thiophene derivatives with bio components and the way they interact and organize in solution and in thin film. The unique example of a peptide-quaterthiophene is synthesized by P. Bäuerle and co-workers.[22] As reported by authors, scanning tunnelling microscopy (STM) investigations showed that the biohybrid quaterthiophene exhibited completely novel features and superstructures, with different supramolecular aggregation modalities from both the peptide sequence and the quaterthiophene derivatives. In fact, the peptide sequence alone showed a 2D-ordering which is due to its tendency to form β-sheets via multiple hydrogen bonding, while the quaterthiophene carboxylic acid exhibited a lamellar long-range ordering in various domains due to interdigitation and van der Waals interactions of the hexyl side chains, as already reported for head-to-tail coupled oligo and polythiophenes.

However, in the paper the authors did not discuss the nature of the interactions responsible for the new aggregation modalities in the peptide-quaterthiophene hybrid derivative. They only suggested the possibility that short peptide sequences may indeed act as auxiliaries influencing the nanoscale structure, and ultimately, the properties of organic semiconducting material.
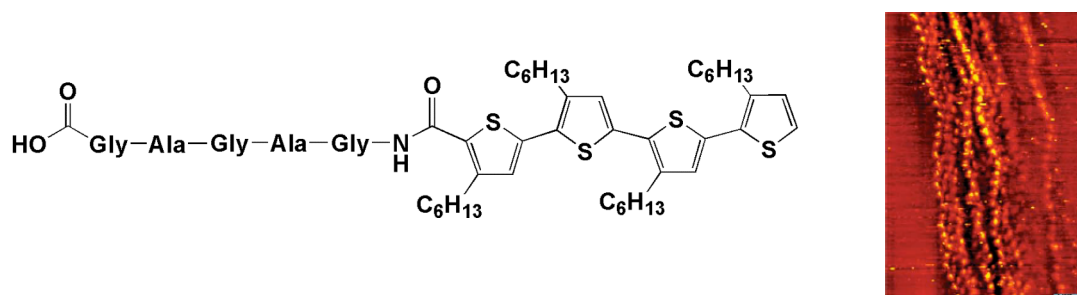

Figure 1.11 *Molecular structure and STM image of the supramolecular organization of biohybrid quaterthiophene.*

1.4 References

[1] (a) M.C. Roco, *Current Opinion in Biotechnology* **2003**, *14*, 337-346. (b) C. Sanchez, H. Arribart, M.M. Giraud Guille, *Nat. Mater.* **2005**, *4*, 277-288. (c) K. Rajagopal, J. P. Schneider *Current Opinion in Structural Biology* **2004**, *14*, 480-486. (d) E. Dujardin, S. Mann *Adv. Mater.* **2002**, *14*, 775-788. (e) B. Samorì, G. Zuccheri. *Angew. Chem. Int. Ed.* **2005**, *44*, 1166-1181.

[2] (a) J.J. Davis, D.A. Morgan, C.L. Wrathmell, D.N. Axford, J. Zhao, N. Wang, *J. Mater. Chem.* **2005**, *15*, 2160-2174. (b) G. Maruccio, R. Cingolani, R. Rinaldi *J. Mater. Chem.* **2004**, *14*, 542-554.

[3] (a) F. E. Alemdaroglu, A. Herrmann, *Org. Biomol. Chem.* **2007**, 5, 1311-1320. (b) K. Tanaka, M. Shionoya *Chem. Letters* **2006**, *35*, 694-699. (c) F. D. Lewis, H. Zhu, P. Daublain, T. Fiebig, M. Raytchev, Q. Wang, V. Shafirovich *J. Am. Chem. Soc.* **2006**, *128*, 791-800. (d) K. V. Gothelf, T. H. LaBean, *Org. Biomol. Chem.* **2005**, *3*, 4023-4037. (e) F. J. M Hoeben, E. W. Meijer, A. P. H. J Schenning, *Chem. Rev.* **2005**, *105*, 1491-1546. (f) E. Katz, I. Willner, *Angew. Chem. Int. Ed.* **2004**, *43*, 6042- 6108. (g) M. A Abdalla, J. Bayer, J. O. Radler, K. Müllen, *Angew. Chem. Int. Ed.* **2004**, *43*, 3967-3970.

[4] E. Katz, I. Willner *Angew. Chem Int. Ed.* **2004**, *43*, 6042-6108.

[5] (a) H. Korri-Youssoufi, F. Garnier, P. Srivastava, P. Godillot, A. Yassar, *J. Am. Chem. Soc.* **1997**, *119*, 7388–7389. (b) K. Faïd, M. Leclerc, *J.Am. Chem. Soc.* **1998,** *120,* 5274–5278. (c) M. Baek, R. C. Stevens, D. H Charych, *Bioconjugate Chem.* **2000**, *11*, 777–788. (d) L. Kumpumbu-Kalemba, M. Leclerc, *Chem. Commun.* **2000**, 1847–1848.

[6] H.A. Klok *J. Polym. Sci. Part A: Polym. Chem.* **2005**, *43*, 1-17.

[7] (a) J. L. Sessler, J. Jayawickramarajah *Chem. Commun.* **2005**, 1939-1949. (b) S. Zhang *Nature Biotechnology* **2003**, *21*, 1171-1178.

[8] C. Chi, A. Mikhailovsky, G. C. Bazan *J. Am. Chem. Soc.* 2007, *129*, 1135-1145.

[9] J. M. Gibbs, S-J. Park, D. R. Anderson, K. J. Watson, C. A. Mirkin, S. T. Nguyen *J. Am. Chem. Soc.* **2007**, *127*, 1170-1178

[10] Y. Kamikawa, T. Kato, *Org. Lett.* **2006**; *8*, 2463-2466.

[11] (a) H. Bock,W. Helfrich, *Liq. Cryst.* **1995**, *18*, 387-399.(b) T. Hassheider, S. A. Benning, H.-S. Kitzerow, M.-F. Achard, H. Bock, *Angew. Chem., Int. Ed.* **2001**, *40*, 2060-2063.

(c) V. Percec, M. Glodde, T. K. Bera, Y. Miura, I. Shiyanovskaya, K. D. Singer, V. S. K. Balagurusamy, P. A. Heiney, I. Schnell, A. Rapp, H.-W. Spiess, S. D. Hudson, H. Duan, *Nature* **2002**, *419*, 384.

[12] R. Iwaura, F. J. M. Hoeben, M. Masuda, A. P. H. J. Schenning, E. W. Meijer, T. Shimizu, *J. Am. Chem. Soc.* **2006**, *128*, 13298-13304.

[13] G. Barbarella, M. Melucci, G. Sotgiu, Adv. Mater. **2005**, *17*,1581-1593.

[14] A. R. Murphy, J. M. J. Fréchet *Chem. Rev.* **2007**, *107*, 1066-1096.

[15] M. Mazzeo, V. Vitale, F. Della Sala, M. Anni, G. Barbarella, L. Favaretto, G. Sotgiu, R. Cingolani, G. Gigli *Adv. Mater.* **2005**, *17*, 34-39

[16] S. Günes, H. Neugebauer, N. S. Sariciftci Chem. Rev. **2007**, *107*, 1324-1338.

[17] K. Peter, R. Nilsson, O. Inganas Nature Materials **2003**, *2*, 419-424.

[18] K. P R. Nilsson, J. Rydberg, L. Baltzer, O. Inganäs *PNAS* **2003,** *100*, 10170–10174**.**

[19] K. Dore, S. Dubus, H-A. Ho, I. Levesque, M. Brunette, G. Corbeil, M. Boissinot, G. Boivin, M. G. Bergeron, D. Boudreau, M. Leclerc *J. Am. Chem. Soc.* **2004**, *126*, 4240-4244.

[20] F.R Raymond, H-A. Ho, R. Peytavi, L. Bissonnette, M. Boissinot, F. J Picard, M. Leclerc and M. G Bergeron *BMC Biotechnology* **2005**, 5:10.

[21] Y. Tang, F. He, M. Yu, F. Feng, L. An, H. Sun, S. Wang, Y. Li, D. Zhu *Macromol. Rapid Commun.* **2006**, *27*, 389–392.

[22]H.A. Klok, A. Rösler, G. Götz, E. Mena-Osteritz, P. Bäuerle *Org. Biomol. Chem.* **2004**, *2*, 3541-3544.

Aim and outline of the thesis

The aim of this Ph.D. thesis is the design and development of new biohybrid oligothiophene derivatives and their characterization in solution and in thin films. To this purpose, conveniently functionalized thiophene-based oligomers have been covalently linked to oligonucleotides in order to obtain novel oligothiophene-oligonucleotide hybrids, which have been characterized in solution and in the solid state. The relationship between the biohybrid molecular structure, its self-assembling behaviour and its functional properties such as light emission and charge transport has been investigated.

In particular, we aimed at: **1) exploring the use of oligothiophene-oligonucleotide biohybrid derivatives to monitor DNA hybridisation events, 2) developing theoretical and experimental tools to understand the interactions of thiophene derivatives with DNA components, 3) investigating the supramolecular organization of the biohybrids in solution and in thin film.**

At the beginning of this work, one of the problems we had to face was the difficulty to synthesize the oligothiophene components with a sufficiently high level of purity.

In fact, thiophene based materials are usually prepared by stepwise formation of carbon-carbon bonds *via* cross-coupling of halogenated precursors with metalated counterparts, in organic solvents using soluble Pd or Ni catalysts (homogeneously catalysed Suzuki or Stille reactions). However, when prepared with these synthetic methodologies, oligothiophenes, and consequently their biohybrid derivatives, are often contaminated by residual metals deriving from catalysts, which are very difficult to remove and alter the optical and electrical properties.

To overcome these drawbacks, we developed heterogeneously catalyzed Suzuki coupling procedures, in which the supported palladium catalyst could easily be removed from the reaction mixture by filtration and be reused in consecutive reactions. To accelerate reaction rates microwave-assistence was employed.

Making use of the newly developed synthetic modalities, quaterthiophene and quinquethiophene biohybrid derivatives – having the oligothiophene moiety covalently linked to two and one dinucleotide pendant group, respectively - were prepared.

Subsequently, the synthesis of four oligothiophene-5-labeled deoxyuridines and their incorporation into oligodeoxynucleotides sequences were carried out.

The biohybrids were applied, on one side, for the detection of DNA single nucleotide polymorphism (SNP) in complementary target sequences and, on the other, for the elucidation of the nature of the interactions between thiophene and DNA bases through the investigation of their self-assembly modalities.

The results were interpreted by the aid of a combination of spectroscopic methods, light transmission, fluorescence and atomic force microscopies, electrical characterizations and molecular mechanics/molecular dynamics calculations.

More in detail, in Chapter 2, we report the use of heterogeneous Suzuki coupling in EtOH/water or isopropanol under microwave irradiation to prepare α-β alkyl substituted oligothiophenes (up to hexamers) and thiophene based co-oligomers containing electron deficient 1,2,3-benzothiadiazole or electron-rich thienothiophene rings.

In Chapter 3, we discuss the synthesis of biohybrid derivatives containing short oligonucleotide sequences, performed in solution phase through phosphorilation reactions, as well as the preparation of oligothiophene-5-labeled deoxyuridines and their subsequent insertion into 19-meric oligonucletide sequences, carried out in solid phase via phosphoramidite chemistry procedures.

In Chapter 4, the oligothiophene-labeled oligonucletide sequences are used as probes to detect a single nucleotide polymorphism (SNP) in complementary target sequences.

In Chapter 5, by means of a combination of spectroscopy and microscopy techniques, electrical characterizations and theoretical calculations, we demonstrate, for quaterthiophene biohybrid compounds, the formation of photoluminescent and electroactive rod-like supramolecular aggregates.

In Chapter 6, the self-assembly modalities in thin film of biohybrid derivatives of quinquethiophene - functionalized with self-complementary dinucleotides at the inner thienyl beta position - are investigated with the aid of microfluidic techniques.

Chapter 2

Microwave-assisted synthesis of oligothiophenes in aqueous media using supported Pd catalysts

Abstract

An innovative heterogeneous procedure for the preparation of highly pure oligothiophene moieties of biohybrid materials via microwave-assisted Pd catalysis by using silica- and chitosan-supported Pd complexes is discussed. The present approach is very efficient and greener than the existing homogeneous methodology as it combines a very efficient reaction with improved catalyst separation. Moreover, this efficient and cleaner microwave methodology smoothly afforded the preparation of coupled products in high yields (up to 87% isolated yield, 30-100 min). Thienyl iodides or activated bromides were employed as starting materials and KF as base. The microwave reaction was carried out in isopropanol or aqueous ethanol. The heterogeneous catalyst can be easily removed from the reaction mixture by filtration and reused in consecutive reactions (up to 4 times).

2.1. Introduction

Actually the most widely employed strategy adopted for the preparation of thiophene-based materials is an organometallic approach,[1] taking advantage of accessible building blocks and Pd or Ni catalysts. Such approach usually consists of cross-coupling reactions between halogenated thienyls and metalated counterparts in the presence of soluble palladium or nickel complexes (homogeneous catalysis). However, the use of organometallic catalysts in the process presents a number of drawbacks including the presence of by-products either originated by the demetalation or dehalogenation of the starting materials or by homo-coupling or boron-halogen exchange side reactions, as well as the presence of catalyst residues. Such impurities may alter the film forming properties of the synthesized materials and therefore the morphology, conductivity and performance of the device prepared. As a consequence, preliminary expensive purification techniques including vacuum sublimation are often required for the successful application of oligothiophenes as active organic materials in electronic and optoelectronic devices .

In previous work, our group demonstrated that the use of microwave-assisted Suzuki-coupling methodologies for the preparation of substituted and unsubstituted oligothiophenes led to higher reaction rates and minimized the formation of undesired by-products. [2] Along these lines, we envisaged that combining microwave assistance with heterogeneous Pd catalysis[3] could be an interesting way to synthesize highly pure, metal free, thiophene based materials in very short time.

Suzuki-Miyaura heterogeneous protocols[4] have been reported for the synthesis of biphenyl systems employing Palladium supported on various materials including carbon,[5,6] metal oxides, ceramics (perovskites), porous aluminosilicates, as well as on polymers[7] and biopolymers,[8,9] the latter ones offering the advantages of being renewable, biodegradable and having low toxicity.

Chitosan and silica based Pd complexes have been demonstrated to be very effective under a wide range of conditions in the Suzuki and Heck couplings, being reusable up to 10 times.[10] Such catalysts, comprising bidentate organic ligands, grafted onto the solid support, that complex the active palladium salts, exhibited excellent stability (chemical and thermal), high surface areas, good accessibility and chemical versatility. Moreover, chitosan is a water-tolerant support that will potentially allow reactions to be

carried out in aqueous media and has major advantages in that it can be formed into fibres, films, attached to reactor walls, etc. making it ideal for incorporation in different reactor designs (continuous/intensive, etc.). On the other hand, silicas can be easily prepared and allow for the robust attachment of organic functionalities and control over their surface chemistries.
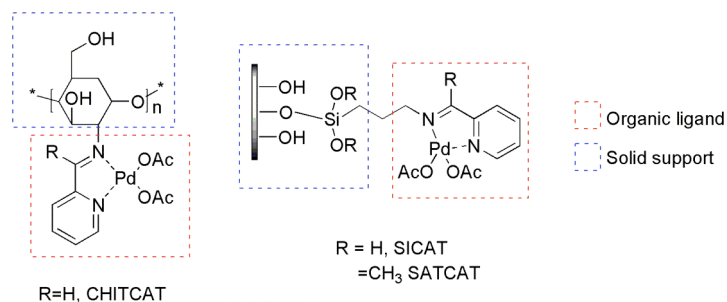
Scheme 2.1 *Structures of the catalysts used in the present investigation. CHITCAT = chitosan supported Pd complex ; SICAT= silica supported Pd complex 1(R=H); SATCAT= silica supported Pd complex 2 (R=Me).*

In this direction we explored the possibility of preparing thiophene-based materials using selective and stable chitosan and silica supported palladium complexes (Scheme 2.1) taking advantage of the use of microwave irradiation.

2.2 Results and discussion

2.2.1 Optimization of the model reaction.

The reaction optimization was performed on two commercially available substrates, namely 5-Bromo-2-thiophenecarboxaldehyde 1 and 2-Thienylboronic acid derivative 2 (Scheme 2.2). Supported palladium catalysts were tested under both conventional heating and microwave-assisted conditions (see Table 2.3).
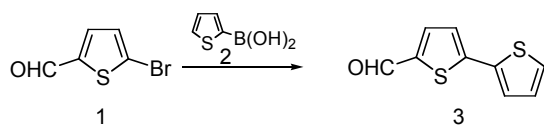
Scheme 2.2 *Model reaction between 5-Bromo-2-thiophenecarboxaldehyde and 2-Thienylboronic acid*

Being based on previous reported studies on the Suzuki cross-coupling of thienyl derivatives, proving that KF was a very suitable base for these systems,[11] we observed

that the use of CHITCAT as catalyst and KF as the base in aqueous ethanol (1:1) afforded a complete conversion of the starting materials to the coupling product **3** in only 2 min of microwave irradiation at 130°C (Table 2.3, entry 2). The same reaction carried out under conventional heating provided a poor 55% conversion after 48 h.

The use of an aqueous environment was also found to be particularly advantageous for an optimum catalytic performance with respect to the use of toluene or other organic compounds as solvents. This can be probably ascribed to the different solubility of KF in toluene and alcoholic solvents as well as to the more efficient absorption of microwaves from polar solvents. Medium to high microwave absorbing solvents, including EtOH, isopropanol and water, may allow a more efficient internal heating compared to microwave-transparent solvents (toluene) usually employed in heterogeneous Suzuki reactions.[15]

Table 2.3 *Catalytic performance of different supported Pd complexes in the model reaction (Scheme 2.2).*

Entry	Base	Catalyst	Solvent	MW conditions	3 Conversion (%)[b]
1	KF	SICAT	EtOH/H_2O (1:1)	100 W, 60 min, 80°C	87
2[a]	KF	CHITCAT	EtOH/H_2O (1:1)	100 W, 2 min, 130°C[d]	>99
3[a]	KF	CHITCAT	toluene	100 W, 60 min, 130°C	8
4[a]	KF	SATCAT	EtOH/H_2O (1:1)	100 W, 60 min, 80°C	82
5[c]	KF	SATCAT	isopropanol	100 W, 60 min, 80°C[d]	96
6	KF	SATCAT	toluene	220 W, 60 min, 80°C	20

[a]carried out with simultaneous cooling; [b]GC conversion; [c]higher power values did not remarkable improve the reaction conversion; [d]the pressure measured was about 80 and 20 psi for entries 2 and 5, respectively.

It was possible to observe that the use of silica supported palladium catalysts (SICAT and SATCAT) required lower reaction temperatures (80°C vs 130°C) but much longer reaction times (60 min) compared to chitosan in order to achieve comparable conversion values.

In fact, the choice of the catalyst has to take into account several factors including the thermal stability of the boronic-substrates and the size of the target oligomer. Chitosan

is possibly more suitable for stable and smaller substrates compared to silica, in which the porous structure is surely an attractive feature in reactions with larger molecules.

A hot filtration test (HF) was performed to prove the truly heterogeneous nature of our catalytic reaction (entries 2 and 4, Table 2.8).[12] The hot reaction mixture (typically less than half way through completion) was filtered off and the liquid filtrate and the solid were recovered separately. Fresh substrates were added both to the liquid filtrate and to the solid and another reaction (under the same conditions) was conducted. The results of the second reuse of CHITCAT are included in Figure 2.4. The catalyst was filtered off after 60 sec of microwave irradiation (~30% conversion), then the reaction mixture without catalyst was further microwaved for 30 additional minutes and finally quenched. No changes in conversion were observed, excluding the presence of a substantial concentration of palladium leached species in solution. After catalyst filtration, the Pd content in solution was determined using ICP. A tiny 1.8 ppm Pd was found, confirming that the Pd leaching in the systems was almost negligible.
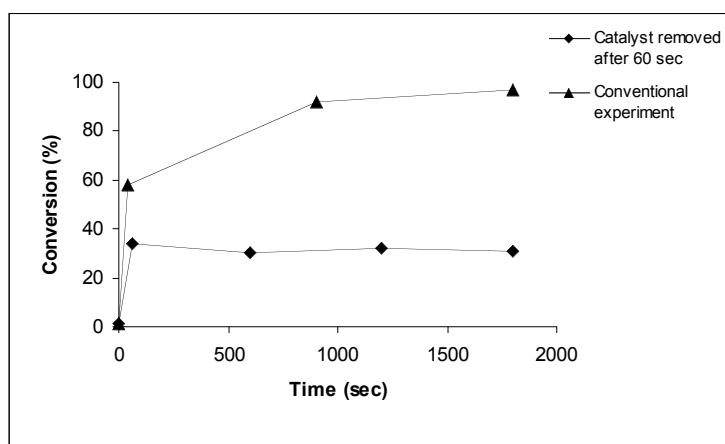
Figure 2.4 *Hot filtration test. Effect of removing the chitosan supported palladium catalyst from the second cycle reaction of 2-Thienylboronic acid and the 5-Bromo-2-thiophenecarboxaldehyde.*

The catalyst reusability was also investigated under the optimized conditions. The catalyst was filtered off after each reaction run, washed with aqueous methanol and pure methanol, dried at 90 °C and subsequently reused in another catalytic cycle. Despite an increase in the time of reaction required for complete conversion, the catalysts were reusable up to 4 times preserving more than 95% of the initial catalytic activity (entry 2,

table 2.8).[15] The observed slight reduction in catalytic activity with recycling probably can be due to a partial blockage or deactivation of the active sites of the catalyst with the salts and/or by-products from the reaction.

Table 2.5 *CHITCAT reusability experiments carried out under microwave irradiation with simultaneous cooling.*

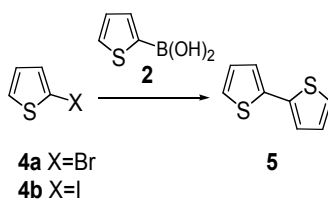| Cycle	Base	Catalyst	Solvent	MW conditions	3 (%)
1st	KF	CHITCAT	EtOH/H_2O (1:1)	100 W, 130°C, 1 min	>99
2nd	KF	CHITCAT	EtOH/H_2O (1:1)	100 W, 130°C, 30 min	97
3rd	KF	CHITCAT	EtOH/H_2O (1:1)	100 W, 130°C, 45 min	98
4th	KF	CHITCAT	EtOH/H_2O (1:1)	100 W, 130°C, 45 min	95

2.2.2 Extension to other substrates

The optimised conditions based on the use of the CHITCAT and SATCAT materials were then extended to various thienyl-based substrates. Several parameters, including the nature and number of halogen atoms, functionalization and size of the starting building blocks were investigated and the results are summarised in Tables 2.7, Table 2.8 and Table 2.11.

Iodo-derivatives were found to be more effective than bromo-derivatives in the preparation of bithiophene (Scheme 3), irrespective of the conditions employed (solvent and/or catalyst). Therefore, only thienyl iodides were employed for the synthesis of longer oligomers.

4a X=Br
4b X=I

Scheme 2.6 *Suzuki reaction for the preparation of bithiophene (5) from a range of halo-thiophenes*

Table 2.7 *Catalytic performance of various Pd catalysts in the preparation of bithiophene from 2-thienyl bromide and 2-thienyl iodide .*

Entry	Reagent	Catalyst	Solvent	MW conditions	Yield 5 (%)[a]
1[b]	4a	CHITCAT	EtOH/H_2O (1:1)	100 W, 130°C, 60 min	8
2[b]	4b	CHITCAT	EtOH/H_2O (1:1)	100 W, 130°C, 60 min	57
3	4a	SATCAT	isopropanol	100 W, 80°C, 60 min	36
4	4b	SATCAT	isopropanol	100 W, 80°C, 60 min	61
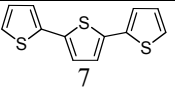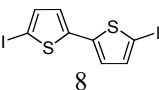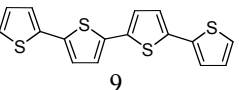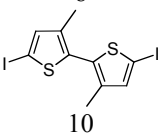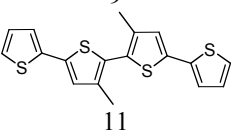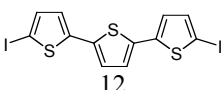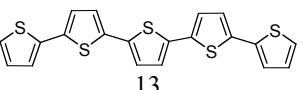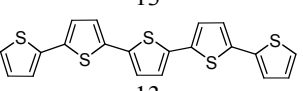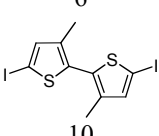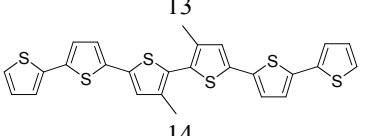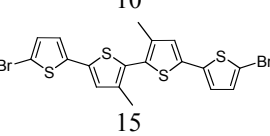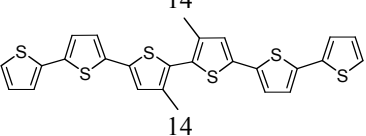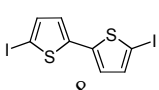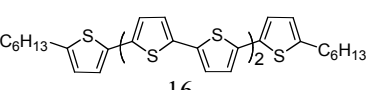
[a] isolated yield. [b] carried out with simultaneous cooling.

The methodology was then further extended to the preparation of larger (α-β alkyl) substituted oligomers. (See Table 2.8).

Terthiophene (**7**) is a useful building block for the preparation of thiophene-based oligomers and polymers.[13] Many synthetic routes to α-terthienyl have been reported. A previously reported solvent-free microwave assisted Suzuki coupling, provided a maximum isolated yield of 60% starting from 2,5-dibromothiophene[7a], much lower than that reported in Table 2.8starting from the di-iodo derivative.

Quaterthiophene (T4, **9**) is one of the most investigated thiophene derivatives for its photoluminescence[14] and charge transport properties.[15] Terminal alkyl substituted T4 compounds are also of interest as they exhibit liquid crystalline behaviour and enhanced solubility that make them particularly suitable for solution processing.[16] T4 derivatives are usually prepared by using the bi-directional 1+2+1 approach consisting in the reaction between two equivalents of boronic or halo-thienyl derivative and one equivalent of the corresponding reaction partner.[17] For the preparation of quaterthiophenes **9** and **11**[22] we chose the reaction between boronic thienyl derivative 2, and the bifunctional iodo-dimers **8** and **10** that afforded good yields for both unsubstituted and β-methyl substituted T4 compounds (entries 2, 3 table 4).

Table 2.8 *Preparation of various oligothiophenes derivatives using supported Pd complexes*

Entry	Starting material	Product	Catalyst	MW conditions	Yield[b] (%)
1[a]	6	7	CHITCAT	100 W, 30 min, 130°C	87
2[a]	8	9	CHITCAT	100 W, 100 min, 130°C	83
3	10	11	SATCAT	100 W, 100 min, 80°C	77
4	12	13	CHITCAT	100 W, 100 min, 130°C	37
5	6	13	SATCAT	100 W, 100 min, 80°C	82
6	10	14	SATCAT	100 W, 100 min, 80°C	65
7[c]	15	14	SATCAT	100 W, 100 min, 80°C	traces
8	8	16	CHITCAT	100 W, 100 min, 130°C	69

[a] In entry 1, the reaction was carried out with simultaneous cooling. For entry 2 we tried both, with and without simultaneous cooling obtaining similar results (66% after 60 min employing simultaneous cooling) [b] isolated yield. [c] The dibromo derivative was more soluble than diiododerivative under the reaction conditions .

Unsubstituted or functionalised α-quinque- and hexathiophenes were also prepared. Such systems show high self-assembly capability and good charge transport properties in Field Effect Transistors (FET). [18,19]

Two different strategies were employed and compared for both compounds. Quinquethiophene (T5, **13**) was prepared either by adding two boro-functionalized monomers to the diiodoterthiophene (**12**) (+1 strategy, Figure 2.9), or by reacting the diiodothiophene (**6**) with two equivalents of borobithiophene (+2 strategy., Figure 2.9).

Similarly, hexathiophene (T6, **14**) was prepared by means of a +2 approach (using the di-iodobithiophene **10**) as well as by the +1 strategy employing di-bromoquaterthiophene **15** as starting material.
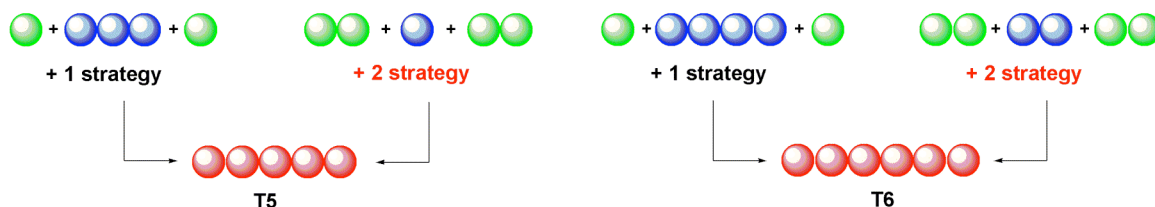
Figure 2.9 *Overview of the strategies investigated for the synthesis of T5 and T6 materials.*

The election of the synthetic pathway is usually dependent on many factors including the availability of the starting materials and the formation of by-products such as deborylated thiophenes, homo-coupling and metal-halogen exchange products that have to be removed from the target compounds. The +1 strategy led to by-products easily separated from the reaction mixture, facilitating the purification of the desired product. However, the starting materials are complex systems, therefore additional synthetic steps are required in order to obtain them. Despite our previous results on homogeneous microwave assisted Suzuki coupling pointing out that the +2 strategy was unfavourable (due to the formation of T4 by-products difficult to remove), it proved to be the most effective for the synthesis of both T5 and T6 oligomers (Table 2.8, entries 5, 6), as it involves readily available precursors and easily purified products, thus improving the green credentials of the reaction.

In the reaction conditions the larger building blocks, including ter- and quaterthiophene, are poorly soluble and consequently less reactive. Moreover, their higher steric hindrance is believed to restrict the oxidative addition to palladium, which is less pronounced than in homogeneous conditions.

Steric effects can also explain why SATCAT and CHITCAT catalyzed reactions show undetectable boron-halogen exchange by-products. The oxidative insertion of Pd in the C-B bond takes place when the C-I bond insertion reaction is very slow. The presence

of supported Pd (0) reduces the probability of such insertion therefore minimizing the presence of undesired boron-halogen exchange by-products.

Preliminary investigations on quinque- and hexathiophenes prepared in this way (**13**, **14**, **16**) pointed out that these compounds may display enhanced film forming properties than the same compounds prepared by conventional homogeneous catalysis, due to the higher level of purity obtained using this methodology. Melted homogeneously prepared T5 powder sandwiched between two glasses rendered a viscous fluid containing black solid aggregates which melt at temperatures over 350°C. Such aggregates can be removed upon purification by vacuum sublimation suggesting they may be residues of the catalyst and/or impurities. No evidence of similar impurities were observed in the preparation of T5 using our heterogeneous protocol (Figure 2.10).
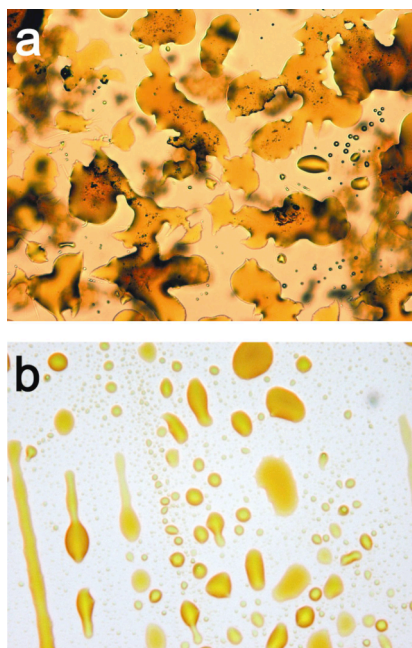
Figure 2.10 *Optical microscopy image of melted T5 powder (image size 800x800μm) prepared by a) conventional homogeneous catalytic method; b) novel heterogeneously catalyzed protocol.*
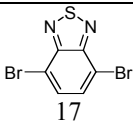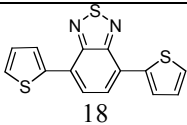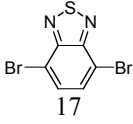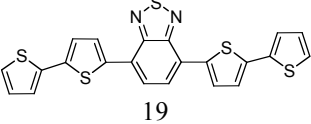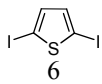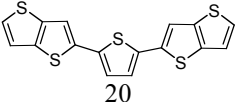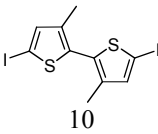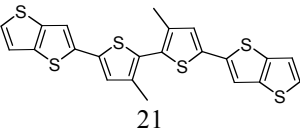
Enhanced properties can be expected for all the materials prepared in their use as Field-Effect Transistors (FET) and further investigations in this area are currently ongoing.

The optimized protocol was also employed in the preparation of thiophene based co-oligomers containing electron deficient 1,2,3-benzothiadiazole or electron-rich

thienothiophene rings. Benzothiadiazole derivatives have been recently proved to have liquid crystal and semiconducting properties and the polymers have been reported as especially suitable materials for photovoltaic applications.[20] High air stability and charge carrier capabilities have been also recently reported for thienothiophene containing oligomers and polymers.[21] Thienothiophene-thienyl co-oligomers would potentially feature a combination of good π-stacking and charge transport properties (from the thienothiophene system) with the chemical versatility of the thienyl ring.

The benzothiadiazole-based compound (**19**), and the newly synthesized thienothiophene based products (**20** and **21**) were chosen as target compounds. The +2 approach (Figure 2.9) - both for odd oligomer (**19** and **20**) and for even oligomer (**21**) - was employed. Data are summarized in Table 2.11. Our heterogeneously catalyzed protocol provided moderate to very good isolated yields to the different synthesized compounds. Product 21 exhibited good solubility in non-polar solvents and highly crystalline cast films, therefore having promising perspectives as active layer in FET.

Table 2.11 *Catalytic performance of CHITCAT and SATCAT in the preparation of thiophene based co-oligomers*

Entry	Starting material	Product	Catalyst	MW conditions	Yield[a] (%)
1	**17**	**18**	CHITCAT	100 W, 100 min, 130°C	75
2[b]	**17**	**19**	CHITCAT	100 W, 100 min, 130°C	47
3	**6**	**20**	SATCAT	100 W, 100 min, 80°C	81
4	**10**	**21**	SATCAT	100 W, 100 min, 80°C	65

[a] Isolated yield. [b] Literature data report 37% yield with a similar compound.[22]

[23]In entries 3 and 4 the starting material 4,4,5,5-Tetramethyl-2-thieno[3,2-b]thiophen-2-yl-[1,3,2]dioxaborolane (TTB) was synthetized starting from thieno[3,2-b]thiophene[24] following a standard procedure.[7a]

2.3 Conclusions

Firstly, we observed that the proposed protocol can be used as standard protocol irrespective of the size and substitution of the thienyl, compared to homogeneous Suzuki methodologies which usually require an optimization of the reaction conditions for each substrate.[7] Oligomers containing up to six thiophene units and substituted oligomers containing fused heterocycles into the aromatic backbone have been successfully prepared using this novel, efficient and greener heterogeneous methodology. The high level of purity obtained avoids tedious and energy intensive-time consuming purification steps and the need to deal with residual metals. Ongoing studies on quinque- and hexathiophenes (**13**, **14** and **16**) pointed out these compounds can display improved film forming properties than those prepared by conventional homogeneously catalyzed methodologies and consequently higher charge mobilities in thin film can be expected.

2.4 Experimental Section

2.4.1 Materials and methods

All the reactions were carried out under air. All commercially available reagents and solvents were used as purchased without further purification. **10**[25], **12**[7b] and **15**[19] were prepared by methods described previously. Microwave experiments were carried out in a CEM-DISCOVER model with PC control and monitored by sampling aliquots of reaction mixture that were subsequently analysed by GC/GC-MS using an Agilent 6890N GC model equipped, with a 7683B series autosampler, fitted with a DB-5 capillary column and an FID detector. Experiments were conducted on a closed vessel (pressure controlled) under continuous stirring. The microwave method was generally power controlled (100 W maximum power input) where the samples were irradiated with the required power output (settings at maximum power) to achieve the desired temperature (80-130$^{\text{o}}$C).

2.4.2 Synthesis of the catalysts

Supported Pd-catalysts used in the present work are prepared following the already reported procedures,[15] obtaining a Pd loading of about 0.5 and 0.2 mmol g^{-1} for CHITCAT and SATCAT, respectively, as confirmed by ICP. Diffuse Reflectance IR analysis of the materials showed a diagnostic peak at 1638 cm^{-1} due to the formation of the pyridylimine unit.

2.4.3 General procedure for CHITCAT and SATCAT catalyzed Suzuki reaction.

The microwave oven reactor was charged with halothienyl-derivative or dihalothienyl-derivative (0.2 mmol), dodecane (0.2 mmol), mono-or bithienylboronic derivatives (0.6 mmol for halides,1.2 mmol for dihalides), Pd catalyst CHITCAT or SATCAT (0.05 mmol for monohalides and 0.1 mmol for dihalides), KF (0.6 mmol for monohalides and 1.2 mmol for dihalides) and of EtOH/ water (1:1) (2 mL) for CHITCAT catalyzed procedure or of isopropanol (2 mL) for SATCAT catalyzed one. After 30-100 min of microwave irradiation, a TLC on silica gel showed the absence of starting materials. The solvent was removed, the solid crude was dissolved in CH_2Cl_2 (table 2.8, entries 1, 2, 3; table 2.11, entry 1) or in hot toluene (table 2.8, entries 4, 5, 6, 7, 8; table 2.11, entries 2, 3, 4) and the catalyst filtered off. Then, the organic phase was washed with water (2 x 15 ml), dried on Na_2SO_4 and the solvent evaporated under vacuum. The shorter oligomers (table 2.8, entries 1, 2, 3; table 2.11, entry 1) were purified by flash chromatography, while the longer oligomers (table 2.8, entries 4, 5, 6, 7, 8; table 2.11, entries 2, 3, 4) were purified by washing steps and crystallization.

2,2':5'2''-terthiophene 7[7a]

Table 2.8, entry 1, yield 87%; yellow solid, mp 93-95°C. Flash chromatography: petroleum ether (40-60) purum. δ_H(270 MHz, $CDCl_3$, Me_4Si) 7.22 (2H, d, *J* 4.8), 7.18 (2H, d, *J* 3.8 H), 7.08 (2H, s), 7.03 (2H, dd, *J* 3.8); δ_C(67.93 MHz, $CDCl_3$, Me_4Si) 137.081, 136.148, 127.851, 124.444, 124.276, 123.650; m/z 248.

2,2':5'2'':5''2'''-quaterthiophene 9[7a]

Table 2.8, entry 3, yield 83%; yellow solid, mp 210-212°C. Flash chromatography: petroleum ether (40-60):EtOAc/99:1. δ_H(400 MHz, DMSOd_6, Me_4Si) 7.529 (2H, d, *J* 4.8), 7.341 (2H, d, *J* 4.0), 7.297 (2H, d, *J* 3.6), 7.272 (2H, d, *J* 3.6), 7.098 (2H, dd, *J* 3.6); m/z 330.

3'',4'-dimethyl-2,2':5'2'':5''2'''-quaterthiophene 11[25]

Table 2.8, entry 4, yield 77%; yellow oil. Flash chromatography: petroleum ether (40-60):EtOAc/99:1. δ_H(200 MHz, $CDCl_3$, Me_4Si) 7.21 (2H, d, *J* 5.2), 7.16 (2H, d, *J* 3.4), 7.02 (2H, s), 7.01 (t, J_3=5.0 Hz, 2H). δ_C(50 MHz, $CDCl_3$, Me_4Si) 137.33, 137.20, 136.66, 128.10, 127.82, 126.76, 124.39, 123.55, 14.97; m/z 358.

2,2':5'2'':5''2''':5''',2''''-quinquethiophene 13[23]

Table 2.8, entry 5, yield 82%; orange solid, mp 251°C. The crude product was washed with petroleum ether and diethyl ether and finally crystallized from toluene. δ_H(400 MHz, DMSOd_6, Me$_4$Si) 7.51 (2H, d, J 5.2), 7.33 (2H, d, J 2.8) 7.30 (2H, s), 7.29 (2H, d, J 3.6), 7.26 (2H, d, J 3.2), 7.10 (2H, dd, J 3.2); m/z 412.

3''',4''-dimethyl-2,2':5'2'':5''2''':5''',2'''':5'''',2''''''-hexathiophene 14[24]

Table 2.8, entry 6, 7, yield 65%; deep red solid, mp 164-166°C. The crude product was washed with petroleum ether and diethyl ether and finally CH$_2$Cl$_2$. δ_H(400 MHz, CDCl$_3$, Me$_4$Si) 7.226 (2H, d, J 4.8), 7.182 (2H, d, J 3.6), 7.084 (2H, d, J 4.4), 7.064 (2H, d, J 3.6), 7.028 (2H, dd, J 3.2), 7.020 (2H, s), 7.227 (6H, s). δ_C(100 MHz, CDCl$_3$, Me$_4$Si) 137.632, 137.288, 136.527, 136.442, 136.076, 128.347, 128.045, 126.885, 124.665, 124.529, 124.334, 123.862, 15.208; m/z 522.

α,ω-dihexylhexathiophene 16[26]

Table 2.8, entry 8, yield 69%, orange powder, mp: 285-288°C. The crude product was washed with petroleum ether and diethyl ether and finally CH$_2$Cl$_2$.; ν_{max}(film)/cm^{-1} 3085 3060, 2956, 2922, 2873, 2855, 1748, 1596, 1538, 1505, 1466, 1442, 1377, 1221, 1206, 1071, 872, 839, 794, 723, 462); m/z 664.

4,7-Di-2-thienyl-2,1,3-benzothiadiazole 18[27]

Table 2.11, entry 1, yield 75%; red solid, mp 123-125°C. Flash chromatography: petroleum ether (40-60):EtOAc/97:3. δ_H(270 MHz, CDCl$_3$, Me$_4$Si) 8.11 (2H, d, J 3.7), 7.86 (2H, s), 7.59 (2H, d, J 5.2), 7.21 (2H, t, J 4.0); δ_C(67.93 MHz, CDCl$_3$, Me$_4$Si) 152.60, 139.33, 127.99, 127.469, 126.78, 125.96, 125.743; m/z 300.

4,7-Bis(-2,2'-dithiophenyl-5-yl)benzo[1,2,5]-thiadiazole 19

Table 2.11, entry 2, yield 47%; violet solid, mp 163–170°C. The crude product was washed with petroleum ether and diethyl ether and finally CH$_2$Cl$_2$. MS: 464; δ_H(400 MHz, DMSOd_6, Me$_4$Si) 8.11 (2H, d, J 3.6), 8.105 (s, 2H), 7.55 (2H, d, J 5.2), 7.437-7.434 (4H, m), 7.134 (2H, dd, J 3.6). δ_C(100 MHz, DMSOd_6, Me$_4$Si) 152.163, 139.230, 137.700, 136.960, 129.273, 129.065, 126.714, 126.149, 125.409, 125.205, 125.179; m/z 464.

2,2'-thiene-2,5-diylbisthieno [3,2-*b*]thiophene 20

Table 2.11, entry 3, yield 81%; yellow solid, mp 164-166°C.

The crude product was washed with petroleum ether, CH$_2$Cl$_2$ and finally crystallized from toluene. δ_H(400 MHz, CDCl$_3$, Me$_4$Si) 7.37 (2H, d, J 4.0), 7.37 (2H, s), 7.23 (2H, d,

J 5.2), 7.13 (2H, s). δ_C(100 MHz, CDCl$_3$, Me$_4$Si) 139.810, 138.675, 138.161, 136.834, 127.337, 124.531, 119.467, 115.858; m/z 360.

3,3'-dimethyl-5,5'-dithieno [3,2-*b*]thien-2-yl-2,2'-bithiophene 21

Table 2.11, entry 4, yield 65%; orange-red solid, mp 182-186°C. The crude product was washed with petroleum ether and diethyl ether and finally CH$_2$Cl$_2$. δ_H(400 MHz, CDCl$_3$, Me$_4$Si) 7.36 (2H, d, *J* 5.6), 7.34 (2H, d, *J$_5$* 0,8), 7.23 (2H, dd, *J$_3$* 5.2, *J$_5$* 0,4), 7.06 (2H, s), 2.24 (6H, s). δ_C(100 MHz, CDCl$_3$, Me$_4$Si) 139.77, 138.88, 138.06, 137.52, 137.00, 128.40, 127.12, 126.91, 119.46, 115.65; m/z 470.

2.5 References

[1] F. Babudri, G. M. Farinosa, F. Naso, *J . Mater. Chem.* **2004**, *14*, 11-34.

[2] (a) M. Melucci, G. Barbarella, G. Sotgiu, *J. Org. Chem.* **2002**, *67*, 8877-8884. (b) M. Melucci, G. Barbarella, M. Zambianchi, P. Di Pietro, A. Bongini, *J. Org. Chem.* **2004**, *69*, 4821-4828.

[3] (a) "Fine chemicals through heterogeneous catalysis" Eds. R.A. Sheldon and H. van Bekkum, Wiley VCH, **2001**; (b) R. B. Bedford, U. G. Singh, R. I. Walton, R. T. Williams, S. A. Davis, *Chem. Mater.* **2005**, *17*, 701 -707; (c) J. Ku Cho, R. Najman, T. W. Dean, O. Ichihara, C. Muller, M. Bradley, *J. Am. Chem. Soc.* **2006**, *128*, 6276–6277; (d) J. Y. Shin, B. S. Lee, Y. Jung, S. J. Kim, S-g. Lee, *Chem. Commun.* **2007**, 5238–5240; (e) H. Oyamada, T. Naito, S. Miyamoto, R. Akiyama, H. Hagio, S. Kobayashi, *Org. Biomol. Chem.* **2008**, *6*, 61-65. (f) Q. Xu, W. Hao, M. Cai, *Catal. Lett.* **2007** *118*, 98-102.

[4] L. Yin and J. Liebscher, *Chem. Rev.* **2007**, *107*, 133-173.

[5] G. Marck, A. Villiger, R. Buchecker, *Tetrahedron Lett.* **1994**, *35*, 3277.

[6] F-X. Felpin, T. Ayad, S. Mitra, Eur. *J. Org. Chem.* **2006**, 2679-2690.

[7] B. M. L. Dioos, I. F. J. Vankelecom, P. A. Jacobs, *Adv. Synth. Catal.* **2006**, *348*, 1413-1446.

[8] D. J. Macquarrie, J. J. E. Hardy, *Ind. Eng. Chem. Res.* **2005**, *44*, 8499-8520.

[9] (a) M. J. Gronnow, R. Luque, D. J. Macquarrie, J. H. Clark, *Green Chem.* **2005**, *7*, 552-557; (b) V.L. Budarin, J.H. Clark, R. Luque, D.J. Macquarrie, R.J. White, *Green Chem.* **2008**, DOI: 10.1039/b715508e.

[10] (a) E. B. Mubofu, J. H. Clark, D. J. Macquarrie, *Green Chem.* **2001**, *3*, 23-25. (b) S. Paul, J. H. Clark, *Green Chem.* **2003**, *5*, 635–638.(c) J. J. E. Hardy, S. Hubert, D. J. Macquarrie, A. J. Wilson, *Green Chem.* **2004**, *6*, 53-56.

[11] Other less strong bases, generally used under heterogeneous conditions such as Na_2CO_3, K_2CO_3, Cs_2CO_3, K_3PO_4 were uneffective.

[12] H. E. B. Lempers, R. A. Sheldon, *J. Catal.* **1998**, *175*, 62.

[13] B. J. J. Smeets, R. H. Meijer, J. Meuldijk, J. A. J. M. Vekemans and L. A. Hulshof, *Organic Process Research & Development* **2003**, *7*, 10-16.

[14] H. E. Katz, J. G. Laquindanum, A. Lovinger, *Chem. Mater.* **1998**, *10*, 633-638.

[15] C. D. Dimitrakopoulos, P. R. L. Malenfant, *Adv. Mater.* **2002**, *14*, 99-117.

[16] K. R. Amundson, H. E. Katz, A. J. Lovinger, *Thin Solid Films* **2003**, *426*, 140–149.

[17] G. Sotgiu, M. Zambianchi, G. Barbarella, C. Botta, *Tetrahedron* **2002**, *58*, 2245-2251.

[18] M. Melucci, M. Gazzano, G. Barbarella, M. Cavallini, F. Biscarini, P. Maccagnani, P. Ostoja, *J. Am. Chem. Soc.* **2003**, *125*, 10266-10274.

[19] G. Barbarella, M. Zambianchi, L. Antolini, P. Ostoja, P. Maccagnani, A. Bongini, E. A. Marseglia, E. Tedesco, G. Gigli, R. Cingolani, *J. Am. Chem. Soc.* **1999**, *121,* 8920-8926.

[20] (a) Y. Zhu, R. D Champion, S. A. Jenekhe, *Macromol.* **2006**, *39*, 8712-8719. (b) R. D. Champion, K-F. Cheng, C-L. Pai, W-C. Chen, S. A. Jenekhe, *Macromol. Rapid Commun.* **2005**, *26*, 1835–1840.

[21] (a) H-S. Kim, Y-H. Kim, T-H. Kim, Y-Y. Noh, S. Pyo, M. H. Yi, D-Y. Kim and S-K. Kwon, *Chem. Mater.* **2007**, *19,* 3561-3567.(b) M. Medina, A. Van Vooren, P. Brocorens, J. Gierschner, M. Shkunov, M. Heeney, I. McCulloch, R. Lazzaroni, J. Cornil, *Chem. Mater.* **2007**, *19*, 4949-4956. (c) H. Ebata, T. Izawa, E. Miyazaki, K. Takimiya, M Ikeda,H. Kuwabara, T. Yui *J. Am. Chem. Soc.* **2007**, *129*, 15732-15733.

[22] E. Bundgaard, F. C. Krebs, *Macromolecules* **2006**, *39*, 2823-2831.

[23] To a stirred solution of thienothiophene[22] (200 mg, 1.4 mmol) in fresh distilled THF (16 mL) was added 2.5 M *n*-BuLi in hexane (0.56 mL ,1.44 mmol, 1.01 eq) dropwise at -78 °C under nitrogen atmosphere. After 1.5 h, 0.36 mL (1.82 mmol, 1.3 eq) of 2-isopropoxy-4,4,5,5-tetramethyl-1,3,2-dioxaborolane was added by syringe and the reaction allowed to warm to room temperature. After 12 h of stirring the mixture was

poured into water and extracted with diethyl ether. The organic phase was washed with brine and dried over Na_2SO_4. The resulting crude product was obtained as a pale yellow oil (317 mg, yield 85%). δ_H(400 MHz, $CDCl_3$, Me_4Si) 7.76 (1H, d, J_5 0.8), 7.48 (1H, d, *J* 5.6), 7.28 (1H, d, J_5 0.8, J_3 5.6) , 1.36 (12 H, s); *m/z* 266.

[24] L. S. Fuller, B. Iddon, K. A. Smith, *J. Chem. Soc., Perkin Trans.* **1997**, *1*, 3465-3470.

[25] G. Sotgiu, M. Zambianchi, G. Barbarella, C. Botta, *Tetrahedron* **2002**, *58*, 2245-2251.

[26] F. Garnier, A. Yassar, R. Hajlaoui, G. Horowitz, F. Deloffre, B. Servet, S. Ries, P. Alnot, *J. Am. Chem. Soc.* **1993**, *115*, 8716–8721.

[27] Q. Hou, Y. Xu, W. Yang, M. Yuan, J. Peng, Y. Cao, *J. Mater. Chem.* **2002**, *12*, 2887-2892.

Chapter 3

Synthesis of oligothiophene-oligonucleotide hybrids

Abstract

In this chapter the synthesis of the different oligothiophene-oligonucleotide hybrid derivatives is reported.

3.1 Introduction

To prepare covalently linked thiophene-oligonucleotide biohybrid compounds, the synthesis of appropriately functionalized oligothiophene components has been developed, when possible, with the new heterogeneous methodologies reported in Chapter 2

Biohybrids with short oligonucleotide sequences were prepared applying the methodologies of the solution syntesis of oligonucleotides. In particular we found that the reagent 2-chlorophenyl-O,O-bis(l-benzotriazolyl)phosphate, previously used by Van Boom's group for the formation of 3'-5'-internucleotide phosphotriester linkages[1] can be use to phosphorylate a protected dinucleotide to give an intermediate still able to couple with the hydroxyl group of a suitable thiophene derivative. Following this synthetic methodology we prepared quaterthiophene-dinucleotide hybrid compounds as well as quinquethiophene-dinucleotide derivatives.

Longer oligonucleotide sequences, containing 5'-thiophene labelled deoxyuridine were prepared applying the protocols of the solid phase synthesis through the preparation of a deoxyuridine amidite. This task was accomplished by firstly preparing the 5'-labelled-thiophene uridine, then preparing the required amidite using either the the 2-cyanoethyl-*N,N*-diisopropylchlorophosphoramidite or the 2-cyanoethy *N,N,N',N'*-tetraisopropylphosphorodiamidite, as phosphytilating agents, the latter allowing a direct use in the automatic synthesizer without isolation.

3.2 Synthesis of quaterthiophene-dinucleotide hybrids

Conjugates $^{5'}$TA$^{3'}$-t4-$^{3'}$AT$^{5'}$ (**29a**), $^{5'}$CG$^{3'}$-t4-$^{3'}$GC$^{5'}$ (**29b**), $^{5'}$AA$^{3'}$-t4-$^{3'}$AA$^{5'}$ (**29c**) and $^{5'}$TT$^{3'}$-t4-$^{3'}$TT$^{5'}$ (**29d**) were prepared following the synthetic pattern shown in Scheme 3.1, taking advantage of microwave assistance in steps a) and b) for the preparation of the parent quaterthiophene.[2] Quaterthiophene **24a** with protected alcoholic groups was obtained in 87% yield in 5 minutes by solvent-free, microwave-assisted, coupling of the diiododerivative 2 with the boronic ester 1, using PdCl$_2$(dppf)/KF Al$_2$O$_3$/KOH 10% as catalytic system. Moreover, it was possible to prepare it, starting from the same building blocks, by using the heterogenous methodology presented in Chapter 2. In fact, the use of CHITCAT as the catalyst and EtOH/H$_2$O as the solvent provided, after 100 min of microwave irradiation, the desired compound **24a** in 78% of yield. After deprotection under microwave activation, the oligomer was reacted with an excess of 5'-protected (4,4'-dimethoxytrityl)-deoxy-dinucleotides **25a-d**, previously phosphorylated with 2-chlorophenyl-*O*, *O*-bis-[1-benzotriazolyl]-phosphate in pyridine as the solvent. After removal of the 5'-dimethoxytrityl group with benzenesulphonic acid, the detritylated compound was treated with N^1,N^1,N^3,N^3-tetramethylguanidine and *syn*-pyridine-2-carboaldoxime, and then with aqueous ammonia. The targeted **29a-d** were obtained from the crude mixture after reversed-phase chromatography and characterized by mass spectroscopy, ^{1}H and ^{31}P NMR. Their UV-Vis, CD and Pl spectra as well as the electrical characterization, the molecular modelling and the solid-state aggregation modalities studies, through optical, fluorescence and atomic force microscopy are reported in Chapter 5.
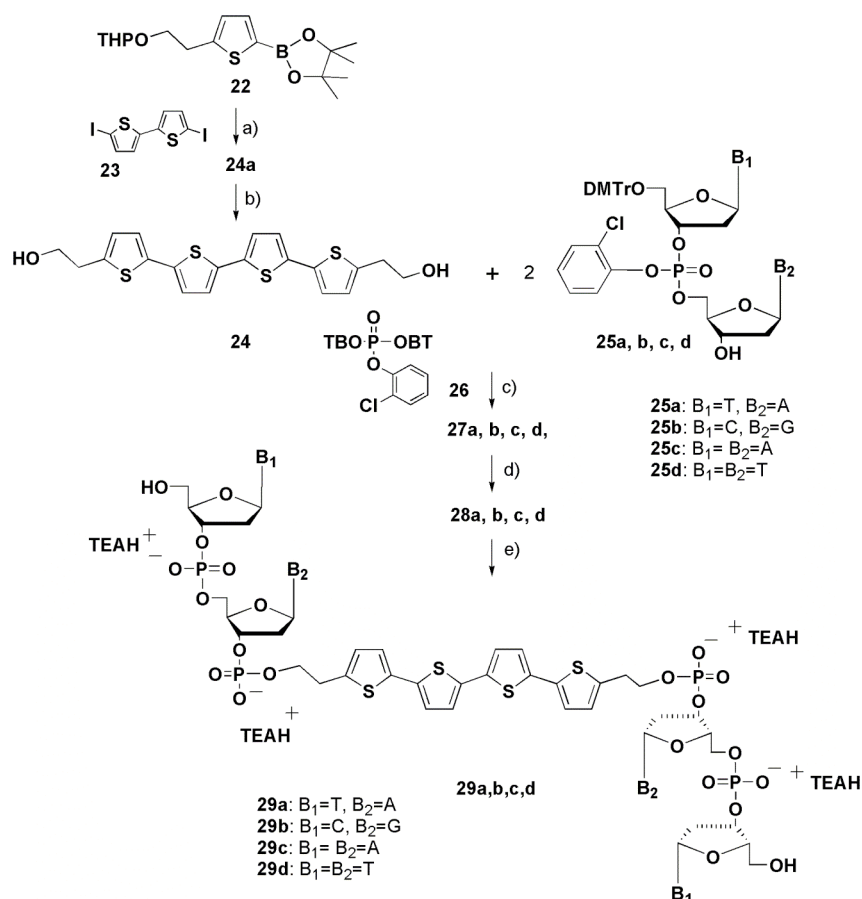
Scheme 3.1 *a) KF, PdCl$_2$(dppf), Al$_2$O$_3$/KOH 10%, MW 5 min. b) HCl 0.2N, THF, MW, 5 min. c) 26, py, 2h, RT. d) benzenesulfonic acid, MeOH/CH$_2$Cl$_2$, 0.5h, RT. e) py, 16h, RT; NH$_3$ 30%, 24 h, 50°C. THP = tetrahydropyran, DMTr = 4, 4'-dimethoxytrityl, BT = benzotriazolyl, TEA= triethylamine.*

3.3 Synthesis of quinquethiophene-dinucleotide hybrids

In the same way, conjugates $^{5'}$TA$^{3'}$-t5 (**36a**) and $^{5'}$CG$^{3'}$-t5 (**36b**) were prepared starting from quinquethiophene **32**, obtained in 55% yield by Stille coupling of the 2,5-dibromo-3-thiopheneethanol **30** with the 5-tributylstannyl-2,2'-bithiophene **31**, using Pd(Ph$_3$)$_4$ as catalyst. The oligomer **32** was then reacted with an excess of 5'-protected (4,4'-dimethoxytrityl)-deoxy-dinucleotides **33a, b** previously phosphorylated. After removal of the protecting groups the targets **36a, b** were obtained from the crude mixture by reversed-phase chromatography. Both compounds were characterized by mass spectroscopy, ^{1}H and ^{31}P NMR. While for compound **36b**, scarcely soluble in both

water and organic solvents only UV-Vis and Pl spectra were recorded, product **36a** was studied, as in the case of quaterthiophene biohybrid derivatives, through UV-Vis, CD and Pl spectroscopy, optical, fluorescence and atomic force microscopy, molecular modelling and a two electrodes device, for the electrical characterization. Moreover, a detailed study of its aggregation modalities, through microfluidic techniques is reported in Chapter 6.
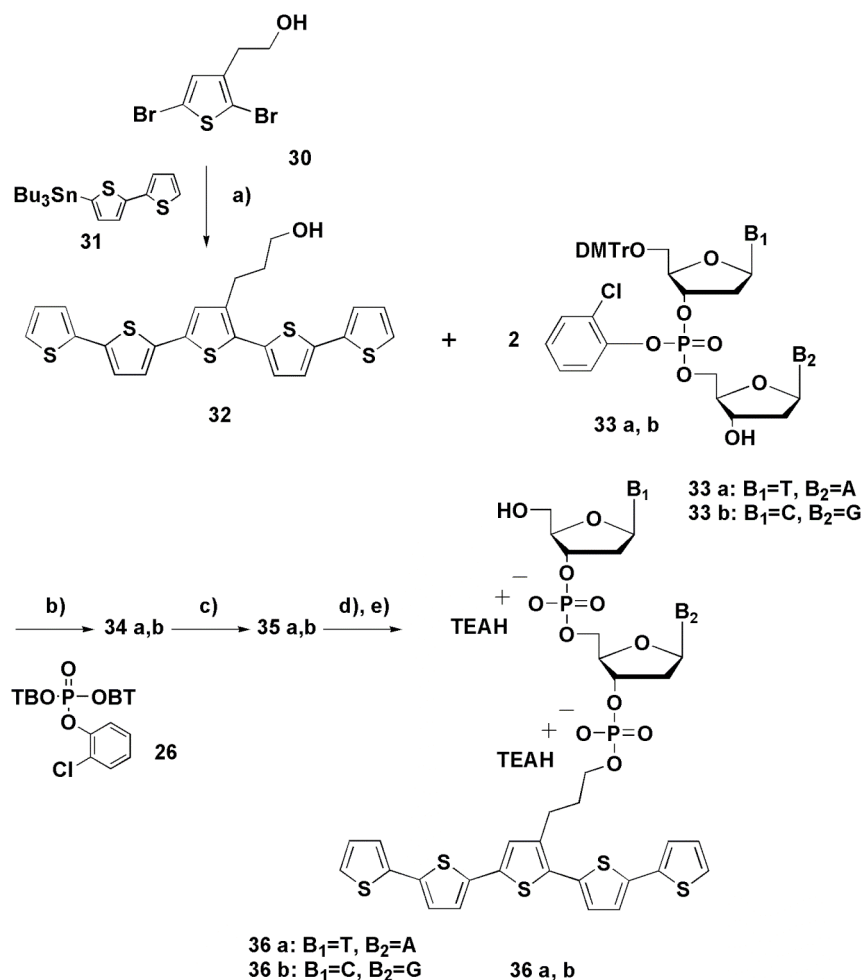
Scheme 3.2 *a)Pd(Ph₃)₄, toluene, reflux, overnight. b) 26, py, 2h, RT. c) benzenesulfonic acid, MeOH/CH₂Cl₂, 0.5h, RT. d) py, 16h, RT; e) NH₃ 30%, 24 h, 50°C. DMTr = 4, 4'-dimethoxytrityl, BT = benzotriazolyl, TEA= triethylamine.*

3.4 Synthesis of modified uridines

Oligothiophene-5-labeled deoxyuridines **42, 49, 52a** and **52b** were prepared from the corresponding 5'-dimethoxytrityl of 5-iodouridine[3] applying Sonogashira's or Stille's coupling. The compounds were then converted to phosphoramidites using the 2-cyanoethyl-*N,N*-diisopropylchlorophosphoramidite or the 2-cyanoethy *N,N,N',N'*-tetraisopropylphosphorodiamidite.
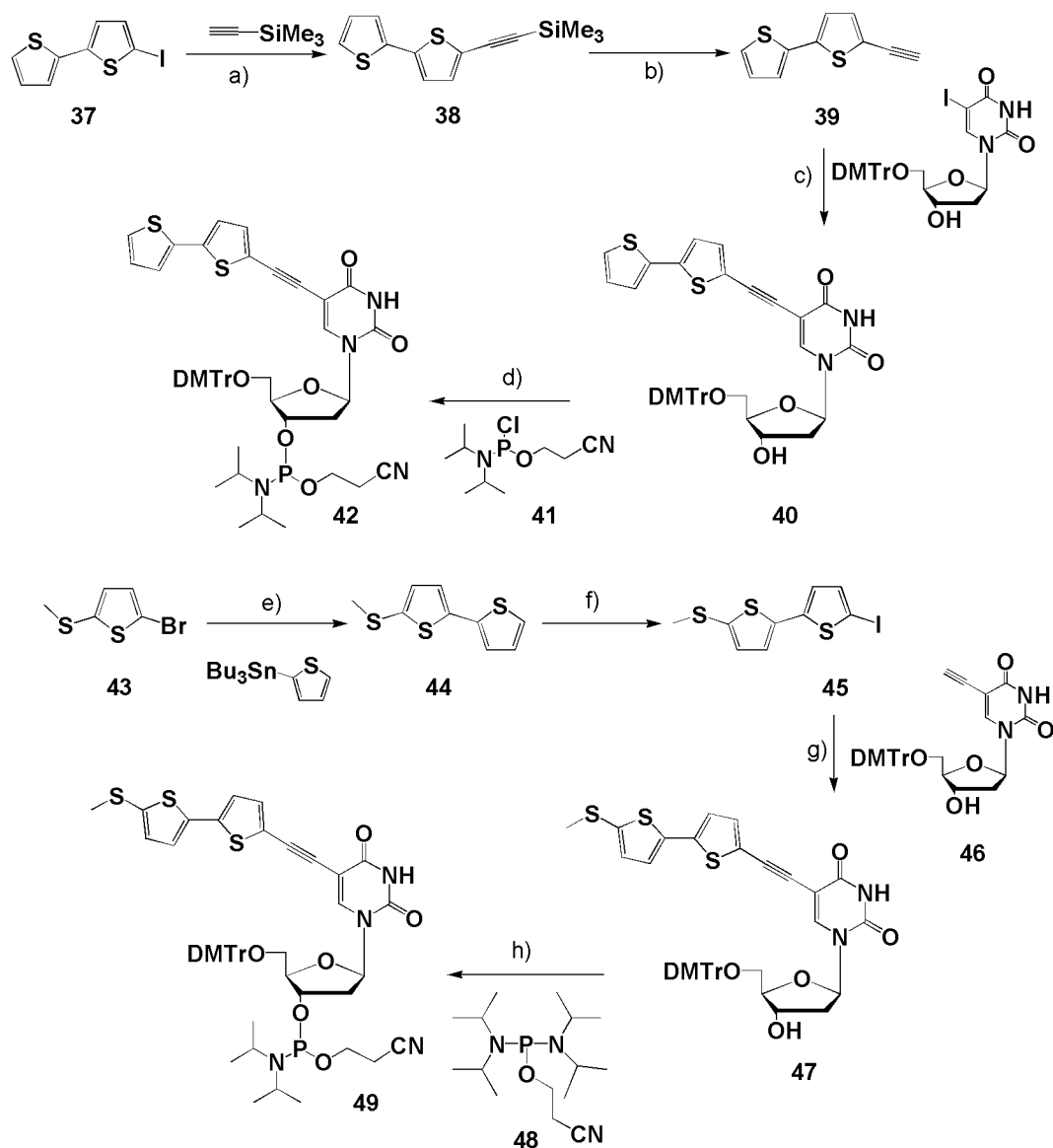
Scheme 3.3. *Synthesis of 5-alkinyl-oligothiophene-deoxyuridine phosphoramidites. a) trimethylsilyl acetylene, Pd(PPh₃)₄, CuI, Et₃N in DMF, 20 min microwave irradiation, (79% yield); b) K₂CO₃ in 8/2 hexane/MeOH, 2 h rT, (74% yield); c) Pd(PPh₃)₄, CuI,*

*Et$_3$N in DMF, 3 h rT, (60% yield), d) DIPEA in CH$_2$Cl$_2$, 30 min rT (76% yield); e) Pd(PPh$_3$)$_4$ in toluene, 45 min microwave irradiation, (70% yield), f) NIS dropwise in 1:1 CH$_2$Cl$_2$/AcOH at –15 °C then 2 h at rT (74% yield); g) Pd(PPh$_3$)$_4$,CuI, Et$_3$N in DMF, 3 h rT, (66% yield); the synthesis and characterization of 5-(ethynyl)-2'-deoxy-5'-O-(4,4'-dimethoxytrityl)uridine **46** employed were reported elsewere[4]. h) 1/1 CH$_2$Cl$_2$/CH$_3$CN, tetrazole, 45 min rT, (yield > 90% on TLC, compound not isolated).*

Compound **40** was obtained via Sonogashira's coupling of the ethynyl-bithiophene **39** with the dimethoxytritylated-iodouridine[3], the S-Me analogue **47** was prepared with the same methodology but a reverse strategy, in which the ethynyl moiety was previously linked to the uridine nucleoside, to allow an easier purification step. Furthermore compound **47** available in a limited amount (80 mg left after analysis) was phosphitylated by using 1 eq of 2-cyanoethyl *N,N,N',N'*-tetraisopropyl-phosphorodiamidite and 1 eq. of tetrazole. This gave, after the filtration of the diisopropylammonium tetrazolide, a concentrated solution that was diluted with CH$_3$CN to a formal concentration of 0.1 M and immediately used for the automated synthesis of the probe P2, Chapter 4. This procedure[5] allowed us to carry out the synthesis of the probe without risk any loss of the amidite **49** (due to hydrolysis or manipulation) in the purification steps.
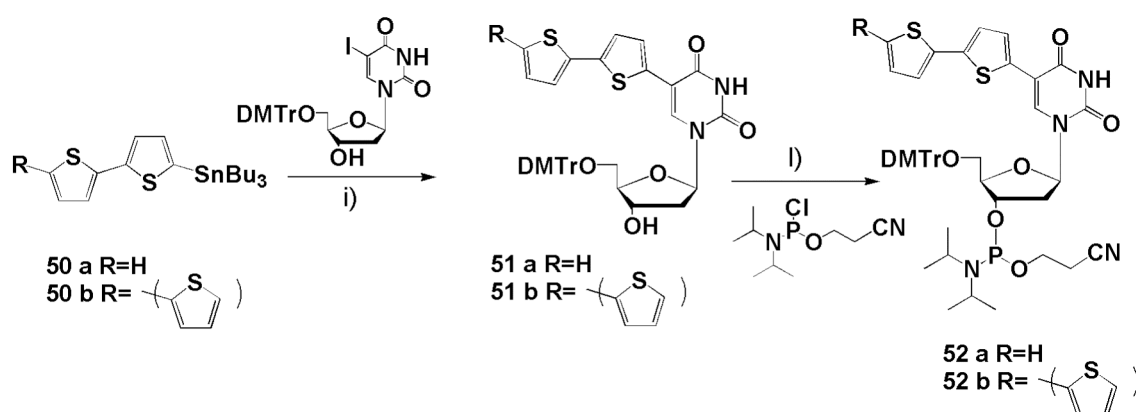
Scheme 3.4 *Synthesis of 5-oligothiophene-deoxyuridine phosphoramidites i) Pd(PPh$_3$)$_2$Cl$_2$ in dioxane, 4 h 95°C, (yields: **50a** 97%, **50b** 40%); l) [(**52a** 2-cyanoethyl-chloro-diisopropylaminophosphoramidite, DIPEA in THF, 30 min rT, 80% yield). (**52b.** 2-cyanoethyl N,N,N',N'-tetraisopropylphosphorodiamidite, tetrazole in 1/1 CH$_2$Cl$_2$/CH$_3$CN, 45 min rT, yield >90 % on TLC, compound not isolated)].*

Compounds **51a** and **51b** were obtained using the Stille's procedure from dimethoxytrityl-iodouridine and tributhylstannyl derivative of the bis or ter-thiophene **50a** and **50b**. The coupling gave an almost quantitative yield in case of the bithiophene derivative **51a**, but a moderate yield in case of the compound **51b** due probably to a lower reactivity of the larger oligothiophene and to severe loss during the chromatographic purification step. Again with this compound, the phosporoamidite **52b** was obtained by use of 2-cyanoethyl *N, N, N', N'*-tetraisopropylphosphorodiamidite without isolation step. In order to study the fluorescence properties of oligothiophenes as markers for proteins and oligonucleotides[6] and to explore their use as diagnostic tools in biotechnologies,[7] we inserted the four deoxyuridine derivatives synthesized, (Scheme 3.5), at the centre of an oligonucleotide probe (P1-4, Scheme 3.6).
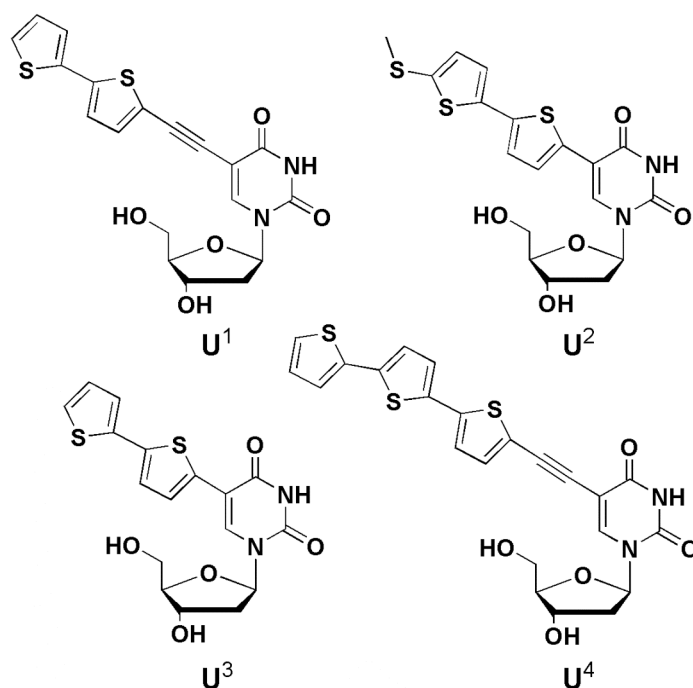
Scheme 3.5 *Structure of the 5-oligothiophene modified deoxyuridines synthesized*

These probes were designed to hybridize with model oligonucleotides corresponding to a region known to contain a SNP (A to G transition), that occurs in some patients that present a mutated form of hemoglobin. For this purpose, the probes (P1-4), the normal

(A) and the three mutated targets containing (G, C and T) mismatches (Scheme 3.6) were prepared and purified.

P1-4 $^{3'}$ AC TGA GGA $\underline{U}$TC CTC TTC A $^{5'}$

Target-A $^{5'}$ TG ACT CCT $\underline{A}$AG GAG AAG T $^{3'}$
Target-G $^{5'}$ TG ACT CCT $\underline{G}$AG GAG AAG T $^{3'}$
Target-C $^{5'}$ TG ACT CCT $\underline{C}$AG GAG AAG T $^{3'}$
Target-T $^{5'}$ TG ACT CCT $\underline{T}$AG GAG AAG T $^{3'}$
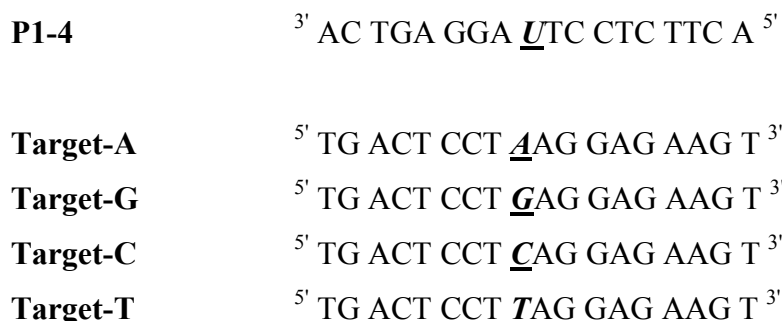
Scheme 3.6 *Oligonucleotide probes (P1-4) and targets (Target-A,-G, -C, -T) used in this work. $\underline{U}$ = modified uridine (compounds $\underline{U}^{1-4}$ as in Scheme 3.5). Triplets correspond to reading codons.*

All the probes were synthesized on a Pharmacia Gene Assembler 2 (see scheme 3.7), repeating two times the coupling step for the modified uridine, without the intervening capping, with a 2 min longer than usual coupling time, on a 1.3 μmol scale. With these precautions we didn't notice any lowering of efficiency of the coupling steps. The oligonucleotide targets (A, C, G, T) were prepared on the same synthesis scale using commercial reagents. All the oligonucleotides, were deblocked by treatment with 30% aqueous ammonia at 50 °C for 16 h, then lyophilized. The targets were purified by precipitation with n-BuOH and judged sufficiently pure by reversed phase HPLC analysis at 260 nm (80-85%). The probes were purified by reversed phase HPLC using a double detection: UV at 260 nm and fluorescence at the maximum of emission of every derivative. Final compounds were judged more than 90% pure by UV and more than 95% pure by fluorescence. The identity of the probes was determined by a careful analysis of the UV-vis spectra (giving the expected ratio UV/vis) and from ESI-MS analysis.
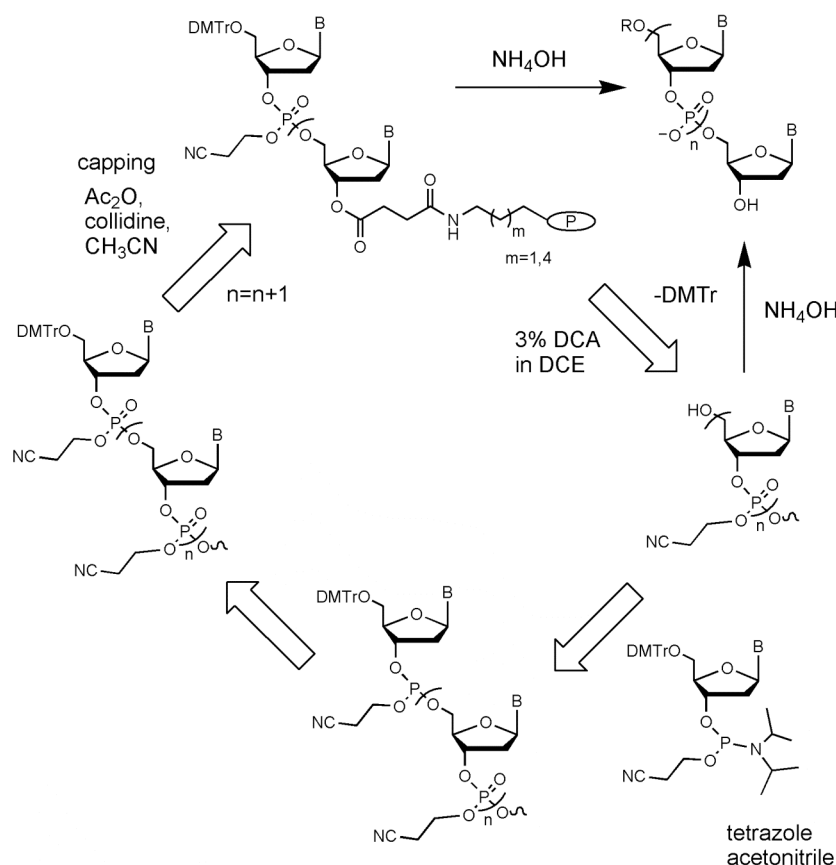
Scheme 3.7 *Synthetic mechanism for the preparations of probes and targets, by using a Pharmacia Gene Assembler 2.*

3.5 Experimental section

Materials. All chemicals were of commercial grade unless otherwise stated. Microwave reactions were performed with a Prolabo synthwave 402 oven. The synthesis of the 19-mer oligonucleotides was achieved with a Pharmacia Gene Assembler 2. NMR analysis were carried out with a Varian VXR-200 or a Varian Mercury 400 spectrophotometer. Mass analysis were performed with a Finningan Mat GCQ or in ESI mode with a Bruker Esquire 3000+. HPLC analysis of the probes P1-4 and purifications were done with a Waters 600 E, using a Waters UV detector and a Varian Pro Star 363 spectrofluorimeter. Experimental Section

2-(2-Thienyl)ethanol, 3,4-Dihydro-2*H*-pyran, p-Toluensulfonic acid, 2,2 diiodo-bithiophene (**23**), 2-Isopropoxy-4,4,5,5-tetramethyl-1,3,2-dioxaborolane, n-Butyllithium (2.5 M in hexane), [1,1'-Bis(diphenylphosphino)-ferrocene]dichloropalladium, 3-

thiopheneethanol, Pd(Ph$_3$)$_4$, 2-tributylstannylthiophene, ethynyltrimethylsilane, tetrakis(triphenylphosphine)palladium, 5-iodo-2'-deoxyuridine, 2-thiomethylthiophene, 2-cyanoethyl-*N,N*-diisopropylchlorophosphoramidite, 2-cyanoethyl *N,N,N',N'*-tetraisopropylphosphorodiamidite were commercial products. The synthesis of compounds, **25a**, **25b**, **25c**, **25d**,[8] **26**,[1] and **33a,b**[8] has been reported elsewhere.

Abbreviations. NBS = *N*-bromosuccinimide; NIS = *N*-iodosuccinimide; TLC thin layer chromatography; R$_H$ - R$_L$ = higher running - lower running isomer; rT = room temperature; sat = saturated; TEA = triethylamine.

2-[2-(Tetrahydropyranyloxy)ethyl]thiophenyl-5-yl-4,4,5,5-tetramethyl-[1,3,2]dioxaborolane 22.

This compound was prepared by using standard procedures,[3c] starting from 2-[2-(Tetrahydropyranyloxy)ethyl]thiophene[9] (386 mg, 1.84 mmol). Compound **22** was obtained as a brown oil (578 mg, 93% yield) and used without further purification.

^{1}H NMR (400 MHz, CDCl$_3$, 25°C, TMS):δ = 7.4635 (d, $_3J$ (H,H)=3.6 Hz, 1H), 6.928 (d, $_3J$ (H,H)=3.6 Hz, 1H), 4.611 (t, $_3J$ (H,H)=3.2 Hz 1H), 4.013-3.93 (m, 1H), 3.81-3.91 (m, 1H), 3.70-3.58 (m, 1H), 3.53-3.45 (m, 1H), 3.15 (t, $_3J$ (H,H)=6.4 Hz ,2H), 1.85 (m, 1H), 1.73(m, 1H), 1.55(m, 4H) 1.32 (s, 12H). MS (m/z): 85, 210, 236, 323, 338.

5,2'''-Di[2-(Tetrahydropyranyloxy)ethyl]-2,2':5',2'':5'':2'''-quaterthiophene, 24a.

The microwave oven reactor was charged with **23** (50 mg, 0.12 mmol), **22** (200 mg , 5 eq., 0.6 mmol), Pd(dppf)Cl$_2$ (8 mg, 0.08 eq., 0.01 mmol), KF (112 mg ,16 eq., 1,92 mmol), basic alumina (240 mg) and few drops of a solution of KOH (10%). The mixture was stirred to homogenize the reagents. After 5 min of irradiation at T$_{max}$= 80°C at a fixed power, the reaction solid crude was purified by chromatography on silica gel using Et$_2$O/CH$_2$Cl$_2$/petroleum ether (1:3:6) as eluent. **24a** was isolated as a deep yellow powder in 87% of yield. Mp/ 142°C. ^{1}H NMR (400 MHz, [D$_6$] DMSO, 25°C, TMS):δ= 7.03 (d, $_3J$ (H,H)=4 Hz, 2H), 7.00-6.98 (m, 4H), 6.76 (d, $_3J$ (H,H)=3.2 Hz, 2H), 4.65 (t, $_3J$ (H,H)=3.2 Hz, 2H), 3.97 (m, 2H), 3.83 (m, 2H), 3.63 (m, 2H), 3.50 (m, 2H), 3.09 (t, $_3J$ (H,H)=6.4 Hz, 4H), 1.85 (m, 2H), 1.74 (m, 2H.), 1.59 (m, 4H.). ^{13}C NMR (100 MHz, [D$_6$] DMSO, 25°C, TMS):δ= 141.5, 136.9, 135.7, 135.6, 126.3, 124.3, 124.0, 123.6, 99.1, 67.9, 62.4, 31.1, 31.0, 30.9, 25.7, 19.6. MS (m/z): 586 [*M*$^+$].

5, 2'''-Di(2-hydroxyethyl)-2,2':5',2'':5'':2'''-quaterthiophene 24. To a THF solution of **3a** (50 mg/2mL, 0.085 mmol) was added HCl 0.2 M (0.5 mL). The mixture was

irradiated at 55°C under fixed power and the reaction was followed by TLC on silica gel using THF/CH$_2$Cl$_2$/ 2:8 as eluent. After 5 min. of irradiation the solvent was evaporated and the solid residue washed with saturated NaHCO$_3$ (2x5 mL) and H$_2$O (2x5 mL) then, chromatographed on silica in the same condition used for TLC. ^{1}H-NMR on the isolated powder (31 mg) showed the presence of large amounts of hydroquinone (THF stabilizer) and several washing with Et$_2$O were required in order to achieve **24** in high purity and in 50% of yield. Mp/ 210 °C. ^{1}H NMR (200 MHz, [D$_6$] DMSO, 25°C, TMS):δ= 7.24 (d, $_3J$ (H,H)=3.8 Hz, 2H), 7.167 (d, $_3J$ (H,H)=3.6 Hz, 2H), 7.136 (d, $_3J$ (H,H)=3.8 Hz 4H), 6.832 (d, $_3J$ (H,H)=3.4 Hz, 2H), 4.87 (bs, 2H), 3.61 (t, $_3J$ (H,H)=6.2 Hz, 2H), 2.90 (t, $_3J$ (H,H)=6.0 Hz, 2H). ^{13}C NMR (50 MHz, [D$_6$] DMSO, 25°C, TMS):δ= 142.3, 136.1, 134.4, 134.0, 125.4, 124.9, 124.2, 123.2, 61.8, 33.4. MS (m/z) 418 [M^+].

General procedure for sinthesys of α,ω-(bis-fully protected-dinucleotide))-quaterthiophene, 27a, b, c, d.

Dinucleotides **25** (0.29 mmol, 2.4 eq.) and quaterthiophene **24** (50 mg, 1 eq., 0.119 mmol) were dissolved in anhydrous pyridine and evaporated to dryness in order to remove any traces of water immediately before being used. Then dinucleotides **25** were dissolved in of anhydrous pyridine (1mL) and a 0.2 M solution of **26** in dioxane (1.6 mL, 0.3 mmol, 2.6 eq.) was added. After 15 min. at RT, TLC of the mixture showed the complete conversion of dinucleotide into the corresponding phosphorylated intermediates. Then, quaterthiophene **24** (50 mg), dissolved in anhydrous pyridine (0.5 mL), was added and the mixture was stirred at RT. After 2h, TLC (SiO$_2$, CH$_2$Cl$_2$/MeOH (95:5)) showed the absence of starting materials. The mixture was diluted with CH$_2$Cl$_2$ and washed with NaHCO$_3$ (saturated solution, 15 mL), citric acid (saturated solution, 15 mL) and water (15 mL), then the organic phase was dried over Na$_2$SO$_4$ and the solvent removed.

The crude products were purified by flash chromatography (eluant: CH$_2$Cl$_2$/MeOH 98:2-90:10) .(Isolated yield : 47-65%).

General procedure for sinthesys of α,ω-(bis(protected-dinucleotide))-quaterthiophene, 28 a, b, c, d.

The 5'-dimethoxytrityl protecting group was removed by treating **27a, b, c, d** with a solution (5 mL) of benzenesulfonic acid (2% by weight) in CH$_2$Cl$_2$/MeOH (7:3) at 0° C

for 30 min. The reaction was quenched by adding NaHCO$_3$ (saturated solution, 15 mL). The organic layer was separated and then washed with water, dried over Na$_2$SO$_4$ and evaporated. After flash chromatography eluant: CH$_2$Cl$_2$/MeOH 98:2-90:10), the detritylated compounds **28a, b, c, d** was isolated as a brown solid in 60-97% of yield.

General procedure for synthesis of α,ω-(bis(-dinucleotide)-quaterthiophenes 29 a, b, c, d.

28a, 28b, 28c or 28d were dissolved in dry pyridine (3 mL), and treated with N^1,N^1,N^3,N^3-tetramethylguanidine (0.6 mL), *syn*-pyridine-2-carboxaldoxime (730 mg), for 16 h at room temperature. The mixture was then added with 30% aqueous ammonia (10 mL) and kept sealed at 50 °C for 24 h. The crude products thus obtained were purified by reversed phase chromatography on a column of C-18 eluting with a linear gradient of triethyl ammonium acetate (TEAA) 0.1 M in H$_2$O from 0 to 80% of CH$_3$CN (300 mL). **29a-d** as brown solids were isolated after lyophilization in 67-83% of yield. **29a** ESI-MS: MW found 1651.7 (Calc.d 1652.2); **29b** ESI-MS found = 1653.5 [M-H]$^-$. Calc PM=1654.2 **29c** ESI-MS: MW found 1669.3 (Calc.d 1670.0); **29d** ESI-MS: MW found 1633.4 (Calc.d 1634.0)

5, 2'' (2-hydroxyethyl)-2,2':5',2'':5''',2''''':5''''',2'''''-quinquethiophene 32.

To a solution of 2,5-dibromo-3-thiopheneethanol (2.0 g, 6.99 mmol) in toluene (300 mL) were added 0.1 eq. (0.69 mmol) of Pd(Ph$_3$)$_4$ and 5-tributylstannyl-2,2'-bithiophene. The mixture was refluxed overnight. The solvent was removed by rotary evaporation and the remaining residue was purified by flash chromatography (petroleum Et$_2$O(30-40)/AcOEt 1:1) to provide 1.932 g (55% yield) as a crystalline orange solid.

mp: 109°C. (MS (m/z): 456 [M$^+$]. ^{1}H NMR 400 MHz (CDCl$_3$) δ 7.25-7.22 (m, 2H), 7.20-7.18 (m, 2H), 7.14-7,13 (d, 1H, J_2= 4 Hz), 7.10-7.07 (m, 4H), 7.05-7.02 (m, 2H).

^{13}C NMR 100 MHz (DMSO-d_6) δ 137.6, 137.0, 136.9, 136.5, 136.0, 135.5, 134.1, 131.1, 130.2, 128.0, 127.0, 126.5, 124.7, 124.6, 124.4, 124.1, 123.9, 123.8, 62.7, 32.6

General procedure for sinthesys of (fully protected dinucleotide)-quinquethiophene, 34 a,b.

Dinucleotides **33a,b** (0.0528 mmol, 1.2 eq.) and quinquethiophene **32** (20 mg, 1 eq., 0.044 mmol), were dissolved in anhydrous pyridine and evaporated to dryness in order to remove any traces of water immediately before being used. Dinucleotides **33a,b** were dissolved in 0.5 mL of anhydrous pyridine and a 0.2 M solution of **26** in dioxane (286

µl, 0.0572 mmol, 1.3 eq.) was added. After 10 min. at RT, TLC of the mixture showed the complete conversion of dinucleotide into the corresponding phosphorylated intermediates. Then, 20 mg of quinquethiophene **32** dissolved in 0.5 mL of anhydrous pyridine were added and the mixture was stirred at RT. After 1h, TLC (SiO$_2$, CH$_2$Cl$_2$/MeOH (95:5)) showed the absence of starting materials. The mixture was diluted with CH$_2$Cl$_2$ and washed with NaHCO$_3$ saturated solution (10 mL), citric acid (saturated solution, 10 mL) and water (10 mL), then the organic phase was dried over Na$_2$SO$_4$ and the solvent removed. The crude products were purified by flash chromatography (eluant: CH$_2$Cl$_2$/MeOH 90:10) .(Isolated yield: 96%- 74%).

General procedure for sinthesys of (protected-dinucleotide)-quinquethiophene, 35 a,b.

The 5'-dimethoxytrityl protecting group was removed by treating **34a**, **b** with a solution (2 mL) of benzenesulfonic acid (2% by weight) in CH$_2$Cl$_2$/MeOH (7:3) at 0° C for 30 min. The reaction was quenched by adding NaHCO$_3$ (saturated aqueous solution) 15 mL. The organic layer was separated and then washed with water, dried over Na$_2$SO$_4$ and evaporated. After flash chromatography eluant: CH$_2$Cl$_2$/MeOH 98:2), the detrytilated compounds **15 a**, **b** was isolated as a brown solid in 66-58% of yield.

General procedure for sinthesys of α,ω-(bis(-dinucleotide)-quinquethiophene, 36a, b. 35a, **b** was dissolved in dry pyridine (3 mL), and treated with N^1,N^1,N^3,N^3-tetramethylguanidine (20 eq.), *syn*-pyridine-2-carboxaldoxime (25 eq), for 16 h at room temperature. The mixture was then added with 30% aqueous ammonia (5 mL) and kept sealed at 50 °C for 24 h. The crude products thus obtained were purified by reversed phase chromatography on a column of C-18 eluting with a linear gradient of triethyl ammonium acetate (TEAA) 0.1 M in H$_2$O from 0 to 80% of CH$_3$CN in 300 mL. 8 a, b as brown solids were isolated after lyophilization in 97-78% of yield. **36a** ESI-MS: MW found 1072.04 . (Calc.d 1074.07) **36b** ESI-MS: MW found 1073.6 (Calc.d 1075.07)

36a [13]C(100MHz, DMSO-d_6) δ 164.4, 156.7, 151.2, 149.7, 137.5, 137.4, 137.3, 136.5, 136.4, 136.6, 136.3, 135.1, 134.6, 133.9, 130.5, 129.2, 128.4, 128.1, 126.6, 126.0, 125.7, 125.6, 125.1, 119.6, 110.2, 86.7, 84.3, 75.9, 64.8, 62.0, 58.2, 30.8, 46.2, 12.9.

5-iodo-[2,2']bithiophene (37). The synthesis and characterization of this compound have already been reported.[10]

[2,2']Bithiophenyl-5-ethynyl-trimethylsilane (38). The microwave oven reactor was charged with 5-iodo-[2,2']bithiophene (**37**) (500 mg, 1.7 mmol), ethynyltrimethylsilane (380 µL, 2.7 mmol), tetrakis(triphenylphosphine)palladium (100 mg, 0.085 mmol), CuI (98 mg 0.51 mmol) and TEA (10 mL). After 20 min of irradiation at 150 °C a TLC on silica gel with *n*-hexane as eluent showed the absence of **37**. The mixture was diluted with Et$_2$O (20 mL) of and washed with 4 M aq HCl (15 ml) and water (15 mL), then the organic phase was dried over Na$_2$SO$_4$ and the solvent removed. After chromatography a brown solid was isolated (355 mg, 79% yield).

MS (*m/z*): 262 [M$^+$] (calcd for C$_{13}$H$_{14}$S$_2$Si 262), 247 [M-CH$_3$]$^+$. ^{1}H NMR (CDCl$_3$ 200 MHz) δ 7.24 (d, 2.7 Hz, 1 H), 7.18 (d, 1.8 Hz, 1 H), 7.14 (d, 1.8 Hz 1 H), 7.03-7.01 (dd, 2 Hz, 2 H), 0.29 (s, 9 H). ^{13}C NMR (CDCl$_3$ 50 MHz) δ 138.84, 136.65, 133.42, 127.9, 125.03, 124.23, 123.24, 121.73, 99.90, 97.36, -0.164.

5-Ethynyl-[2,2']bithiophene (39). The 5-trimethylsilyl protecting group was removed from [2,2']bithiophenyl-5-ethynyl-trimethylsilane (**38**) (355 mg, 1.35 mmol) by reacting it with K$_2$CO$_3$ (560 mg 4.05 mmol, 3 eq) in of *n*-hexane/MeOH (8:2) (15 mL) at rT for 2 h. The reaction was quenched by adding water (1 mL), diluted with Et$_2$O (20 mL) and washed with water (2 × 15 mL). The organic layer was dried over Na$_2$SO$_4$ and evaporated. The desilylated compound was isolated as a yellow oil (190 mg, 74% yield) and used in the following step without further purification.

MS (*m/z*): 190 [M$^+$] (calcd for C$_{10}$H$_6$S$_2$ 190). ^{1}H NMR (CDCl$_3$ 400 MHz) δ 7.25 (d, 5.2 Hz, 1 H), 7.19 (d, 3.6 Hz, 1 H), 7.17 (d, 3.6 Hz, 1 H), 7.03-7.01 (m, 2 H), 3.4 (s, 1 H).

5-(5-Ethynyl-[2,2']bithiophenyl)-2'-deoxy-5'-O-(4,4'-dimethoxytrityl)uridine (40). 5-Ethynyl-[2,2']bithiophene (**39**) (200 mg, 2 eq., 1.05 mmol), 5'-O-(4,4')-dimethoxytrityl)-5-iodo-2'-deoxyuridine[3] (346 mg, 1 eq., 0.527 mmol), Pd(PPh$_3$)$_4$ (30 mg, 0.026 mmol, 0.05 eq), CuI (7 mg, 0.037 mmol, 0.07 eq) and TEA (368 µL, 2.635 mmol, 5 eq) were dissolved in DMF (7 mL). The solution was stirred under nitrogen for 3 h at 25 °C. The reaction mixture was concentrated in vacuo, then diluted with CH$_2$Cl$_2$ (15 mL), washed with water (2 x 10 mL) and purified by flash chromatography eluting with CH$_2$Cl$_2$/MeOH (95:5) to achieve the desired product (227 mg, 60% yield) as a yellow solid.

ESI-MS (*m/z*): 740.8 [M + Na]$^+$ (calcd for C$_{40}$H$_{34}$N$_2$O$_7$S$_2$ + Na 741), 303 [DMT]$^+$. ^{1}H NMR (CDCl$_3$, 400 MHz): δ 9.60 (bs, 1 H), 8.11 (s, 1 H), 7.36-7.08 (m, 11 H), 7.01 (d,

3.2 Hz, 1 H),6.895 (dd, 3.6 Hz, 1 H), 6.808 (d, 4 Hz, 1H), 6.77-6.66 (m, 4 H), 6.28 (t, 6.6 Hz, 1 H), 4.51 (t, 2.4 Hz, 1 H), 4.09 (d, 2.4 Hz 1 H), 3.61 (s, 6H), 3.34-3.24 (m, 2 H), 2.54-2.50 (m, 1H), 2.28-2.23 (m, 1H). ^{13}C NMR (CDCl$_3$, 100 MHz): δ 161.42, 158.5, 149.37, 144.26, 142.38, 138.99, 136.61, 135.50, 135.31, 133.35,129.94, 129.84, 127.98, 127.86, 126.96, 124.87, 124.06, 123.09, 120.96, 113.27, 100. 20, 87.01, 86.84, 86.07, 84.59, 72.42, 55.15, 63.53, 35.4.

5-(5-Ethynyl-[2,2']bithiophenyl]-2'-deoxy-5'-O-(4,4'-dimethoxytrityl)uridine-3'-O-(2-cyanoethyl-*N,N*-diisopropyl)phosphoramidite (42). 5-(5-Ethynyl-[2,2']-bithiophenyl)-2'-deoxy-5'-O-(4,4'-dimethoxytrityl)uridine (**40**) (200 mg, 0.279 mmol, 1 eq.) and ethyl-*N,N*-diisopropylamine (238 μL, 1.4 mmol, 5 eq.) were stirred in dichloromethane (2 mL) and treated with 2-cyanoethyl-*N,N*-diisopropylchlorophosphoramidite (93 μL, 0.42 mmol, 1.5 eq.) under nitrogen. After 30 min at rT, the reaction mixture was diluted with dichloromethane (5 mL) and washed with sat aq NaHCO$_3$ (5 mL). The aqueous phase was re-extracted twice with dichloromethane (2 × 5 mL) and the combined organic phases were dried over Na$_2$SO$_4$. After solvent evaporation, the crude residue was purified by flash chromatography (silica gel, column prepared with CH$_2$Cl$_2$/TEA 9:1 and eluted with CH$_2$Cl$_2$/TEA/MeOH 98:1:1) to yield **42** (191 mg, 76 % yield) as a yellow solid mixture of diasteroisomers.

^{31}P NMR (80 MHz, CDCl$_3$): δ 149.07 R$_L$, 148.65 R$_{Hr}$. ^{1}H NMR (CDCl$_3$, 400 MHz): δ 9.60 (bs, 2H, R$_H$ + R$_L$), 8.22 (s, 1 H, R$_H$), 8.17 (s, 1 H, R$_L$), 7.44-7.15 (m, 22 H, R$_H$ + R$_L$), 7.10 (d, 4 Hz, 1H, R$_L$), 7.09 (d, 3.6 Hz, 1H, R$_H$), 6.99 (dd, 4 Hz, 3.6 Hz, 2H, R$_H$ + R$_L$), 6.90 (d, 4 Hz, 1 H, R$_L$), 6.88 (d, 4 Hz, 1 H, R$_H$), 6.817-6.775 (m, 6 H, R$_H$ + R$_L$), 6.72 (d, 3.6 Hz, 1 H, R$_L$), 6.68 (d, 3.6 Hz, 1 H, R$_H$), 6.34 (t, 6 Hz, 1H, R$_L$), 6.32 (t, 6 Hz, 1H, R$_H$), 4.6 (m, 2 H, R$_H$ + R$_L$), 4.2 (m, 4 H, R$_H$ + R$_L$), 3.88-3.80 (m, 2 H, R$_H$ + R$_L$), 3.72 (s, 6 H, R$_L$), 3.71 (s, 6H, R$_H$), 3.67-3.50 (m, 4 H, R$_H$ + R$_L$), 3.50-3.26 (m, 4 H, R$_H$ + R$_L$), 2.63 (m, 4 H, R$_H$ + R$_L$), 2.44 (t, 6.4 Hz, 2 H, R$_H$ + R$_L$), 2.35 (m, 2 H, R$_H$ + R$_L$), 1.18 (d, 6.5 Hz,12 H, R$_L$), 1.16 (d, 6.0 Hz,12 H, R$_H$).

2-Bromo-5-thiomethylthiophene (43). To a solution of 2-thiomethylthiophene (500 mg, 3.8 mmol, 1 eq) in CH$_2$Cl$_2$/CH$_3$COOH (1:1) (33 mL) under nitrogen was added NBS (547 mg, 3.07 mmol, 0.8 eq.) at −15° C in 30 min. After 2 h the reaction mixture was diluted with CH$_2$Cl$_2$ (20 mL) and washed with 10% aq KOH (40 mL), sat aq NaHCO$_3$ (40 mL) and water (40 mL). The organic layer was dried over Na$_2$SO$_4$ and

evaporated. The crude product was isolated as a colorless oil (583 mg, 73% yield) and used in the following step without further purification.

MS (*m/z*): 208, 210 [M$^+$] (calcd for $C_5H_5BrS_2$ 208, 210), 193, 195, [M-Me]$^+$. ^{1}H NMR (CDCl$_3$, 400 MHz) δ: 6.90 (d, 4.0 Hz, 1H), 6.87 (d, 4.0 Hz, 1 H), 2.46 (s, 3 H).

5-Thiomethyl-[2,2']bithiophene (44). The microwave oven reactor was charged with 2-bromo-5-thiomethylthiophene (**43**) (583 mg, 2.79 mmol, 1 eq), 2-(tributylstannyl)-thiophene (886 µL 2.8 mmol, 1 eq), Pd(PPh$_3$)$_4$ (322 mg, 0.28 mmol, 0.1 eq.) of in toluene (10 mL). After 45 min of irradiation at 120 °C a TLC on silica gel with *n*-hexane as eluent showed the absence of **43**. The solvent was removed in vacuo and the crude mixture was directly charged on a chromatography column. After chromatography, eluting with *n*-hexane the title compound was isolated (414 mg 70% yield).

MS (*m/z*): 212 [M$^+$] (calcd for $C_9H_8S_3$ 212), 197 [M-Me]$^+$. ^{1}H NMR (CDCl$_3$, 200 MHz) δ: 7.21 (d, 4.2 Hz, 1 H), 7.13 (d, 3.4 Hz, 1 H), 7.03-6.97 (m, 3 H), 2.5 (s, 3 H). ^{13}C NMR (CDCl$_3$, 50 MHz) δ: 139.95, 137.10, 136.70, 131.79, 127.79, 124.53, 123.82, 123.76, 22.11.

5-Iodo-5'-thiomethyl-[2,2']bithiophene (45). To a solution of 5-thiomethyl-[2,2']bithiophene (414 mg, 1.95 mmol, 1 eq) in CH$_2$Cl$_2$/CH$_3$COOH (1:1) (33 mL) under nitrogen was added NIS (395 mg, 1.76 mmol, 0.9 eq.) at −15° C in 30 min. After 2 h the reaction mixture was diluted with CH$_2$Cl$_2$ (30 mL) and washed with 10% aq KOH (40 mL), sat aq NaHCO$_3$ (40 mL) and distilled water (40 mL). The organic layer was dried over Na$_2$SO$_4$ and evaporated. After chromatography, eluting with *n*-hexane, the target product (488 mg 74% yield) was isolated as a colorless oil.

MS (*m/z*): 338 [M$^+$] (calcd for $C_9H_{12}IS_3$ 338), 323 [M-Me]$^+$, 196 [M-Me-I]$^+$. ^{1}H NMR (CDCl$_3$, 400 MHz) δ: 7.14 (d, 4.0 Hz, 1 H), 6.96 (d, 3.6 Hz, 1 H), 6.95 (d, 3.6 Hz, 1 H), 6.79 (d, 4.0 Hz, 1 H), 2.5 (s, 3 H). ^{13}C NMR (CDCl$_3$, 100 MHz) δ: 142.87, 138.08, 137.62, 137.12, 131.48, 124.98, 124.20, 22.92.

5-(5-ethynyl-5'-tiomethyl-[2,2']-bithiophenyl)-2'-deoxy-5'-O-(4,4'-dimethoxytrityl)-uridine (47). To a solution of 5-iodo-5'-thiomethyl-[2,2']-bithiophene (68 mg, 0.2 mmol) in anhydrous DMF (2 mL) under nitrogen was added CuI (8 mg, 0.04 mmol, 0.2 eq), TEA (140 µl, 5 eq.), 5-(ethynyl)-2'-deoxy-5'-O-(4,4'-dimethoxytrityl)uridine **46** (111 mg, 0.2 mmol) and Pd(PPh$_3$)$_4$ (23 mg, 0.1 eq., 0.02 mmol). The mixture was

stirred 3 h at rT. The reaction mixture was concentrated in vacuo, then diluted with CH_2Cl_2 (20 mL), washed with sat aq citric acid (15 mL), sat aq $NaHCO_3$ (15 mL) and water (15 mL). The organic phase was dried over Na_2SO_4, the solvent removed and the crude mixture purified by flash chromatography eluting with 5% MeOH in CH_2Cl_2. The desired product was obtained as brown oil (110 mg, 66% yield).

ESI-MS (m/z): 786.9 [M + Na]$^+$ (calcd for $C_{41}H_{36}N_2O_7S_3$ + Na 787). ^{1}H NMR ($CDCl_3$, 200 MHz) δ: 8.11 (s, 1 H), 7.80 (bs, 1 H) , 7.90 (dd, 3.6 Hz, 1 H), 7.58-7.50 (m, 1 H), 7.44-7.38 (m, 2 H), 7.36-7.14 (m, 9 H), 6.84-6.70 (m, 4 H), 6.33 (t, 6.6 Hz, 1 H), 4.60 (m, 1 H), 4.08 (d, 2.4 Hz 1 H), 3.65 (s, 6 H), 3.40-3.20 (m, 2 H), 2.54-2.50 (m, 1 H), 2.50 (s, 3 H), 2.28-2.23 (m, 1 H).

5-(5-ethynyl-5'-tiomethyl-[2,2']bithiophene)-2'-deoxy-5'-O-(4,4'-dimethoxytrityl)uridine-3'-O-(2-cyanoethyl-*N*,*N*-diisopropyl)phosphoramidite (49).

A 0.45 M solution of tetrazole (0.104 mmol, 0.232 mL, 1 eq.) in anhydrous CH_3CN was added, under stirring in a flow of nitrogen, to a solution of 5-(5-ethynyl-5'-thiomethyl-[2,2']-bithiophenyl)-2'-deoxy-5'-O-(4,4'-dimethoxytrityl)uridine (**47**) (80 mg, 0.104 mmol, 1 eq.) in anhydrous CH_3CN (222 μL), followed by a solution of 2-cyanoethyl *N, N, N', N'*-tetraisopropylphosphorodiamidite (**48**) (32 μL, 0.0708 mmol, in 40 μL of anhydrous CH_3CN). TLC analysis showed that the reaction was completed within 45 min with formation of two diastereoisomers. The precipitated diisopropylammonium tetrazolide was removed by filtration and the solution diluted with anhydrous CH_3CN (1 mL) to give a 0.1 M solution of **49**. The solution was immediately used in the phosphitlylation step on the automated synthesizer, without further purification or analysis except for a check of the presence of the correct phosphoroamidite specie by phosphorous NMR analysis, on a small aliquot of the solution. ^{31}P NMR ($CDCl_3$, 80 MHz) δ: 149.46, 149.75.

5-(5-[2,2']bithiophenyl)-2'-deoxy-5'-O-(4,4'-dimethoxytrityl)uridine (51a).

A mixture of 5'-O-(4,4'dimethoxytrityl)-5-iodo-2'-deoxyuridine (100 mg, 0.152 mmol 1 eq), 5-tributylstannyl-[2,2']-bithiophene (**51a**) (*21*) (277 mg, 0.610 mmol 4 eq) and $Pd(PPh_3)_2Cl_2$ (11 mg, 0.0152 mmol, 0.1 eq) in dioxane (5 mL) was heated at 95° C for 4 h. The solution was cooled and evaporated and the mixture was purified by flash-chromatography eluting with $CH_3CN:H_2O$ (80:20). **51a** was obtained as a yellow solid (102 mg, 97% yield).

ESI-MS (m/z): 716.8 [M + Na$^+$] (calcd for $C_{38}H_{34}N_2O_7S_2$ + Na 717). ^{1}H NMR (400 MHz, DMSO-*d6*) δ: 9.5 (brs, 1H), 7.92 (s,1 H), 7.38 (d,7.2Hz, 2 H),7.30-7.10 (m, 9 H), 6.99 (d, 3.6 Hz, 1 H), 6.94 (dd, 3.6 Hz, 1 H), 6.76-6.71 (m ,5 H),6.19 (t, 6.5 Hz,1 H), 4.49-4.47 (m, 1 H), 4.15-4.12 (m,1 H), 3.65 (s, 6 H), 3.45-3.41 (m, 1 H), 3.35-3.31 (m, 1 H), 2.05-1.95 (m, 1 H), 2.35-2.25 (m,1 H).

5-(5-[2,2']-bithiophenyl)-2'-deoxy-5'-O-(4,4'-dimethoxytrityl)uridine-3'-O-(2-cyanoethyl-*N,N*-diisopropyl)phosphoramidite (52a). 5-(5-[2,2']bithiophenyl)-2'-deoxy-5'-O-(4,4'-dimethoxytrityl)-uridine (**51a**) (100 mg, 0.144 mmol, 1 eq.) and ethyl-*N,N*-diisopropylamine (123 μL, 0.72 mmol, 5 eq) were stirred in THF (1 mL) and treated with 2-cyanoethyl-*N,N*-diisopropylchlorophosporamidite (48 μL, 0.216 mmol, 1.5 eq.) under nitrogen. After 30 min at rT, the reaction mixture was diluted with dichloromethane (5 mL) and washed with sat NaHCO$_3$ (5 mL). The aqueous phase was re-extracted twice with CH$_2$Cl$_2$ (2 × 5 mL) and the combined organic phases were dried over Na$_2$SO$_4$. After solvent evaporation, the crude residue was purified by flash chromatography (silica gel, column eluted with EtOAc/TEA/*n*-hexane 80:1:19) to give **52a** (102 mg, 80% yield) as yellow solid mixture of diasteroisomers.

^{31}P NMR (80 MHz, CDCl$_3$): δ 150.27, 149.77 (R$_L$ + R$_H$). ^{1}H NMR (CDCl$_3$, 400 MHz): δ 9.60 (bs, 2 H, R$_H$ + R$_L$), 7.98 (s, 1 H, R$_H$), 7.93 (s, 1 H, R$_L$), 7.69-7.63 (m, 2 H, R$_H$ + R$_L$), 7.57-7.51 (m, 2 H, R$_H$ + R$_L$), 7.48-7.15 (m, 20 H, R$_H$ + R$_L$), 6.98-6.93 (m, 4 H, R$_H$ + R$_L$), 6.76-6.67 (m, 10 H, R$_H$ + R$_L$), 6.38 (t, 7.2 Hz, 1 H, R$_L$), 6.37 (t, 7.2 Hz, 1 H, R$_H$), 4.65 (m, 2 H, R$_H$ + R$_L$), 4.40 (m, 4 H, R$_H$ + R$_L$), 3.71 (s, 12H, R$_L$ + R$_H$), 3.64-3.45 (m, 8 H, R$_H$ + R$_L$), 2.63-2.15 (m, 4 H, R$_H$ + R$_L$), 2.42-2.38 (m, 4 H, R$_H$ + R$_L$), 2.35-2.20 (m, 4 H, R$_H$ + R$_L$), 1.18 (d, 6.5 Hz,12 H, R$_L$), 1.16 (d, 6.0 Hz,12 H, R$_H$).

5-(5-[2,2'],[5',2'']-terthiophene)-2'-deoxy-5'-O-(4,4'-dimethoxytrityl)-uridine (51 b). A mixture of 5'-O-(4,4'dimethoxytrityl)-5-iodo-2'-deoxyuridine (230 mg, 0.35 mmol, 1 eq), 5-(tributylstannyl)-[2,2'],[5',2'']terthiophene (**50b**)[11] (750 mg, 1.4 mmol, 4 eq), and Pd(PPh$_3$)$_2$Cl$_2$ (25 mg, 0.035 mmol, 0.1 eq) in dioxane (10 ml) was heated at 95° C for 4 h. The solution was cooled and evaporated and the mixture was purified chromatografically on reversed-phase C-18 silica gel, eluting with CH$_3$CN/H$_2$O (80:20). **51b** was obtained as a yellow solid (109 mg, 40% yield).

ESI-MS (m/z): 774.7 [M-H]$^+$ (calcd for $C_{42}H_{35}N_2O_7S_3$ 775). ^{1}H NMR (400 MHz, DMSO-*d6*) δ:11.8 (s, 1 H), 7.97 (s,1 H), 7.4-7.3 (m,4 H),7.30-7.14 (m, 9 H), 7.09

(dd,3.6 Hz, 1 H), 7.03 (d,4.0 Hz, 1 H), 6.99 (d,4.0 Hz, 1 H) 6.80 (dd, 5.6 Hz,4 H), 6.19 (t, 6.5 Hz,1 H), 4.45 (brs, 1 H), 3.95-3. 90 (m,1 H), 3.65 (s, 6 H), 3.40 (m, 1 H), 2.70-2.90 (m, 1 H), 2.25-2.35 (m,1 H), 1.60 (m, 2 H).

5-(5-[2,2'],[5',2"]-terthiophenyl)-2'-deoxy-5'-O-(4,4'-dimethoxytrityl)-uridine-3'-O-(2-cyanoethyl-N,N'-diisopropyl)-phosphoramidite (52b). A 0.45 M solution of tetrazole (0.07 mmol, 0.157 ml, 1 eq) in anhhydrous CH_3CN was added at rT, stirring under N_2 atmosphere, to a solution of 2'-deoxy-5'-O-(4,4'-dimethoxytrityl)-5-[-[2,2'],[5',2"]-terthiophene]-uridine (**51b**) (55 mg, 0.07 mmol, 1 eq.) in 350 µL of anhydrous CH_3CN followed by 2-cyanoethyl *N, N, N', N'*-tetraisopropylphosphorodiamidite (0.0708 mmol, 22.5 µL, 1eq). TLC analysis showed that the reaction was completed within 45 min with formation of two diastereoisomers. The precipitated diisopropylammonium tetrazolide was removed by filtration and the solution diluted with CH_3CN (350 µL) to give a 0.1 M solution of **52b** which was immediately used in the following step without further purification.

^{1}H and ^{31}P NMR spectra of $^{5'}$TA$^{3'}$-t4-$^{3'}$AT$^{5'}$ (29a)
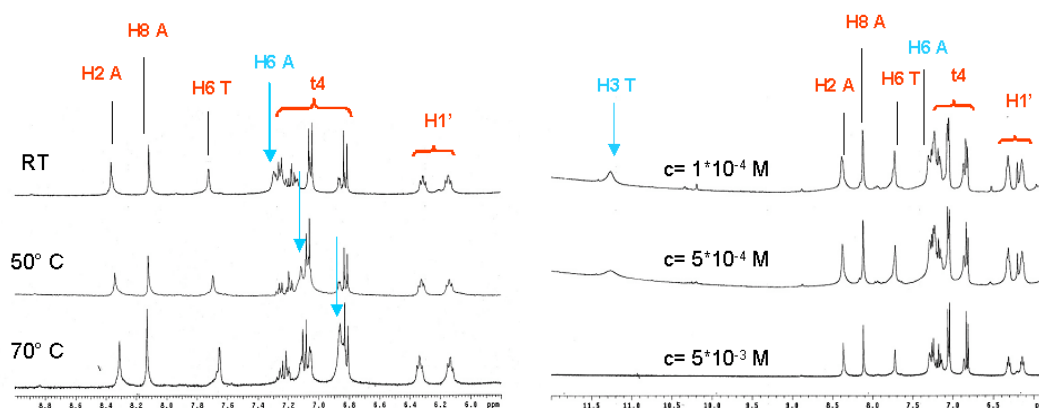
Figure 3.8 *Aromatic region of the ^{1}H-NMR spectrum of* **29a** *(5x10^{-3} M in DMSO-d$_6$) at variable concentration and temperature.*
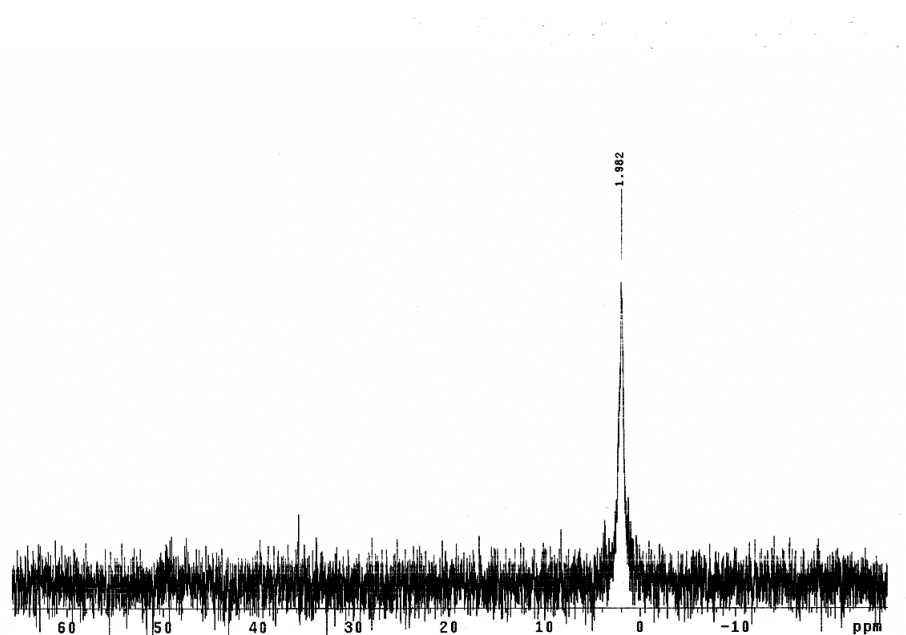
Figure 3.9. *^{31}P -NMR spectrum of* **29a** *in D$_2$O. δ (H$_3$PO$_4$) = + 1.982 ppm.*

^{1}H and ^{31}P NMR spectra of $^{5'}$TA$^{3'}$-t5 (36a)

(a)

(b)

70°

50°

RT

C=1*10^{-4}

C=5*10^{-4}

C=5*10^{-3}
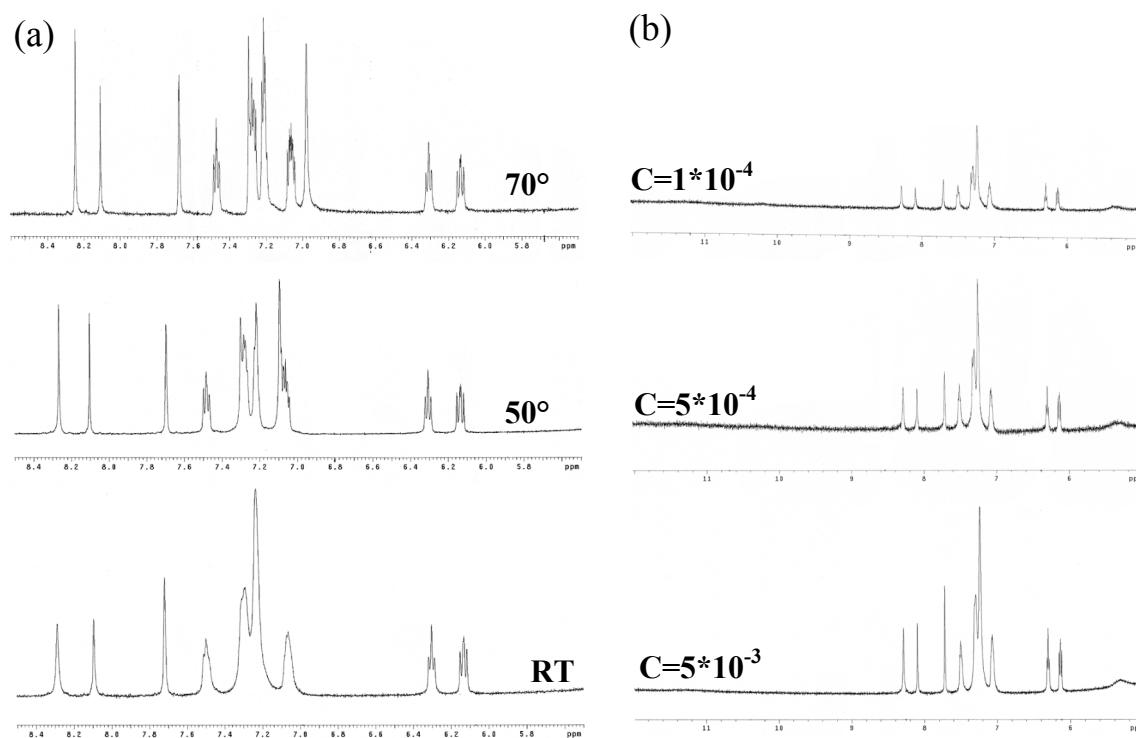
Figure 3.10 *Aromatic region of the ^{1}H-NMR spectrum of* **36a** *(5x10^{-3} M in DMSO-d$_6$) at variable (a) temperature and (b) concentration.*
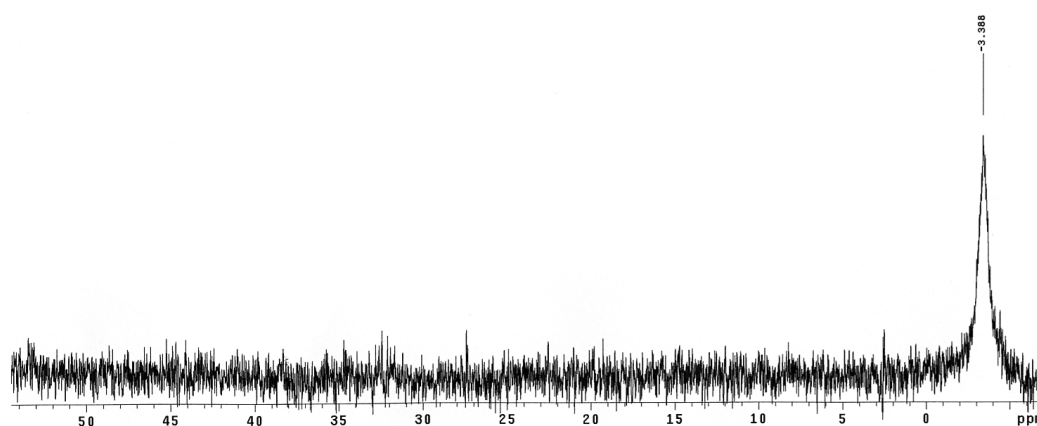

Figure 3.11 *^{31}P -NMR spectrum of* **36a** *in D$_2$O. δ (H$_3$PO$_4$) = -3.388 ppm.*

3.6 References

[1] J. E. Marugg, M. Tromp, P. Jhuran, C. F. Hoyng, G. A. van der Marel, J. H. van Boom, J. H. *Tetrahedron* **1984**, *40*, 73-78.

[2] a) Y. Kanemitsu, K. Suzuki, Y. Masumoto, *Phys. Rev. B* **1994**, *50*, 2301-2305; b) R. S. Becker, J. Seixas de Melo, A. L. Maçanita, F. Elisei, *J. Phys. Chem.* **1996,** *100,* 18683-18695; c) M. Melucci, G. Barbarella, M. Zambianchi, P. Di Pietro, A. Bongini, *J. Org. Chem.* **2004**, *69*, 4821-4828; d) M. Melucci, G. Barbarella, G. Sotgiu, *J. Org. Chem.* **2002**, *67*, 8877-8884.

[3] (a) R. D. Sheardy, N. C. Seeman, *J. Org. Chem.* **1986**, *51*, 4301-4303.(b) M. Ahmadian, P. M. Zhang, D. E. Bergstrom, *Nucleic Acids Res.* **1998**, *26*, 3127-3135.

[4] D. J. Hurley, Y. Tor, *J. Am. Chem. Soc.* **1998**, *120*, 2194-2195.

[5] J. Liu, A. Van Aerschot, I. Luyten, P. Wigerinck, C. Pannecouque, J. Balzarini, E. Declercq, P. Herdewijn, *Nucleos. Nucleot.* **1995**, *14*, 525-528.

[6] (a) G. Barbarella, *Chem. Eur. J.* **2002**, *8*, 5072-5077.

(b) G. Barbarella, M. Zambianchi, A. Ventola, E. Fabiano, F. Della Sala, G. Gigli, M. Anni, A. Bolognesi, L. Polito, M. Naldi, M. L. Capobianco, *Bioconjugate Chem.* **2006**, *17*, 58-67.

[7] A. Cazzato, M. L. Capobianco, M. Zambianchi, L. Favaretto, C. Bettini, G. Barbarella, *Bioconjugate Chem.* **2007**, *18*, 318-322.

[8] M. Cirilli, F. Bachechi, G. Ughetto, F. P. Colonna, M. L. Capobianco, *J. Mol. Biol.* **1993**, *230*, 878-889.

[9] (a) M Kiuchi, K. Adachi, T. Kohara, M. Minoguchi, T. Hanano, Y. Aoki, T. Mishina, M. Arita, N. Nakao, M. Ohtsuki, Y. Hoshino, K. Teshima, K. Chiba, S. Sasaki, T. Fujita, *Journal of Medicinal Chemistry* **2000**, *43*, 2946-2961. ([b]) J. Liu, R. D. Mc Cullough, *Macromolecules* **2002**, *35*, 9882-9889. (c) G. Barbarella, M. Zambianchi *Tetrahedron* **1994**, *50*,11249-11256.

[10] (a) J. S. Field, R. J. Haines, E. I. Lakoba, M. H.Sosabowski, *J. Chem. Soc. Perkin Trans. 1*, **2001**, 3352-3360. (b) T. M. Pappenfus, K. R. Mann, *Org. Lett.* **2002**, *4*, 3043-3046.

[11] A. Bilge, A. Zen, M. Forster, H. B. Li, F. Galbrecht, B. S. Nehls, T. Farrell, D. Neher, U. Scherf *J. Mater. Chem.* **2006**, *16*, 3177-3182.

Chapter 4

Oligothiophene-5-labeled deoxy-uridines for the detection of Single Nucleotide Polymorphisms

Abstract

The oligothiophene-5-labeled deoxyuridines, incorporated into oligodeoxynucleotides, as discussed in Chapter 3 (Paragraph 3.4), have been used as probes to discriminate, through changes in fluorescence emission, between the hybridization with a perfectly complementary strand and those with a single nucleotide mismatch facing to the modified uridines. Upon hybridization remarkable differences (up to 47%) of the emitted light can be observed depending on the uridine facing base.

4.1 Introduction

In previous works our group studied the fluorescence properties of oligothiophenes as markers for proteins and oligonucleotides[1] and explored their use as diagnostic tools in biotechnologies[2]. As part of this study we wondered if it could be possible to use emission and charge transport properties of oligothiophene-oligonucleotide biohybrids, developed in Paragraphs 3.4, Chapter 3, in order to monitor a particular type of biological event, as mutations of nucleosides inside DNA[3]. Single mutations, known as Single Nucleotide Polymorphism (SNP)[4], can be randomly produced during DNA replication, even in absence of mutagens, with an esteemed frequency in the range 10^{-7}-10^{-11} per replication and can be inherited. Most of the times SNPs occur in untranscribed DNA or into introns, but seldom they can affect an exon and alter the gene translation leading to a truncated or a mutated protein. Detection of SNPs is thus of great importance in medicine and biology and a great effort has been devoted to find suitable methods of analysis. Among a plethora of methodologies ,[5a-e] based on sequencing, selective hybridization,[6] amplification,[7a,b] colorimetric,[8] mass spectrometry[5a-c] etc., those based on the variation of the emitted light of a modified nucleosides, inserted into a probe in front of the mutation spot of the oligonucleotide to be analyzed, are perhaps the most straightforward.[9] The methods rely on the fact that the electronic distribution of a nucleobase is modified by the presence (or absence) of the Watson-Crick hydrogen bonds formed with the facing nucleoside in a duplex.

If a suitable fluorophore is conjugated on the nucleobase opposite the presumed mutated base it can be affected from that variation, and fluoresce in a different way if correctly paired or mispaired.

In this direction, fluorescence variations of oligothiophene-5-labeled deoxyuridines incorporated into probe oligonucletide sequences have been used to transduce a SNP in complementary target sequences into an observable response. The observed photoluminescence variations, comparable or even superior to those reported in similar studies, suggested that the developed biohybrid systems can potentially be used for an easy SNP recognition in biological samples.

4.2 Results and discussion

The UV-vis and the fluorescence emission spectra of the each sequences probe, (P1-4, Scheme 3.6, Chapter 3), synthesized in chapter 3, were registered at 25 and at 70 °C at 1 μM concentration in an aqueous buffer containing 100mM NaCl and 10mM sodium cacodylate at pH 7.0. They didn't reveal any significative changes but a 10-15% loss of fluorescence emission at the higher temperature. This behavior was already observed in our previous work[2] with this class of fluorophores and was attributed to a slight loss of coplanarity of the thiophene rings and increasing collisional quenching due to the heating.

Three more cuvettes were prepared for each probe at 1 μM concentration in the same buffer and checked against the first sample, UV and fluorescence intensity were found in a range of less than 0.5-1% difference. Each cuvette of 3000 μL was then added of 1.2 eq (10-20 μL from concentrated aqueous solution) of the four complementary strands. The samples were heated to 90 °C and left to cool in a becker (in about three hours) to favor the annealing. The UV-melting profile was then recorded at 260 nm during both heating and cooling, in the range 10-75 °C, at a rate of 0.5 °C/min. The found melting temperatures are reported on Table 4.1.

	P1 (ethynyl-t_2)	**P2** (ethynyl-t_2-SMe)	**P3** (t_2)	**P4** (t_3)
A	50	50	52	48
C	49	49	49	47
G	47	49	49	46
T	46	48	49	47

Table 4.1 *Melting temperatures (T_m, in °C) at 1μM concentration in aqueous buffer containing 100 mM NaCl, 10 mM sodium cacodylate at pH 7.0. (precision +/- 1 °C). (t_2 and t_3 refers to the number of thiophene rings).*

After the melting experiments the very same samples were used to measure the variation of fluorescence of the four hybrids of the P1-P4 probes. All the probes were excited at the maximum of their visible absorption. To ensure that the measurements of the mixtures were not affected by the presence of accidental quenchers in the target solutions, we recorded the fluorescence of every mixture at 70 °C and found them equal to those obtained with the corresponding isolated probe at the same temperature.
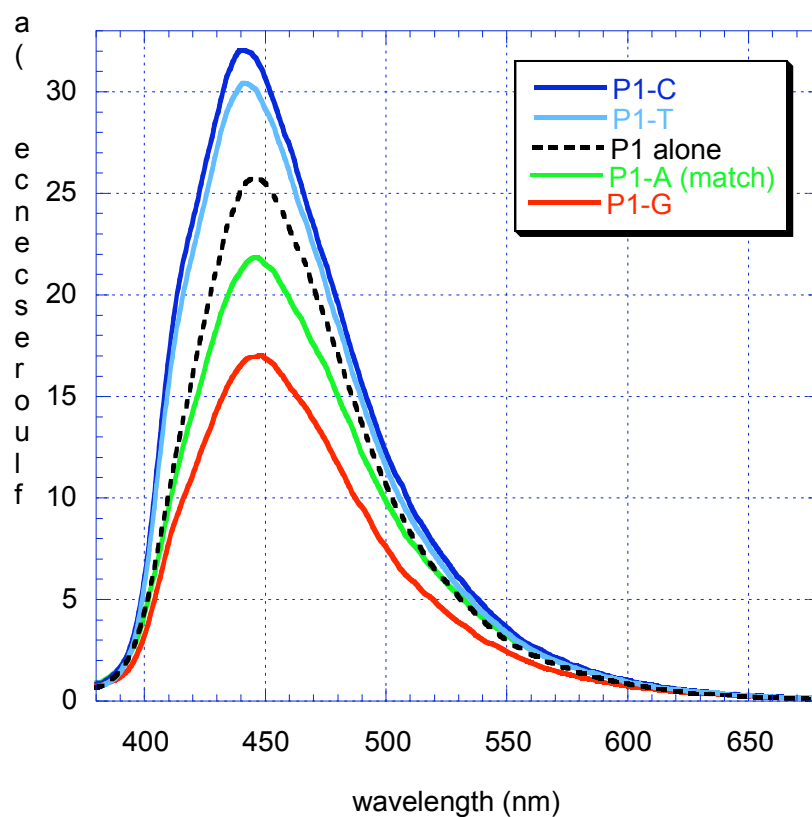
Figure 4.2 *Fluorescence emission of P1(ethynyl-t₂) alone and hybridized with the four targets after irradiation at 360 nm.*

Fluorescence emissions of P1 alone and hybridized with the four targets are shown in Figure 4.2. The graph shows that P1 is able to discriminate between the perfect match with target-A (-20% in the emitted intensity respect to unhybridized P1), target-G (-35%) and the couple of targets C and T (+15, +18%).
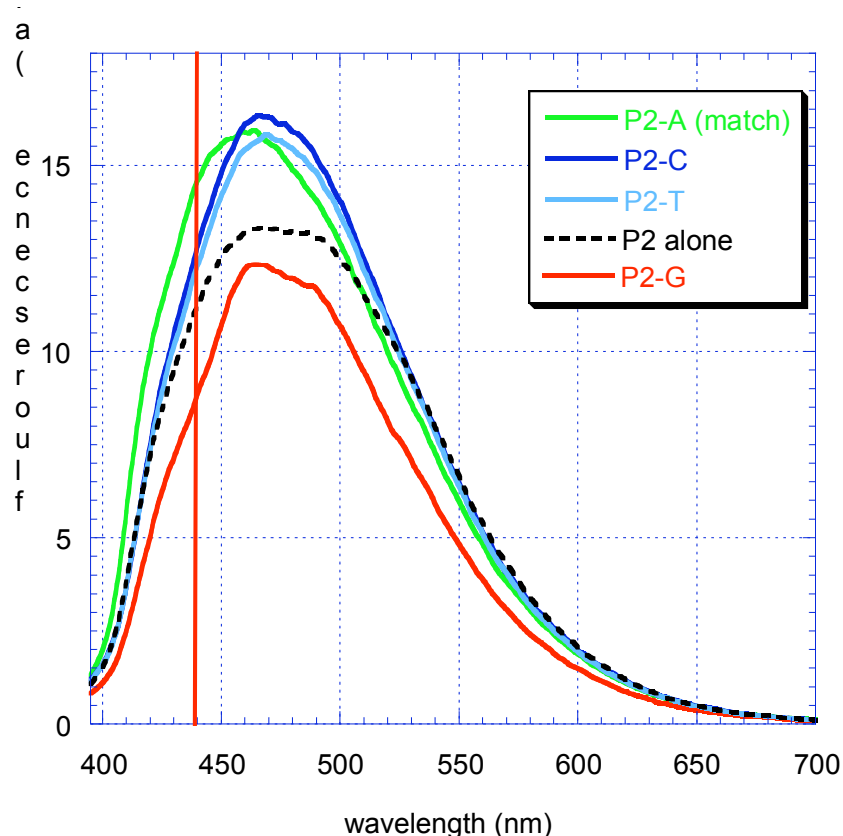
Figure 4.3 *Fluorescence emission of P2 (ethynyl-t₂-SMe) alone and hybridized with the four targets after irradiation at 375 nm.*

Compared to the previous probe, P2 shows lower and broader signals (Figure 4.3), reflecting the increased dimension of the molecular orbital, now including a S-Me substituent. Here we can see that hybrids formed with probes C and T show very similar signals, the hybrid with probe A has a similar intensity than the previous two but its maximum is blue shifted by about 10 nm. The three signals are about 18% more intense than the isolated probe. The hybrid with probe-G shows a signal 10% weaker than that showed by the single strand probe. If we look at the value of the emitted light at 440 nm we can easily observe that the emission of the probe alone is half way from that of the mismatch with probe-G (-20%) and that of the match with probe-A (+36%). Again the mismatches with probe-C and T (+18%) are too close to be distinguished. This can be considered an ideal probe to look for a G to A transition: it is sufficient to record the emission of the probe alone, hybridize it with the unknown target then if the emission is

higher than before this reveals a match, if it is lower it's a G-mismatch, (beside C and T mismatch can also be detected with a careful measurement).

Figure 4.4 *Fluorescence emission of P3 (t_2) alone and hybridized with the four targets after irradiation at 360 nm.*

The graphics of the fluorescence emission of P3 and its hybrids, reported in Figure 4.4, showed that there isn't clear intensity difference between the signal of the single strand and those of the hybrids with A and G targets, instead the intensity of the maxima of the hybrids with targets T (+18%) and C (+44%) can clearly be distinguished. Small differences perhaps exploitable for the recognition of the formed hybrids can be seen in the position of the maxima: they move from 492 (P3 alone), to 488 (P3-G, P3-A), to 482 (P3-T), to 478 (P3-C).

Comparing the emission of this probe with those of P1 it can be seen that the intensity of the emission is between three and four times lower in absence of the ethynyl linker.
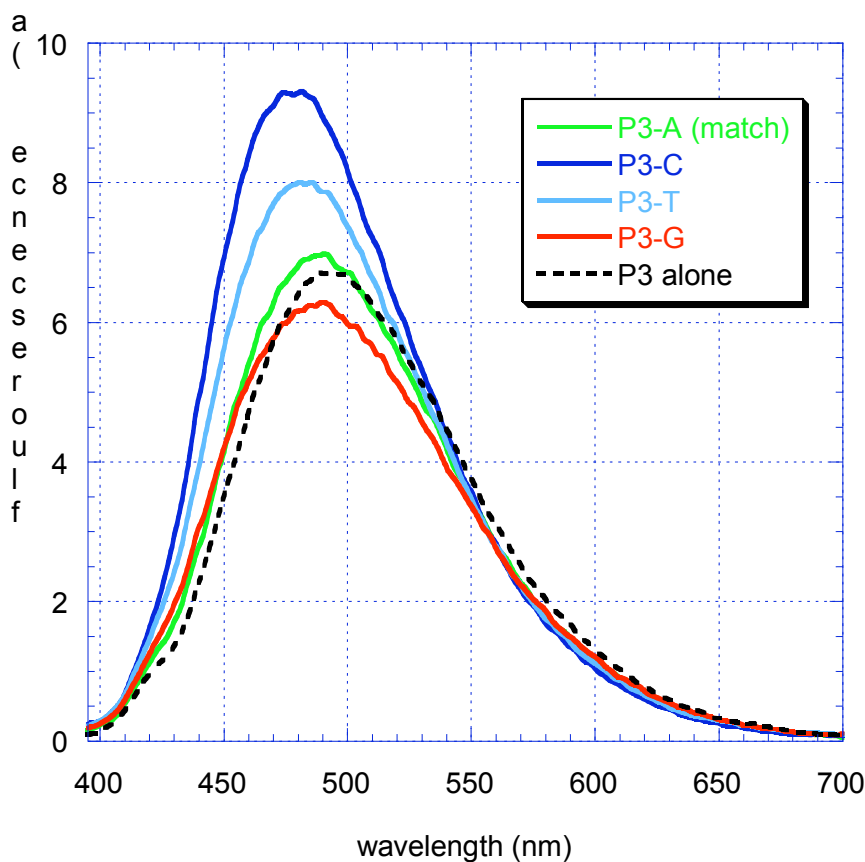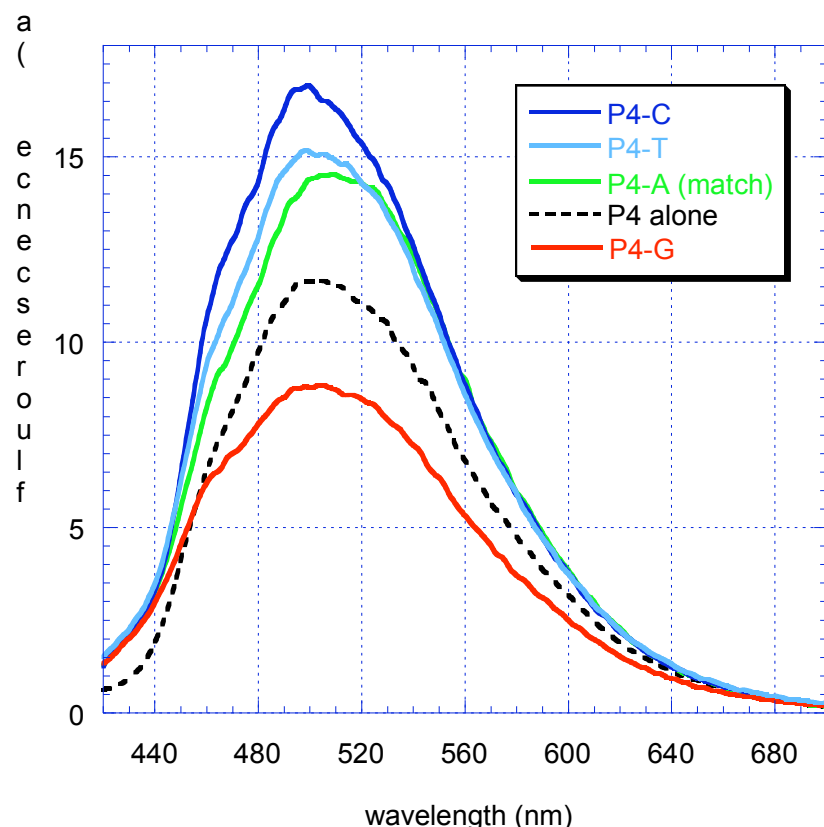
Figure 4.5 *Fluorescence emission of P4 (t₃) alone and hybridized with the four targets after irradiation at 400 nm.*

The graphics of the fluorescence emissions of P4 hybrids, and isolated P4, are reported in Figure 4.5. These emissions are the widest and the most structured among the four probes. Respect to the signal of the P4 probe alone, hybrids with targets C (+47%), T (+30%) and A (+26%) are clearly distinguishable even if the last two are closely grouped, the hybrid with target G can also be neatly recognize (-22%). Furthermore all compounds have an emission maximum centered at 500 nm except for the hybrid with target-A that is shifted to 510 nm.

Only few methods of mismatch detection based on fluorescence of the facing base have been reported in the literature. Among the most recent ones: Tor reports the use of 1,10-phenantroline-etynyl-5-uridine[9a] and demonstrates a fair sensitivity in recognizing the pairing nucleosides comparing the emission ratio at two different wavelengths in a range from 0.95 for the match with adenosine to 1.2 for the worst tolerated mismatch with cytidine; Kim shows to be able to appreciate by naked eye the correct pairing of a

5-(1-ethynylpyrenyl)2'-deoxyuridine incorporated into an oligonucleotide respect the three possible mismatches[9b] however all of them are very little fluorescent and their emission quite similar.

Our results demonstrate that the new uridines, integrated into an oligonucleotide, are apt to discriminate between the correct pairing and mispairings.

Moreover, despite the steric hindrance of the labels, modified uridines didn't interfere significantly with the hybridization process, (differences between the match and mismatches are less than 3 °C), neither showed any tendency to intercalate between base pairs, as demonstrated by invariance of absorbance in visible part of the spectra, and by preliminary studies of molecular modeling performed on P3 with all the probes. Akin to the case of molecular beacons[2], the emissions of oligothiophene derivatives are exquisitely sensitive to the local environment, and this characteristic is potentially exploitable for the analysis of SNPs. Usually the mutation to be analyzed is well known, and consists of a single nucleoside exchange: A to G (as in our case), but if different exchanges are possible, probes like P3 and P4 can be used to reveal each of them.

In our case we observed the lowest emission when any of the probes was facing G, a feature common to several fluorophores.[2,10] The behavior of the single probes with C, T, and A is still unclear and might be the object of a future communication. At this stage the prevision of a higher or lower fluorescence emission, in case of match or mismatch is still unpredictable and can be solved only experimentally. So it could be interesting to see what pattern of results can be obtained by tagging nucleosides other than dU.

4.3 Conclusions

In conclusion all the probes synthesized in Chapter 3, Paragraph 3.4, containing a deoxyuridine modified with oligothiophene derivatives at the 5 position. All the probes fluoresce at a different wavelength, and all show variations of emission intensity (from 10 to 47% higher or lower than those of the isolated probes), upon hybridization with target sequences containing all the four bases opposite to the uridine. Those variations are comparable or even superior to those reported in similar studies and could be potentially exploited for an easy SNP recognition in biological laboratories equipped with a bench spectrofluorimeter, or automatic high-throughput devices.

These results are the first step toward a procedure for SNP recognition based on the variation of fluorescence of specific probes. To get a real method the probes have to be studied in a variety of conditions and environments and their behavior, in the presence of real biological samples, has to be carefully analyzed. However, the reported variations show that this kind of derivatives can potentially be useful to develop such a method.

4.4 Experimental Section

UV–vis and melting temperature were recorded with a Perkin Elmer lambda 20 spectrophotometer. Fluorescence measurements were performed with a Perkin Elmer LS-50B spectrofluorimeter.

4.5 References

[1] (a) G. Barbarella, *J. Chem. Eur.* **2002,** *8*, 5072-5077. (b) G. Barbarella, M. Zambianchi, A. Ventola, E. Fabiano, F. DellaSala, G. Gigli, M. Anni, A. Bolognesi, L. Polito, M. Naldi, M. L. Capobianco, *Bioconjugate Chem.* **2006**, *17*, 58-67.

[2] A. Cazzato, M. L. Capobianco, M. Zambianchi, L. Favaretto, C. Bettini, G. Barbarella, *Bioconjugate Chem.* **2007**, *18*, 318-322.

[3] http://nci.nih.gov/cancertopics/understandingcancer/geneticvariation National-Cancer-Institute.

[4] http://nci.nih.gov/cancertopics/understandingcancer/geneticvariation National-Cancer-Institute.

[5] (a) C. Jurinke, P. Oeth, D. van den Boom, *Molec. Biotech.* **2004**, *26*, 147-163.(b) E. Petkovski, C. Keyser-Tracqui, R. Hienne, B. Ludes, *J. Forensic Sci.* **2005**, *50*, 535-541. (c) S. Sauer, *Clin. Chim. Acta* **2006**,*363*, 95-105. (d) L. Wang, R. Luhm, M. Lei, *Adv. Exp. Med. Biol.* **2007**, *593*, 105-116. (e) K. Cottingham, *Anal. Chem.* **2004**, *76*, 179-181.

[6]M. Salimullah, K. Hamano, M. Tachibana, K. Inoue, K. Nishigaki, *Cell. Mol. Biol. Lett.* **2005**, *10*, 237-245.

[7] (a) A. Solinas, L. J. Brown, C. McKeen, J. M., Mellor, J. T. G. Nicol, N. Thelwell, T. Brown, *Nucleic Acids Res.* **2001**, *29*, 96. (b) N. J. Gibson, *Clin. Chim. Acta* **2006**, *363*, 32-47.

[8] T. Ihara, Y. Chikaura, S. Tanaka, A. Jyo, *Chem. Comm.* **2002**, 2152-2153.

[9] (a) D. J. Hurley, S. E. Seaman, J. C. Mazura, Y. Tor, *Org. Lett.* **2002**, *4*, 2305-8. (b) G. T. Hwang, Y. J. Seo, B. H. Kim, *J. Am. Chem. Soc.* **2004**, *126*, 6528-9.

[10] (a) A. O. Crockett, C. T Wittwer, *Anal. Biochem.* **2001**, *290*, 89-97. (b) I. Nazarenko, R. Pires, B. Lowe, M. Obaidy, A. Rashtchian, *Nucleic Acids Res.* **2002**, *30*, 2089-2095.

Chapter 5

Water soluble, electroactive and photoluminescent quaterthiophene-dinucleotide conjugates

Abstract

Quaterthiophene-dinucleotide conjugates were synthesized and analyzed by means of a combination of spectroscopy and microscopy techniques, electrical characterizations and theoretical calculations. Circular Dichroism experiments demonstrated a transfer of chirality from the dinucleotides to quaterthiophene at high ionic strength and in cast films. The films were photoluminescent and electroactive. CD as well as photoluminescence spectra and current density-voltage plots (measured under dynamic vacuum) displayed significant variations on changing the dinucleotide scaffold. Molecular Mechanics and Molecular Dynamics calculations indicated that conformation and packing modes of the conjugates are the result of a balance between intra- and intermolecular nucleobase-thiophene stacking interactions and intramolecular hydrogen bondings between nucleobases.

5.1 Introduction

The opportunity to employ water soluble conjugated polyelectrolytes to reveal chemical and biochemical events through changes in absorption or photoluminescence signals, electrical conductivity or redox potentials,[1,2] has been widely discussed in Chapter 1. Despite the fact that the methodologies employing cationic polythiophene transducers to detect biomolecules, such as DNA sequences, have been demonstrated to be very sensitive and specific[1] a few thiophene based materials, with charged pendant groups making them soluble in water, have been studied and used as optical transducers in biosensors.[1] On these grounds, we addressed our attention to the use of oligonucleotides -readily available and easy to graft to organic molecules by means of known methodologies - as scaffolds to prepare water soluble functional molecules capable, on one side, to recognize the presence of relevant biomolecules in physiological/pathological processes and, on the other, to self-assemble over different length scales in thin films via biomolecular recognition. We aimed, in particular, at developing theoretical and experimental tools to understand the interactions of thiophene derivatives with DNA components by means of the synthesis of oligothiophene-oligonucleotide hybrid structures and the study of the way they interact and organize in solution and in thin film. As first step in this direction, we synthesized a set of quaterthiophene-dinucleotide conjugates (**29a-d**, Chapter 3, Paragraph 3.2), where the thiophene oligomer was linked to adenosine-thymidine (TA), guanosine-cytidine (CG), adenosine-adenosine (AA) and thymidine-thymidine (TT) dinucleotides at both terminal positions, as shown in Figure 5.1.

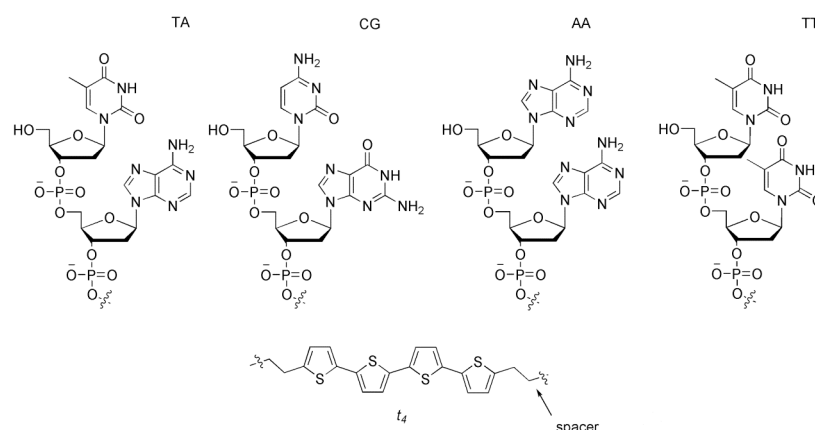**Figure 5.1.** *Building blocks composing the molecular structure of conjugates $^{5'}TA^{3'}$-t4-$^{3'}AT^{5'}$ **29 a**, $^{5'}CG^{3'}$-t4-$^{3'}GC^{5'}$ **29 b**, $^{5'}AA^{3'}$-t4-$^{3'}AA^{5'}$ **29 c** and $^{5'}TT^{3'}$-t4-$^{3'}TT^{5'}$ **29 d**.*

Their synthesis has already been discussed in Chapter 3, Paragraph 3.2. In the present chapter, by means of a combination of spectroscopic methods, fluorescence microscopy, electrical characterizations and theoretical calculations, we demonstrate that the bioconjugates are photoluminescent and electroactive compounds and that their conformational preferences and packing modalities originate from a critical balance between *intra-* and *inter*molecular nucleobase-thiophene stacking interactions and *intra*molecular hydrogen bonds formed by the nucleobases.

5.2 Results and discussion

5.2.1 UV-Vis, PL and CD data

Conjugates **29a-d** are photoluminescent compounds in water solutions and in cast films. Their UV-vis and photoluminescence (PL) spectra in H_2O and in films cast from 10^{-3} M water solutions are shown in Figures 5.2 (a) and 5.2 (b), respectively, while absorption and PL wavelengths are reported in Table 5.3.
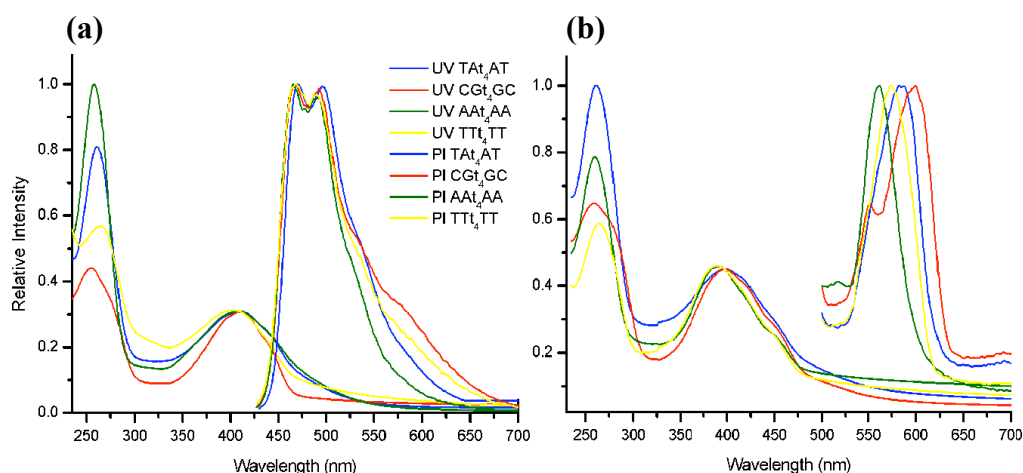
Figure 5.2 *UV-vis and PL spectra (λ_{exc}=410 nm) of conjugates $^{5'}TA^{3'}$-t4-$^{3'}AT^{5'}$, $^{5'}CG^{3'}$-t4-$^{3'}GC^{5'}$, $^{5'}AA^{3'}$-t4-$^{3'}AA^{5'}$ and $^{5'}TT^{3'}$-t4-$^{3'}TT^{5}$, **29a-d**, in H_2O (a) and in films cast from a 10^{-3} M water solution (b).*

The UV-vis spectra in solution consist of a signal around 260 nm, due the oligonucleotide moiety, and a signal around 400 nm due to quaterthiophene *t4*. The PL spectra in solution, arising from the *t4* moieties, consist of a main signal split in two bands near 500 nm and two red shifted shoulders in the region 550-600 nm. These

spectra are very similar to those of 'free' quaterthiophene, and, in general, to those of thiophene oligomers in solution.[3]

Compound	Conditions	$\lambda_{max}(nm)$	λ_{PL} (nm)
$^{5'}TA^{3'}$-*t4*-$^{3'}AT^{5'}$ (**8a**)	(a)	261, 412	470, 496
	(b)	262, 402	590
$^{5'}CG^{3'}$-*t4*-$^{3'}GC^{5'}$ (**8b**)	(a)	255, 411	466, 492
	(b)	260, 398	600
$^{5'}AA^{3'}$-*t4*-$^{3'}AA^{5'}$ (**8b**)	(a)	258, 409	466, 492
	(b)	260, 392	562
$^{5'}TT^{3'}$-*t4*-$^{3'}TT^{5'}$ (**8c**)	(a)	265, 403	469, 488
	(b)	264, 390	574

(a) Aqueous solution, $5 \cdot 10^{-6}$ M, pH=7.4. (b) Cast film from a 10^{-3}M solution in H_2O.

Table 5.2 *Maximum absorption and photoluminescence wavelengths of 29a-d.*

The UV-vis signals of the conjugates in cast films are almost superimposable and *blue* shifted by 10-17 nm with respect to those in solution, whereas the signals pertaining to the dinucleotide scaffolds remain unchanged. Instead, the PL signals of **29a-d** in cast films are remarkably sharpened with respect to the solution, well separated from each other and *red* shifted by 70 to near 100 nm. This behaviour recalls that shown in the formation of H-type aggregates, as those described, for example, for trans-stilbene in Langmuir-Blodgett films[4a] or for supramolecular assemblies of chiral oligothiophenes[4b] and indicates that the *t4* components form oriented ordered domains in the film.[4c] Further studies are required to fully elucidate the relationship between the aggregation modalities of **29a-d** and their photophysical properties and investigations in this direction are currently under way.

Circular dichroism (CD) experiments demonstrated a transfer of chirality from the dinucleotide substituents to the quaterthiophene moiety at high ionic strength and in films. The CD spectra of the bioconjugates in 10^{-5} M in aqueous buffer (pH = 7.4), aqueous buffer containing 1 M NaCl and in cast films from H_2O solutions are shown in Figure 5.4 (a) and (b). The detailed CD data of **29a-d** are reported in Table 5.5.

(a)   **(b)**

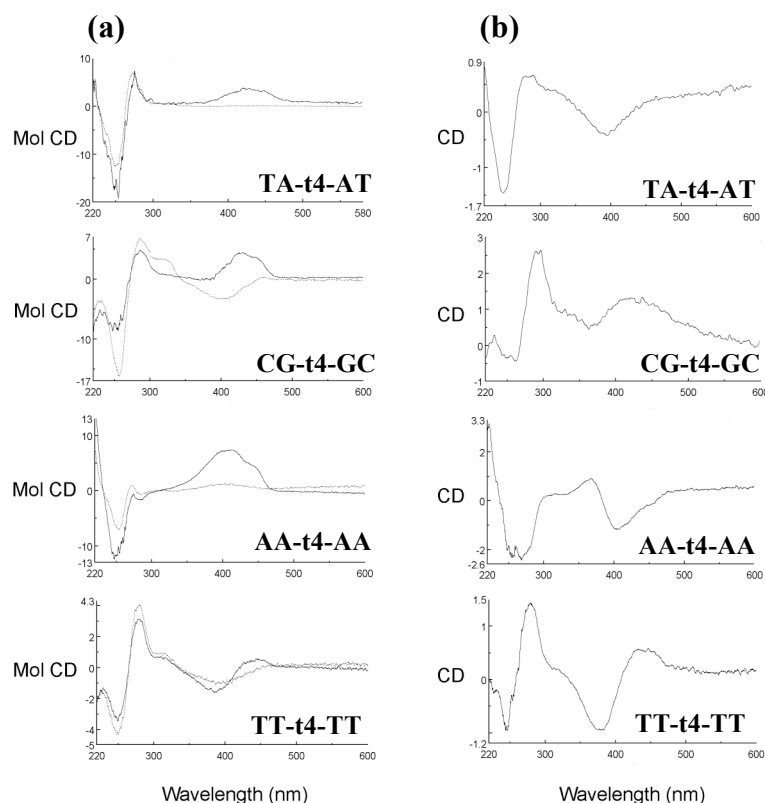**Figure 5.4** *CD spectra of conjugates $^{5'}TA^{3'}$-t4-$^{3'}AT^{5'}$, $^{5'}CG^{3'}$-t4-$^{3'}GC^{5'}$, $^{5'}AA^{3'}$-t4-$^{3'}AA^{5'}$ and $^{5'}TT^{3'}$-t4-$^{3'}TT^{5}$, **29a-d**, (a) in aqueous buffer (pH = 7.4, (dotted line) and in aqueous buffer with 1 M NaCl (solid line), (b) in cast film from 10^{-3} M solutions in H_2O.*

The spectra consist of two regions, one with a bisignated signal at 250-280 nm assigned to TA, CG, AA and TT dinucleotides, and the other with a signal around 400 nm corresponding to the π-π* absorption region of *t4* and related to long-range electronic interactions between the *t4* moieties. Upon increasing the ionic strength of **29a-d** solutions by addition of NaCl hence increasing molecular aggregation, the dinucleotide signals display only minor variations while the *t4* signals show changes both in intensity and shape. Conjugate **29a** shows a very weak *positive* signal at 437 nm in aqueous buffer, but the chirality factor *g* increases in intensity by more than two orders of magnitude following addition of NaCl (see Table 5.5). Conjugate **29b** displays a signal inversion by adding NaCl, accompanied by a red shift of about 25 nm.

Conjugate **29c** shows a weak *positive* signal at 410 nm with the *g* value increasing by six times upon addition of NaCl. In this case the increase in g value of the signal at 410 nm is accompanied by the appearance of a further weak *positive* signal near 450 nm.

Conjugate **29d** shows a *negative* and broad signal around 387 nm in aqueous buffer, which upon addition of NaCl gives rise to a non symmetric bisignated signal with a stronger *negative* component at 384 nm and a weaker *positive* component at 443 nm with zero crossing at 420 nm. The bisignated signal is characteristic of an exciton coupling between chromophores in a chiral orientation.[5] In this specific case it indicates a *right-handed* helical arrangement of interacting *t4* moieties. In cast film **29d** shows the same bisignated signal displayed in solution at high ionic strength, with the zero crossing wavelength blue shifted to 407 nm. While conjugate **29a** in cast film shows an inverted, *negative*, signal blue shifted to 400 nm, for compound **29 b** the positive signal observed under addition of NaCl is retained in cast film.

Compound	Conditions	λ_{max}(nm)	$\Delta\varepsilon$	$g \times 10^4$	ψ
$^{5'}$TA$^{3'}$-t4-$^{3'}$AT$^{5'}$ **29a**	(a)	273, 250	+7.11,-12.50	+1.4,-2.1	
		437	+0.15	+0.06	
	(b)	276,254	+6.29,-19.25	+1.4,-2.7	
		437	+3.34	+1.4	
	(c)	279, 247			+0.75,-1.46
		400			-0.43
$^{5'}$CG$^{3'}$-t4-$^{3'}$GC$^{5'}$ **29b**	(a)	286,255	+6.74,-16.8	+3.2,-3.8	
		406	-3.16	-1.0	
	(b)	285,255	+4.80,-8.55	+1.8,-1.7	
		430	+4.43	+2.2	
	(c)	296,263			+2.69,-0.45
		419			+1.35
$^{5'}$AA$^{3'}$-t4-$^{3'}$AA$^{5'}$ **29c**	(a)	273, 253	+1.03,-7.03	+0.2,-1.2	
		410	+1.34	+0.3	
	(b)	273, 247	-0.81,-12.20	-0.1,-1.3	
		413	+7.37	+1.8	
	(c)	316,269			+0.3,-2.43
		367,407			+0.92,-1.16
		383			0
$^{5'}$TT$^{3'}$-t4-$^{3'}$TT$^{5'}$ **29d**	(a)	281,250	+4.01,-4.32	+1.2,-1.1	
		387	-1.09	+0.37	
	(b)	280,249	+3.14,-3.40	+1.0,-0.9	
		384,443	-1.61 ,+0.58	- 0.58,+0.22	
		420	0		
	(c)	278,246			+1.44,-0.95
		379,446			-0.94,+0.58
		407			0

(a) Aqueous buffer, pH = 7.4. (b) Aqueous buffer, 1 M NaCl. (c) Cast film from H_2O, from 10^{-3} M solutions.

Table 5.5. *CD data for **29a-d** conjugates.*

The behaviour of conjugate **29c** in cast film is more complex. The bisignated signal pertaining to the oligonucleotide scaffold becomes broad and there is the appearance of an exciton couplet in the region of *t4*, composed of a *negative* band at 367 nm and a *positive* band at 407 nm (zero crossing at 383 nm). This behaviour indicates that the interacting *t4* moieties are organized in a helical *left-handed* fashion.[5] The spectrum also shows some signal in the region around 450 nm, overlapping with the negative part of the bisignated signal.

Circular dichroism is one of the most sensitive techniques available for the analysis of the aggregation modalities in π-π* conjugated systems.[5,6] In the present case, CD spectra indicate fine variations in aggregation modalities of the conjugates on changing the oligonucleotide scaffold. In cast film it is the interplay between molecule-molecule and molecule-substrate interactions that governs the aggregation process. When molecule-molecule interactions are weak it is the interaction of the molecules with the surface that drives the formation of the supramolecular aggregate. Sign inversions in CD spectra from solution to film are commonly observed also in the case of oligothiophenes.[4b,d] The fact that in **29b** and **29d** the shape of the spectra do not change from solution to cast film is an indication that the aggregate formed by this conjugate is intrinsically more stable than those formed by **29a** and **29c**.

5.2.2 Shape of the aggregates

Conjugates **29a-d** are amphiphilic molecules, with hydrophobic (t4) and hydrophilic (TA, GC, AA, TT) moieties. As is typical of amphiphilic compounds,[7] casting of **29a-d** from water leads to the formation of spherical, globular or even dendritic aggregates depending on experimental conditions. However, in carefully controlled deposition conditions, we observed for all conjugates the formation of rod-like aggregates, showing that despite the very different intimate nature of **29a-d** aggregates on surfaces revealed by CD spectroscopy, their morphological habit in cast film was always the same. It consisted of an amorphous matrix containing numerous randomly oriented rods, the length of which could reach up to a hundred micrometers depending on the rate of solvent evaporation and the hydrophilicity of the surface employed (glass, glass covered with amylose, SiO_2 and mica were tested).

The samples were prepared in solvent saturated environment at room T to obtain the deposition in quasi-equilibrium conditions; 50 µl of a 1 mg/200µL H_2O solution were cast on glass and after complete solvent evaporation (~12 h) they were analyzed in ambient conditions by optical and fluorescence microscopies and AFM (see Figure 5.6).
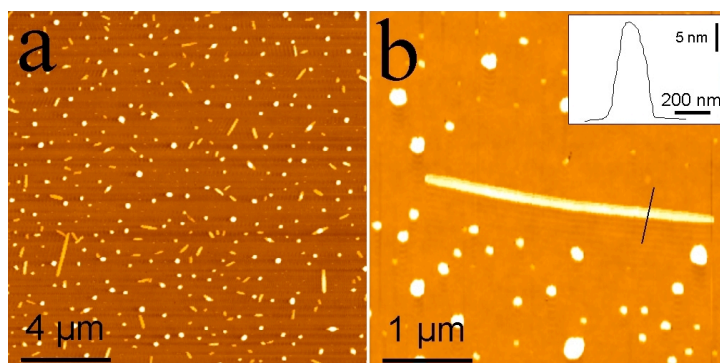

Figure 5.6 *(a) AFM image of a cast film of $^{5'}TA^{3'}$-t_4-$^{3'}AT^{5'}$ (29a) on glass displaying the formation of rod-like aggregates. Dimensions in (b): 3000x200x50 nm.*

No rod-like aggregates were observed when the solvent was quickly removed under vacuum. The longest rods were obtained employing a surface made of amylose deposited on glass. Upon UV irradiation all films displayed intense yellow-orange fluorescence emission. Figure 5.7 shows the fluorescence microscopy image and the corresponding optical microscopy image of a cast film of $^{5'}AA^{3'}$-t4-$^{3'}AA^{5'}$ (**29c**, 40 µl of a solution of concentration 1 mg/mL in H_2O) deposited at RT on a glass substrate covered with an amylose layer (50 µl of a solution of concentration 2 mg/ml in DMSO) and showing the formation of rod-like aggregates up to 100 micron length.
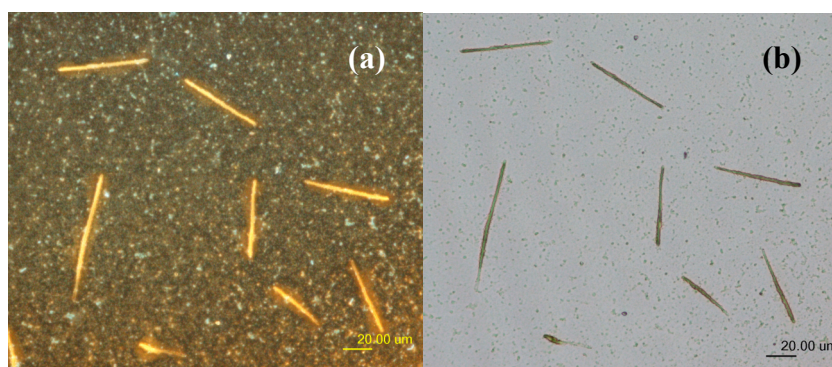

Figure 5.7. *Fluorescence (a) and optical (b) microscopy image of rod-like aggregates formed by deposition of $^{5'}AA^{3'}$-t4-$^{3'}AA^{5'}$, **29c**, on a glass substrate covered with a thick layer of amylose.*

Amylose, a linear polymer of α-1,4-linked glucose,[8] has a helical structure and once cast on glass forms a chiral surface. Thus, it cannot be excluded that chiral-chiral interactions between the chiral surface and the chiral conjugates contribute to the formation of the longest rods. However, since the formation of rod-like aggregates such as those shown in Figure 5.7 has never been observed with oligothiophenes, including those made amphiphilic by the presence of ethylene oxide chains,[4b] it is reasonable to ascribe their formation to the orienting effect of the dinucleotide scaffolds in **29a-d**.

5.2.3 Electrical characterization

The cast films of the conjugates were electroactive. Here are presented the electrical characteristics of **29c** and **29d**, for which cast films of suitable and comparable thickness in controlled conditions could be obtained. For comparison, the data relative to the precursor quaterthiophene **24a** (*t4*-OTHP), (see Figure 5.8), are also given.
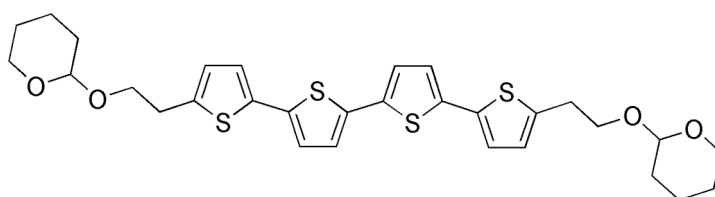
Figure 5.**8** *Molecular structure of quaterthiophene precursor* **24a** (*t4-OTHP*).

Cast films of **29c**, **29d** and the precursor quaterthiophene were deposited onto substrates consisting of two interdigitated Au electrodes fabricated by evaporating gold onto oxidised silicon wafers and patterned with photolithography .
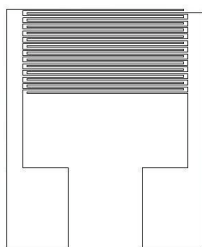

Figure 5.9 *Sketch of the interdigitated gold electrodes used for the electrical characterization.*

The electrical characterizations were performed at ambient temperature in a home made chamber, both in air and under dynamic vacuum. The procedure was repeated twice using samples from different preparations to ensure reproducibility of the results. When performing the electrical characterization in air, a dramatic dependence of the current on environment was observed for conjugates **29c**, **29d** (but not for **24a**). As an example, Figure 5.10 shows the current density-time (*J-t*) curves obtained for **29d** at constant applied voltage (100 V) in three different conditions. First, the current was measured in air and decreasing values with time at constant *d.c.* voltage were observed (curve 1). Soon after, the current was again measured in air (first portion of curve 2 in Figure 5.10 (a)) and lower values were obtained, indicating that the behaviour of the sample is affected by its past story. Then the rotary pump was turned on and an abrupt fall of the current was observed (curve 2). Finally, the current was measured at a pressure of 10^{-3} mbar, after two hours of pumping (curve 3). In this case, much lower currents were measured, but the *J-t* curve still showed a decreasing behaviour with time. These findings suggest a space-charge polarization effect of the sample, due to ionic currents, likely promoted by moisture, leading to increasing resistivity with time.[9] In order to avoid the ionic conduction, the samples were left in the measurement chamber for several hours under dynamic vacuum, until a constant current with time was observed under constant *d.c.* applied voltage. Figure 5.10 (b) shows the current density-voltage (*J-V*) curves of **29c**, **29d** and **24a** measured at ambient temperature under dynamic vacuum of 10^{-4} mbar. The figure shows that the reference compound *t4*-OTHP displays the highest currents, those of **29c** and **29d** being smaller by four and three orders of magnitude, respectively. It should be noted that the samples considered here are only hole-transporting samples because gold acts as a hole injecting contact, for which the work function (5.2 eV) is energetically matched to the highest occupied molecular orbital energy levels of the investigated materials[10] and prevents electron injection from the negatively biased electrode. We observed that for all samples the current density has a good quadratic dependence on the voltage in the high field region, as better shown in Figure 5.10 (b).
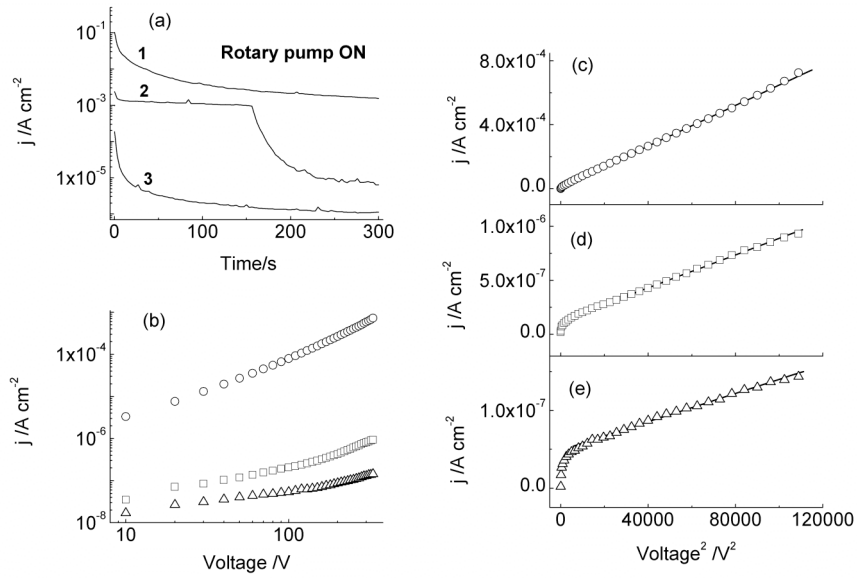
Figure 5.10 *(a). Current density versus time for **29d** sample at an applied voltage of 100 V: 1) in air; 2) while turning on the rotary pump after 150 s in air; 3) at a pressure of 10^{-3} mbar after two hours of pumping. (b). J-V characteristics of t4-OTHP (circles), **29d** (squares) and **29c** (triangles), measured at ambient temperature and under dynamic vacuum of 10^{-4} mbar. (c). Current density versus V^2 for t4OTHP sample. (d). Current density versus V^2 for **29d** sample. (e). Current density versus V^2 for **29c** sample. The lines represent the linear fit to the experimental data. The measurements were carried out at ambient temperature and under dynamic vacuum of 10^{-4} mbar.*

This behaviour is typical of space-charge limited current (SCLC,[11] given by $j = \dfrac{9}{8}\varepsilon_0\varepsilon_r\mu\dfrac{V^2}{L^3}$ in the trap-free regime, where ε_0 is the vacuum permittivity, ε_r is the relative dielectric constant of the material, μ is the charge carrier mobility and L is the electrode separation). By setting $\varepsilon_r = 3$, hole mobilities, μ_h, of 1.7×10^{-4}, 2.4×10^{-8} and 2.0×10^{-7} cm^2 V^{-1}s^{-1} were estimated for t4-OHP, **29c** and **29d**, respectively, from the slope of the linear portion of the J-V^2 curves (Figure 5.10(a)). That these values are reasonable is shown by the fact that the estimated hole mobility for t4-OHP is of the same order of magnitude as the FET (Field Effect Transistor, a 3-electrode device) hole mobility measured for cast films of quaterthiophene, [12] while those of **29c** and **29d** are of the same order as the FET hole mobilities recently measured for cast films of oligo(p-

phenylene vinylene) functionalized with ureido-*s*-triazine groups.[13] Of course, a more precise evaluation of the hole mobilities of conjugates must await for FET measurements to be carried out. However, what is significant in the present context is that a change in the dinucleotide scaffold leads to almost one order of magnitude difference in the measured currents of **29c** and **29d**. Moreover, it is tempting to make a correlation with CD data and ascribe the higher current measured for **29d** to its more ordered molecular organization.

5.2.4 Molecular Modeling

In order to shed light on the molecular mechanism of self-assembly of the quaterthiophene-dinucleotide conjugates, theoretical calculation were carried out on the homogeneous set of compound **29a**, **29c** and **29d**, all constituted by A or T nucleotides. Conformational preferences and the ability to form stable supramolecular aggregates in water solution were investigated by Molecular Mechanics and Molecular Dynamics calculations. The search of minimum energy conformations for monomers and dimers was carried out by means of simulated annealing protocols in gas phase as well as in the presence of the solvent.[14a] The calculations were performed within the AMBER force field.[14b] Furthermore, an implicit solvent model was used to simulate the presence of water and reduced charges on the phosphate groups to account for the presence of the counterions.[14c]

For the monomeric conjugates, two main conformations were found, one with syn and the other with anti oligonucleotide arms with respect to the mean plane of nearly planar t4, as shown in Figure 5.11. For all systems the syn form was energetically favoured over the anti form by a few kJ mol^{-1} (Figure 5.11).

In the syn conformation the dinucleotide arms are folded over the t4 backbone, aligned at stacking distance, and forming intramolecularly H-bonded A···A or T···T pairs. The distance between the π-system of t4 and the adjacent base pair falls in the range of 3.3-3.5 Å, as in the B-form of DNA,[15] close to that found in stilbene-oligonucleotide conjugates,[6] but shorter than that, 3.7 Å, calculated in stacks of chiral oligothiophenes.[4b]
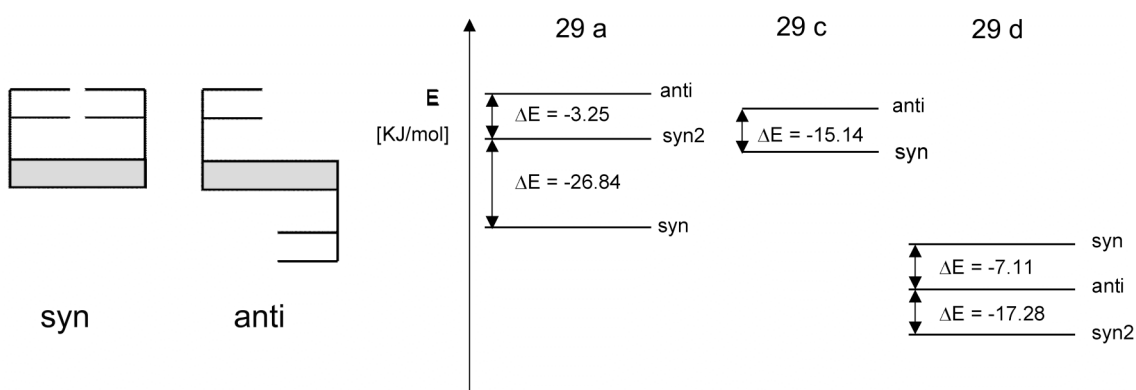
Figure 5.11 *Sketch of the syn and anti forms of conjugates 29a, 29c, 29d and calculated energy differences (kJ mol^{-1}). Green = t4, black = oligonucleotide arms.*

The most favoured syn conformations and stacking distances of the conjugates are reported in Figure 5.12, showing that the preferred conformation is made of a hydrophobic core surrounded by phosphate groups.

Figure 5.12 *Most favored syn conformations and stacking distances of conjugates 29a, 29c and 29d.*

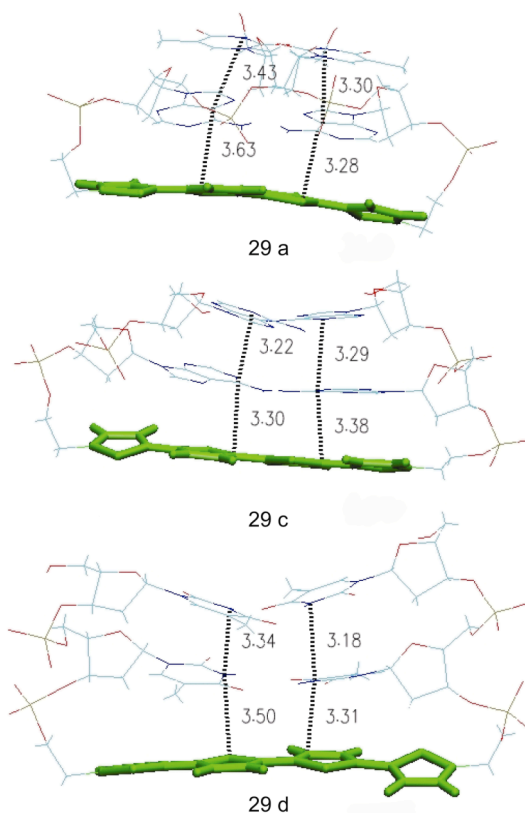During the aggregation process the syn and anti monomeric conformations give rise to different supramolecular systems. The free energies of both types of aggregates were calculated using the equation $\Delta G_{298} = E\ (MM) - RTlnQ$, where E is the energy and Q the partition function. For all conjugates the aggregate of the syn form is more stable than that of the anti form. The largest difference, -50.16 KJmol^{-1}, is that for **29d** and the smallest difference, -20.9 KJmol^{-1}, that for the **29a** conjugate, probably due to a greater stabilization of the aggregate of the anti form since the base pairing occurs between self-complementary bases. The calculated free energies of the dimers formed by the syn and anti conformers of conjugates **29a**, **29c** and **29d** are reported in Table 5.13, together with electrostatic, van der Waals and solvation contributions to the total energy.

systems	$\Delta\Delta G$ (300K-0K) [KJ/mol]	ΔE [KJ/mol]	$-T\Delta S$ [KJ/deg-mol]	Van der Waals [KJ/mol]	Total Energy [KJ/mol]	Solvation [KJ/mol]	Electrostatic [KJ/mol]
Dimer-*C* 29c	-65.151	-124.215	56.410	-511.36	-3203.54	-660.22	-3026.10
Dimer-*H* 29c	-24.136	-83.912	54.012	-537.09	-3163.21	-730.37	-2913.70
Dimer-*C* 29a	-59.609	-117.668	70.212	-557.55	-4271.62	-707.85	-4037.61
Dimer-*H* 29a	-37.322	-96.261	72.912	-530.25	-4250.15	-703.88	-4044.76
Dimer-*C* 29d	-48.499	-101.745	52.204	-493.91	-5243.58	-766.71	-4995.82
Dimer-*H* 29d	+0.820	-52.425	55.205	-481.18	-5194.24	-761.35	-4956.31

* C = dimer from the syn conformation; H = dimer from the anti conformation

Table 5.13. *Sketch of the dimers formed by the syn (C) and anti (H) conformers of conjugates **29a**, **29c** and **29d** and the corresponding calculated free energies.*

The calculated free energies indicate that the aggregation process is not driven by entropy differences, as the entropic contribution is very similar for both aggregates. Figure 5.14 displays the geometry of the dimers of the favoured syn forms of **29a**, **29c** and **29d**, together with the corresponding top views showing the relative orientation of the two *t4* moieties.
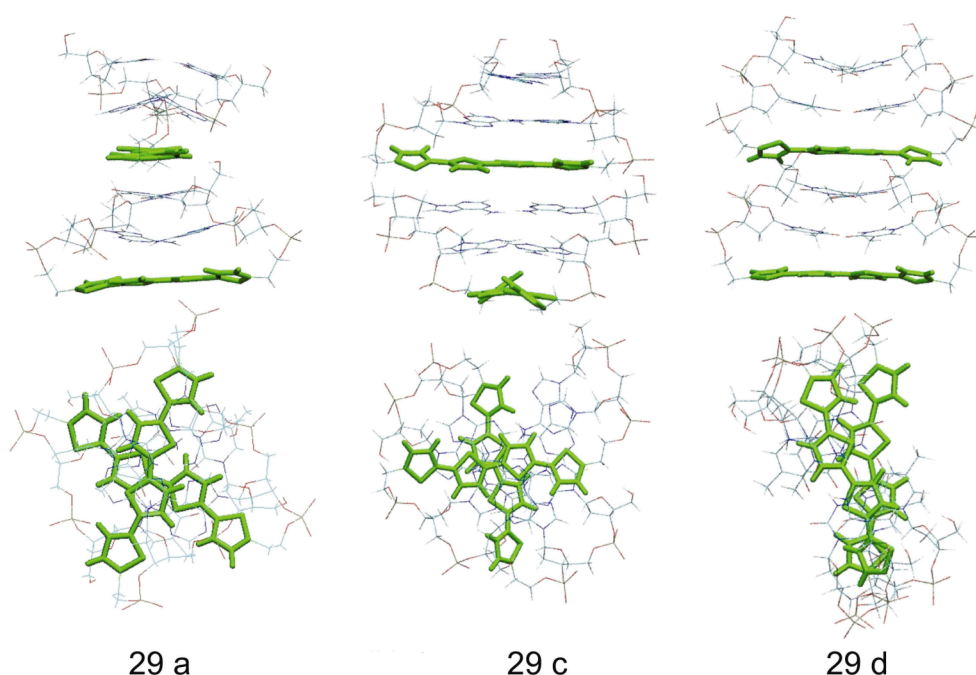
29 a   29 c   29 d

Figure 5.14 *Most stable dimers of conjugates **29a**, **29c** and **29d** and corresponding top views showing the relative orientation of the t4 backbones. In **29a** and **29c** the adjacent t4s form a nearly perpendicular dihedral angle while in **29d** they form a dihedral angle of about 10°.*

The calculations show that the formation of the dimers of the favoured syn form is driven by the stacking interactions between the upper base-pairs in 5' of the first monomer and the quaterthiophene of the second monomer in order to maximize the intermolecular stacking interactions during the aggregation process. Even in **29a** with self-complementary TA ends – for which there was the possibility that it would form *inter*molecularly connected A···T Watson & Crick base-pairs - the stacking interactions impose the same conformation and aggregation modalities as in the other conjugates, with the formation of intramolecularly connected A···A and T···T base pairs.

The dihedral angle that the quaterthiophene of the second monomer forms with that of the first monomer is determined by the orientation of the upper base pair in the single monomer. As a consequence, the *t4* moieties within the dimers are rotated with respect to each other by an angle which depends on the nature of the dinucleotide ends. While

in the dimers of **29a** and **29c** the quaterthiophene moieties are almost perpendicular, in the dimer of **29d** they form a dihedral angle of about 10° (Figure 5.14).

Finally, our calculations (not reported) show that on increasing the number of aggregated molecules, the energy difference between the aggregates of the syn and anti forms increases, with the former becoming more and more favoured owing to electrostatic contributions to the total energy.

The calculations offer a key to the interpretation of the CD spectra. Besides the intrinsic molecular chirality due to the presence of the chiral nucleotide scaffolds, there is an additional supramolecular chirality arising from the way the molecules pile up during the aggregation process, indicated by the presence of a CD signal in the region pertaining to the π-π* transition of t4. Assuming, as is reasonable, that quaterthiophene transition dipoles are polarized along the long molecular axis, the presence of an exciton coupling in **29d** in solution at high ionic strength (with a -/+ pattern indicative of a right-handed helical organization) is in agreement with the value of 10° calculated for the dihedral angle between adjacent *t4*s.[5,6] A columnar helical aggregate is formed in which adjacent *t4* moieties are progressively staggered by 10° in the same direction; the aggregate is stable enough to be frozen as such in cast film. No exciton coupling is expected when the transition dipoles are perpendicular,[5,6] as indicated by the calculations for **29a**, **c**. In agreement with this, no exciton coupling is displayed by the CD spectra of these compounds in solution.

The calculations also offer a clue to the understanding of the formation of rod shaped supramolecular structures in cast films of **29a**, **29c** and **29d** prepared in quasi-equilibrium conditions. Shape and dimension of the aggregates suggest that they are formed via a self-assembly process starting with syn **29a**, **29c** and **29d** piling up in columns. Then side-to-side aggregation of the columns takes place via electrostatic interactions between negatively charged phosphate groups and positively charged counterions leading to the formation of bi- and tridimensional rods.

5.3 Conclusions

In conclusion, we demonstrated that the quaterthiophene-dinucleotide hybrid systems described here lead to the formation of chiral supramolecular assemblies and afford cast films which are photoluminescent and electroactive. Thiophene-nucleobase stacking

interactions orient the molecular conformation towards the form with syn dinucleotide ends and the self-assembly modalities towards the formation of columnar aggregates. The films show fine changes in optical and electrical properties on changing the dinucleotide scaffold. These results pave the way to the synthesis of oligothiophene-oligonucleotide hybrid structures in which different competing intra- and intermolecular interactions (thiophene-nucleobase stacking interactions, hydrogen bonding interactions between nucleobases, oligothiophene-oligothiophene van der Waals interactions, etc) can be exploited by varying oligonucleotide length, substitution pattern and oligothiophene size, to build supramolecular assemblies with programmed functional properties.

5.4 Experimental Section

UV-Vis spectroscopy: Absorption spectra were recorded with a Perkin-Elmer Lambda 20 spectrometer in aqueous solution ($5 \cdot 10^{-6}$ M, pH=7.4) and in cast film on quartz (100 µl of 10^{-3} M solution) after solvent evaporation.

CD spectroscopy: CD spectra were recorded with a Spectropolarimeter JASCO J-715, under ambient condition, in aqueous solution ($\sim 10^{-5}$ M, pH=7.4) and in cast film on quartz (100 µl of 10^{-3} M solution) after solvent evaporation.

Fluorescence microscopy: Nikon Eclipse 80i optical microscope was used for optical measurements. The images were recorded with a digital color camera Nikon Digital Sight DS-2Mv. Glass substrate were furnished by Knittel gläser and were previously washed with Acetone spectroscopic grade (Aldrich). Films were cast from H_2O (~ 50 µL, c$\sim 10^{-4}$ M) on glass substrates and the solvent was evaporated under saturated atmosphere.

Molecular modeling: The supramolecular assemblies structures were fully optimized using the AMBER* force field. All the molecular mechanics calculations were performed with the MacroModel software package.[16]

Electrical characterization: Substrates consisted of two interdigitated comb-like gold electrodes (13 pairs of electrode fingers, see Figure S8) deposited onto a layer of silicon dioxide thermally grown on silicon plates. The thickness of the oxide was 1 µm and that of the metal layer was 0.6 µm. The gap between the interdigitated electrodes and the width of the Au electrodes were 20 µm and 40 µm, respectively. The length of the Au

fingers was 3.0 mm. The surface configuration was chosen to avoid metal diffusion through the organic layer, a common problem of evaporated electrodes onto sandwich-type structures. The organic films were deposited onto the substrates by casting a chloroform solution (5 μL), in the case of t4-OTHP, or H_2O solution (5 μL), for **8b** and **8c**, in order to completely cover the interdigitated area. The concentration of the solutions was 25 gL^{-1}, leading to films with a thickness (0.7 – 1.0 μm, as measured by a Tencor Alphastep 200 profilometer) greater than that of the electrodes layer. The samples were dried at ambient condition. The electrical characterization was performed, at ambient temperature, in a home-made chamber, both in air and under dynamic vacuum. The characterization in dynamic vacuum was carried out after several hours of pumping. The current-voltage and current-time measurements were carried out by using a Keithley 487 source-picoammeter.

5.5 References

[1] a) H. A. Ho, M. Béra-Abérem, M. Leclerc, *Chem. Eur. J.* **2005**, *11*, 1718–1724; b) A. Herland, P. Björk, K. P. R. Nillson, J. D. Olsson, P. Åsberg, P. Konradsson, P. Hammarström, O. Inganäs, *Adv. Mater.* **2005**, *17*, 1466-1471; c) H. A. Ho, K. Dorè, M. Boissinot, M. G. Bergeron, R. M. Tanguay, D. Boudreau, M. Leclerc, *J. Am. Chem. Soc.* **2005**, *127*, 12673-12676; d) K. Peter, R. Nilsson, O. Inganas, *Nature Materials* **2003**, *2*, 419-424.

[2] B. Liu, G.C. Bazan. *Chem. Mater* **2004**, *16*, 4467-4476; b) H. A. Ho, M. Boissinot, M. G. Bergeron, G. Corbeil, K. Doré, D. Boudreau, M. Leclerc. *Angew. Chem. Int. Ed.* **2002**, *41*, 1548-1551, Angew. Chem. **2002**, *114*, 1618-1621.

[3] a) Y. Kanemitsu, K. Suzuki, Y. Masumoto, *Phys. Rev. B* **1994**, *50*, 2301-2305; b) R. S. Becker, J. Seixas de Melo, A. L. Maçanita, F. Elisei, *J. Phys. Chem.* **1996,** *100,* 18683-18695; c) M. Melucci, G. Barbarella, M. Zambianchi, P. Di Pietro, A. Bongini, *J. Org.*

Chem. **2004**, *69*, 4821-4828; d) M. Melucci, G. Barbarella, G. Sotgiu, *J. Org. Chem.* **2002**, *67*, 8877-8884.

[4] a) D. G. Whitten, *Acc. Chem. Res.* **1993**, *26*, 502-509; b) O. Henze, W. J. Feast, F. Gardebien, P. Jonkheijm, R. Lazzaroni, P. Leclère, E. W. Meijer, A. P. H. J. Schenning, *J. Am. Chem. Soc.* **2006**, *128*, 5923-5929; c) F. Meinardi, M. Cerminara, S. Blumstengel, A. Sassella, A. Borghesi, R. Tubino, *Phys. Rev. B* **2003**, *67*, 184205-1-6; d) M. Melucci, G. Barbarella, M. Gazzano, M. Cavallini, F. Biscarini, A.Bongini, F. Piccinelli, M. Monari, M. Bandini, A. Umani-Ronchi, P. Biscarini, *Chem. Eur. J.* **2006**, *12*, 7304 – 7312.

[5] a) *Circular Dicroism*, (Eds.: N. Berova, K. Nakanishi, R. W. Woody), Wiley, New York, **2000**; b) *Circular Dichroic Spectroscopy*, (Eds.: N. Harada, K. Nakanishi), Oxford University Press, Oxford, **1983**.

[6] F. D. Lewis, L. Zhang, X. Liu, X. Zuo, D. M. Tiede, H. Long, G. C. Schaz, *J. Am. Chem. Soc.* **2005**, *127*, 14445-14453.

[7] H. W. Jun, S. E. Paramonov, J. D. Hartgerin, *Soft Matter* **2006**, *2*, 177-181.

[8] K. Ohdan, K. Fujii, M. Yanase, T. Takaha, T. Kuriki, *Biocatalysis and biotransformation* **2006**, *24*, 77-81.

[9] D.R. Lamb, *Electrical Conduction Mechanisms in Thin Insulating Films,* Methuen, London, 1967.

[10] C. D. Dimitrakopoulos, P. R. L. Malenfant, *Adv. Mater.* **2002**, 14, 99-117

[11] M. A. Lampert, P. Mark, *Current Injection in Solids,* Academic Press, New York, **1970**.

[12] H. E. Katz, J. G. Laquindanum, A. Lovinger, *J. Chem. Mater.* **1998**, *10*, 633-638

[13] P. Jonkheijm, N. Stutzmann, Z. Chen, D. M. de Leeuw, E. W. Meijer, A. P. H. J Schenning, A. P. H. J., F. Würthner, *J. Am. Chem. Soc.* **2006**, *128*, 9535-9540.

[14] a) A. Acocella, A. Venturini, F. Zerbetto, *J. Am. Chem. Soc.* **2004**, *126*, 2362-2367. b) J. Scott, P. A. Weiner, D.A.; Kollman, U. Case. *J. Comput. Chem.* **1990**, *11*, 440–467. c) C. Singh, C. Ghio, G. Alagona, S. Profeta, P. Weiner, *J. Am. Chem. Soc.* **1984**, *106*, 765–784. d) W. Clark Still, A. Tempczyk, R. C. Hawley, T. Hendrickson, *J. Am. Chem. Soc.* **1990**, *112*, 6127–6129.

[15] *Nucleic Acids. Structures, Properties and Functions*, (Eds.: V. A. Bloomfield, D. Crothers, I. Tinoco), University Science Books, Sausalito, CA, 2000.

[16] F. Mohamadi, N. G. J. Richards, W. C. Guida, R. Liskamp, M. Lipton, C. Caufield, G. Chang, T. Hendrickson, W. C. Still. *J. Comput. Chem.* **1990**, *11*, 440-467.

Chapter 6

Dinucleotide-driven self-organization of quinquethiophene semiconductors

Abstract:

The optical and self-organization properties of the quinquethiophene bioconjugates, synthesized in Paragraph 3.3, Chapter 3, have been investigated by means of Uv-vis and Photoluminescence spectroscopy, circular dichroism and optical/fluorescence microscopy. Molecular Mechanics and Molecular Dynamics calculations predict for compound TA-t5 a radial self-assembly process driven by intermolecular stacking between quinquethiophene and the nucleobases. Such intrinsic tendency to aggregate trough dendritic modalities was expressed also at micrometer scale and observed in cast as well as in microfluidic (MIMIC) deposited films. Characterization in two contacts devices, under SCLC conditions, revealed semiconducting behaviour with an estimated charge mobility value one order of magnitude higher than that of the quaterthiophene-dinucleotide bioconjugates reported in Chapter 5.

6.1 Introduction

The studies, described in Chapter 5, on quaterthiophene biohybrid compounds, where quaterthiophene was linked, at both terminal positions, to TA, CG, AA and TT dinucleotides allowed us to achieved useful informations on the dynamics and interactions between nucleotides and thienyl rings. In particular we highlighted that the crucial driving force for their self-assembly are the intra and intermolecular p-stacking interactions between oligothiophene and nucleobases.

In this chapter we discuss the quinquethiophene based systems **36a** and **36b** synthesized in Chapter 3, Paragraph 3.3., having a different molecular design respect to that of quaterthiophene bioconjugates, consisting of asymmetric systems having a couple of self-complementary nucleotide at the inner thienyl beta position (Figure 6.0).
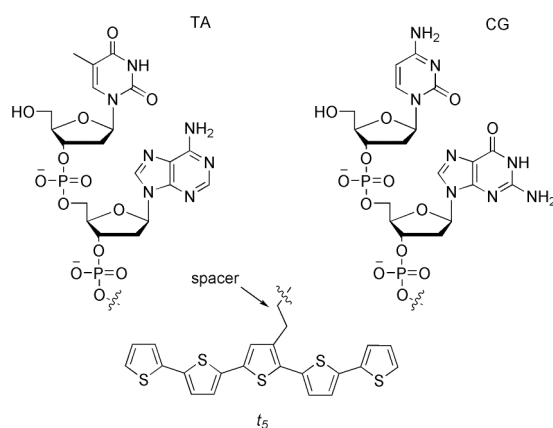

Figure 6.0 *Building blocks composing the molecular structure of conjugates $^{5'}TA^{3'}$-t5 36 a, $^{5'}CG^{3'}$-t5 36 b.*

As in the case of quaterthiophene-dinucleotide conjugates, the characterization of the quinquethiophene-dinucleotide hybrids was carried out by means of a combination of different spectroscopy and microscopy techniques, Molecular Mechanics and Molecular Dynamics calculations and electrical measurements. For compound TA-t5 (**36a**) we observed that the peculiar interplay of conformational flexibility and the regiochemistry of the substitution of the aromatic skeleton allow a high tendency to aggregation into dendritic structures upon solution casting from water.

Moreover, we demonstrated that fine control of its morphology and confined deposition over a micrometer range can be achieved by Micro-molding in capillaries (MIMIC).

6.2 Results and discussion

6.2.1 Optical properties (UV, PL, CD)

Conjugates **36a**,**b** are photoluminescent compounds in water solutions and in cast films. Their UV-vis and photoluminescence (PL) spectra in H_2O and in cast films prepared from a 10^{-3} M aqueous solutions are shown in Figures 6.1 (a) and 6.1 (b), respectively, while absorption and PL wavelengths are reported in Table 6.2.
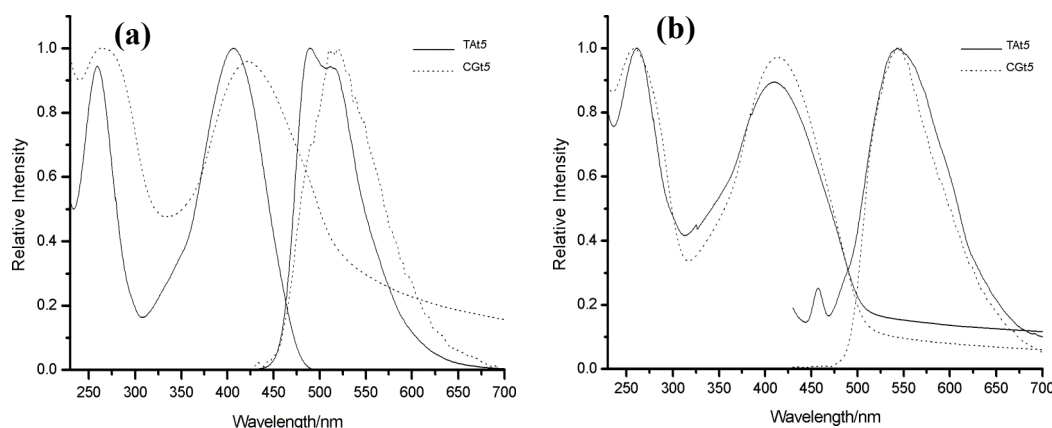

Figure 6.1 *UV-vis and PL spectra (λ_{exc}=410 nm) of conjugates $^{5'}TA^{3'}$-t5 **36a** and $^{5'}CG^{3'}$-t5 **36b** in H_2O (a) and in films cast from a 10^{-3} M water solution (b).*

Compound	Conditions	λ_{max}(nm)	λ_{PL} (nm)
$^{5'}TA^{3'}$-t5 (**36a**)	(a)	259, 406	499, 512
	(b)	262, 411	544
$^{5'}CG^{3'}$-t5 (**36b**)	(a)	263, 422	520
	(b)	259, 413	547

(a) Aqueous solution, $5 \cdot 10^{-6}$ M, pH=7.4 (b) Cast film from a 10^{-3}M solution in H_2O.

Table 6.2 *Maximum absorption and photoluminescence wavelengths of conjugates 36a and 36b.*

The UV-vis spectra in solution consist of a signal around 260 nm, due the oligonucleotide moiety, and a signal around 410 nm due to quinquethiophene. For compound **36a** the PL spectrum in solution, arising from the *t5* moieties, consists of a main signal split in two bands near 500 nm and one red shifted shoulder in the region 550-600 nm. These spectra are very similar to those of 'free' quinquethiophene, and, in

general, to those of thiophene oligomers in solution.[1] PL spectrum in solution of compound **36b** is very similar to that one obtained in solid state, due to its scarce solubility in water. The UV-vis signals of both the conjugates in cast films are almost superimposable and *blue* shifted by 5-9 nm with respect to those in solution, whereas the signals pertaining to the dinucleotide scaffolds remain unchanged. PL signals in cast films are *red* shifted by 30 nm with respect to the solution. Although these blue shifts in the UV-Vis spectra and red shifts of the PL band are smaller, compared to those obtained for the bioconjugates of the quaterthiophene (see Chapter 5), also for compounds **36a** and **36b** the formation of H-type aggregatescan be hypothesized. Anyway, contrarily of bioconjugates of quaterthiophene, the PL signals of **36a,b** in cast films did not exhibit a remarkably sharpening with respect to the solution and the contemporaneous emission of different types of aggregates can not be excluded.

However, further studies are required to fully elucidate the relationship between the aggregation modalities of **36a** and **36b** and their photophysical properties.

Because of the scarce solubility of compound **36b** in both organic solvents and water, the circular dichroism (CD) experiments, the characterization of the aggregates and the electrical measurements were carried out only on compound **36a**.

As in the case of quaterthiophene-dinucleotide derivatives, discussed in Chapter 5, Paragraph 5.2.1, CD measurements showed a transfer of chirality from the dinucleotide substituents to the quinquethiophene moiety in solution and in cast films. The CD spectra of the bioconjugate **36a** 10^{-5} M in aqueous buffer (pH = 7.4), aqueous buffer containing 1 M NaCl and in cast films from H_2O solutions are shown in Figure 6.3(a) and 6.3(b). The detailed CD data of **36a** are reported in Table 6.4.The spectra consist of two regions, one with a bisignated signal at 250-280 nm assigned to TA dinucleotide, and the other with a signal around 400 nm corresponding to the π-π* absorption region of *t5* and related to long-range electronic interactions between the *t5* moieties.
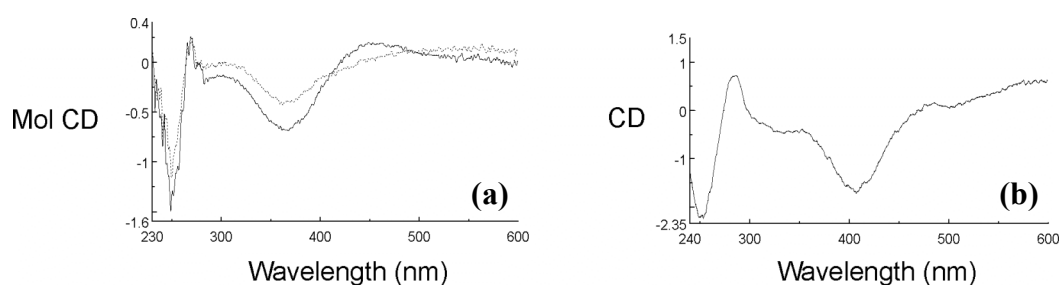
Figure 6.3 *CD spectra of conjugates $^{5'}TA^{3'}$-t5* **36a**, *(a) in aqueous buffer (pH = 7.4, (black line) and in aqueous buffer with 1 M NaCl (red line), (b) in cast film from 10^{-3} M solutions in H_2O.*

Compound	Conditions	λ_{max}(nm)	$\Delta\varepsilon$	g x 10^4	ψ
$^{5'}TA^{3'}$-t5 **36a**	(a)	270, 250	+0.21,-1.16	+0.08,-0.29	
		362	-0.41	-0.43	
	(b)	269, 249	+0.26,-1.49	+0.09,-0.44	
		457	+0.19,-0.68	+0.19,-0.6	
		366			
	(c)	276, 253			+0.73,-2.23
		407			-1.71
		383			0

a) Aqueous buffer, pH = 7.4. b) Aqueous buffer, 1 M NaCl. c) Cast film from H_2O, from 10^{-3} M solutions.

Table 6.4 *CD data for36a conjugate.*

Upon increasing the ionic strength of **36a** solutions by addition of NaCl hence increasing molecular aggregation, the *t5* signals show the appearance of a weak *positive* band near 450 nm other than the signal at 362 nm, already present in aqueous buffer. In cast film **36a** shows the t5 negative signal red shifted of 55 nm (to 407 nm), with respect to that observed in solution. According to the trimeric structure proposed by theoretical calculations no exciton coupling signal was detected for compound **36a**.

As in the case of quaterthiophene biohybrid derivatives **29b** and **29d**, CD spectra of **36a** do not present changes in shape or sign inversions[1b,d] , from solution to cast film, suggesting that the aggregates formed by this conjugate are intrinsically stable.

6.2.3. Shape of the aggregates

 Preliminary studies on **36a** cast films showed the presence of an amorphous matrix containing numerous open dendritic structures randomly-oriented. Highly curved multifiber and star-shaped aggregates, were also observed. Aggregates lengths reach up to hundred micrometers when the samples were prepared casting 50 µl of a 1 mg/mL H_2O solution on glass and the solvent evaporation occurs in saturated environment at room T, for 12 h. No formation of aggregates were observed when the solvent was quickly removed under vacuum. Upon UV irradiation cast films displayed intense yellow-orange fluorescence emission. Figure 6.5 shows the fluorescence microscopy image of a cast film of $^{5'}TA^{3'}$-t5 **36a.** Noteworthy, cast films of quinquethiophene **32** show an amorphous morphology independently on the deposition conditions, this highlighting the key role of the dinucleotides on the aggregation phenomena.
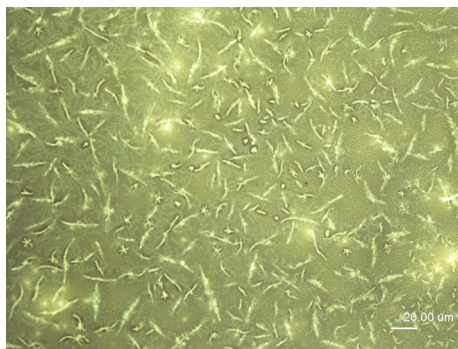

Figure 6.5 *Fluorescence microscopy image of aggregates formed by deposition of $^{5'}TA^{3'}$-t5´, 36a, on a glass substrate.*

6.2.4 Microfluidic-induced self-assembly

Micro-molding in capillaries (MIMIC)[2] is based on microfluidic properties of liquids in restricted geometries, characterized by the fact that the imbibition of liquids and the consequent filling motion are driven by capillary forces and surface effects, which dominate over the bulk dynamics. In particular, this means that microfluidic systems usually fulfil a *fast diffusion regime,* in which the interactions of liquid molecules with surface dominate over molecular diffusion components of the capillary dinamycs.[3] Therefore, the capillarity phenomena usually result from the balance of two opposing forces: liquid adhesion to solid surface, which tends to spread the liquid, and the cohesive surface tension force of the liquid, which acts to reduce the liquid-vapour

interfacial area.[4] Thus it is clear how such phenomena, depending from surface effects, interfacial properties and geometry, play a very important role in the control of the liquid dynamics, as well as in the possibility to finely address self-assembly and supramolecular organization of functional materials in micron and nano-structures.[5]
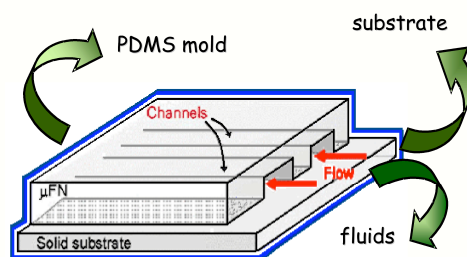

Figure 6.6 *The used micro-channels network were obtained by structured elastomeric elements in poly(dimethylsiloxane) (PDMS), realized by replica molding [5b,6] from silicon masters with 28 μm – large and about 1.5 μm height stripes (see Experimental Section).*

The replicas have been imbibed with aqueous solutions of quinquethiophene conjugate (**36a**) at different concentrations, that have filled elastomeric channels by capillary effect. After the complete evaporation of H_2O the PDMS mould have been peeled off, leaving a striped pattern of molecular material deposited on the silicon substrate.

The optical characterization of the stripes of TA*t*5, patterned by microfluidics, shows remarkable differences in the supramolecular organization of the molecular material in the solid state at changing both of the solution concentration and of the kinetics of evaporation. The volume of solution, deposited and penetrated inside the PDMS channels by capillarity, has been kept constant for all samples.

In the case of samples prepared with a concentration of 1 mg /ml and evaporated in 1 hour, atomic force microscopy (AFM) measurements reveal well-defined quadrangular-plate aggregates, put one on the top of the other in an orderly way (See Figure 6.7).
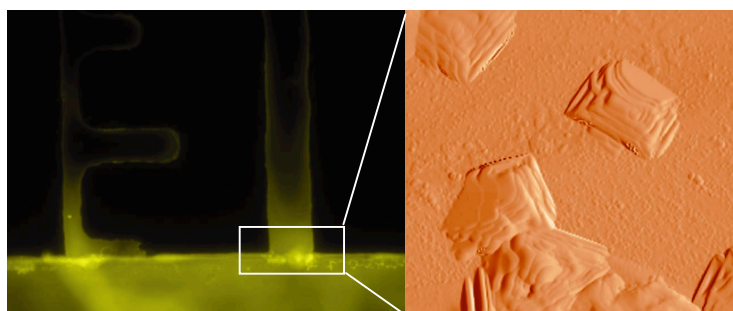
Figure 6.7 *Confocal and AFM characterization of quadrangular-plate aggregates obtained in diluted samples*

Conversely, in the AFM topography of more concentrated samples (2 mg/1 ml) evaporated in 1 h we observe that TA-t*5* organizes under capillary driving forces in a supramolecular structure made up of rod-like aggregates, spatially arranged at precise angles. The macroscopic feature of these sample seems like a star with a lateral dimension of about 10 μm (Figure 6.8).
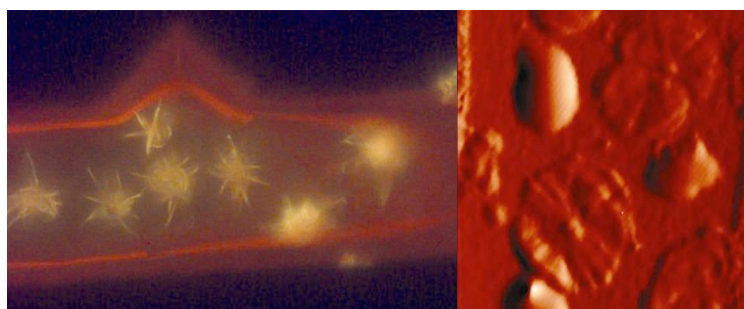

Figure 6.8 *Confocal and AFM characterization of star-shaped aggregates in concentrated samples*

It is worthwhile to highlight the presence of a sort of nucleation site in the vertical arrangement of the molecular material. This morphology is in good agreement with theoretical calculations regarding to the more probable self-assembly dynamics with a star-shape arrangement and to the existence of a sort of vertical axis, around which the supramolecular organization develops.

In order to deeper investigate the structural characteristic of the TA-t*5* films, we carried out integrated and spatially resolved photoluminescence (PL) spectra by confocal

microscopy. All samples showed similar PL spectra with a maximum at 540 nm and spatially resolved confocal spectra allowed to attribute the PL emission to the patterned area and to self-assembled material with a nanometer resolution.

Finally, samples of compound **36a** with a concentration of 6 mg /ml have been deposited. Because of the higher viscosity of such a solution, we chose to modulate the evaporation time during the driving motion, in order to reduce the typical velocity of a capillary motion, described by [5b]

$$\frac{dz}{dt} = \frac{G\Delta p}{\eta z}$$

where G is a geometric factor, Δp the capillary pressure and η the solution viscosity.

We observed an useful reduction of the capillary velocity by saturating the external condition during the dynamical process, in order to raise the evaporation time of water and thus to realize a fine control of the driving flow. More importantly, the reduction of the fluidic velocity, resulting at long times in saturated conditions, realizes a better control of the self-assembly process and an enhancing of order in the supramolecular organization of TA-t5.

Figure 6.9 shows the AFM topography of the striped pattern and, in particular, of the dendritic self-assembled molecular formation. We can recognize in the AT-t5 morphology the same rod-like crystals arranged at precise angles around a vertical axis, that acts as nucleation site. Besides, the optical images in 6.9 reveal that the self-assembly processes under saturated and at slow evaporation conditions keep on with the evaporation process and the supramolecular structure, thus formed, takes up all the available channel area.

Finally, the optical properties of these samples, detected by confocal spatially resolved PL spectra, are quite similar to the properties of other samples with a maximum at about 540 nm.

As demonstrated from MIMIC experiments TA-t5 posses an high tendency to aggregation, resulting into micrometric dendritic structures, able to cover all the microfluidic channel area.
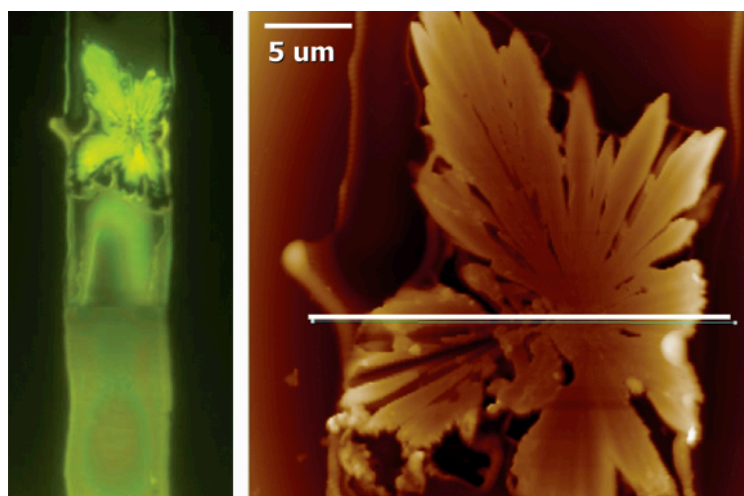
Figure 6.9 *Confocal and AFM characterization of dendridic aggregates formated in more concentrated samples with long evaporation time*

6.2.5 Electrical characterization

Solution-cast films of **36a** were deposited onto substrates consisting of two interdigitated Au electrodes fabricated by evaporating gold onto oxidised silicon wafers and patterned with photolithography. The surface device configuration was chosen to avoid metal diffusion through the organic layer, a common problem of evaporated electrodes onto sandwich-type structures. In order to avoid ionic conduction, activated by moisture the electrical characterization was performed under a dynamic vacuum of $2x10^{-5}$ mbar. In addition, the samples were left in the measurement chamber for several hours under dynamic vacuum, until a constant current with time was observed under constant d.c. applied voltage, before starting the electrical characterization.

It should be noted that the samples here considered are hole-only devices because gold acts as a hole injecting contact, for which the work function (5.2 eV) is energetically matched to the highest occupied molecular orbital energy levels of the investigated materials[7] and prevents electron injection from the negatively biased electrode. Furthermore, the complete symmetry of the two gold electrodes does not lead to a built-in voltage.

The current density–voltage (J-V) characteristic of a **36a** film onto interdigitated Au electrodes obeys to Ohm's law at low voltages, then the current shows a good quadratic

dependence on the voltage (Figure 6.10). This behaviour is typical of space-charge limited current (SCLC),[8] given by $j = \dfrac{9}{8}\varepsilon_0\varepsilon_r\mu\dfrac{V^2}{L^3}$ in the trap-free regime, where ε_0 is the vacuum permittivity, ε_r is the relative dielectric constant of the material, μ is the charge carrier mobility and L is the electrode separation. Even when the trap-free limit is not experimentally accessible, the above formula can be used to extract a lower limit for the intrinsic mobility of the material, at least in the case in which one type of carriers (holes in the present case) is responsible for charge transport. By using $\varepsilon_r = 3$, a hole mobility of 5.8×10^{-6} cm^2 V^{-1} s^{-1} was calculated for **36a**. This value has to be considered as a lower limit for the hole mobility of **36a**, the SCLC current being reduced by the presence of traps.
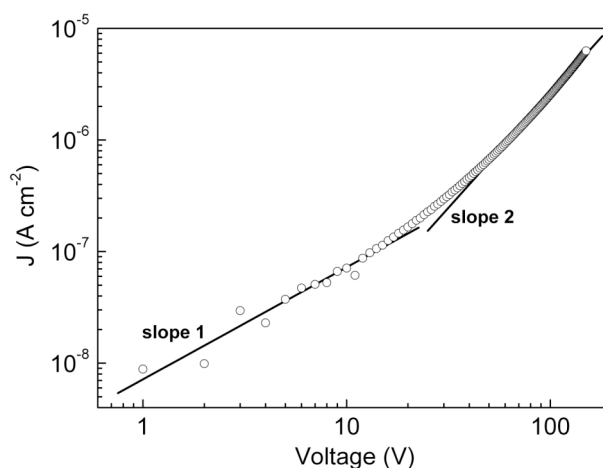

Figure 6.10 *Log-log plot of the J-V characteristic of a **36a** film onto gold interdigitated electrodes. The measurement was carried out at room temperature and under dynamic vacuum of 2×10^{-5} mbar.*

The present hole mobility value is one or two order of magnitude higher than those measured for bioconjugates of the quaterthiophene, as discussed in Chapter 5, probably because of the minor distance between the quinquethiophene units in the most stable trimeric aggregate, as suggested by the theoretical calculations.

6.2.1 Molecular Modeling

As in the case of the quaterthiophene biohybrid derivatives, the ability of quinquethiophene bioconjugates **36a** and **36b** to form stable supramolecular aggregates in water solution were investigated by Molecular Mechanics and Molecular Dynamics calculations by means of simulated annealing protocols in gas phase as well as in the presence of the solvent.[9a] The calculations were performed within the AMBER force field.[9b] Furthermore, an implicit solvent model was used to simulate the presence of water and reduced charges on the phosphate groups to account for the presence of the counterions.[9c]

For both the monomeric conjugates of **36a** and **36b**, two main conformations were found. One of them shows the planar quinquethiophene stacking on both the covalently linked bases (A form). The other displays the quinquethiophene stacking only with the directly linked base (adenosine in **36a** and guanosine in **36b**) (B form). For both the systems considered the A form was energetically favored over the B form by a few kJ mol^{-1} (See Figure 6.11).

In the A conformation the dinucleotide arms are folded over the *t5* backbone, aligned at stacking distance, and forming an intramolecular H bond between A and T base pair in the case of the bioconjugate **36a**. No evidence of intramolecularly H-bonded C-G pair was found for the energetically favoured A conformation of **36b**. The distance between the π-system of *t5* and the adjacent base pair falls in the range of 3.3-3.64 Å, as in the case of previously studied quaterthiophene biohybrid derivatives.
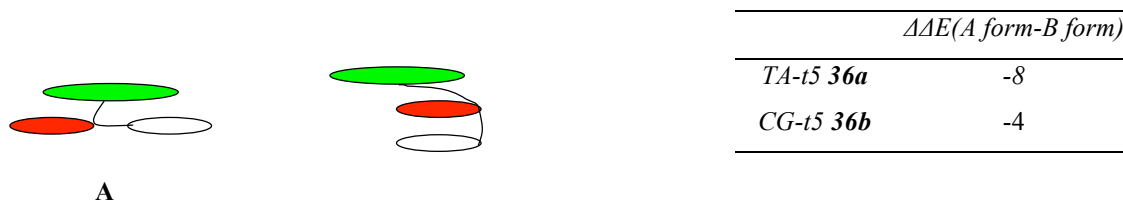

	ΔΔE(A form-B form)
TA-t5 **36a**	*-8*
CG-t5 **36b**	-4

Figure 6.11 *Sketch of the A and B forms of conjugates **36a** and **36b** and calculated energy differences (kJ mol^{-1}). Green= t5, red= Adenosine in **36a** (Guanosine in **36b**), white= Thymidine in **36a** (Cytidine in **36b**)*

The most favored A conformations and stacking distances of the conjugates are reported in Figure 6.12, showing that the preferred conformation is made of the hydrophobic moiety constituted by quinquethiophene and nucleobases, interacting each others by stacking and the hydrophilic one constituted by sugar backbones and phosphate groups (in the background).
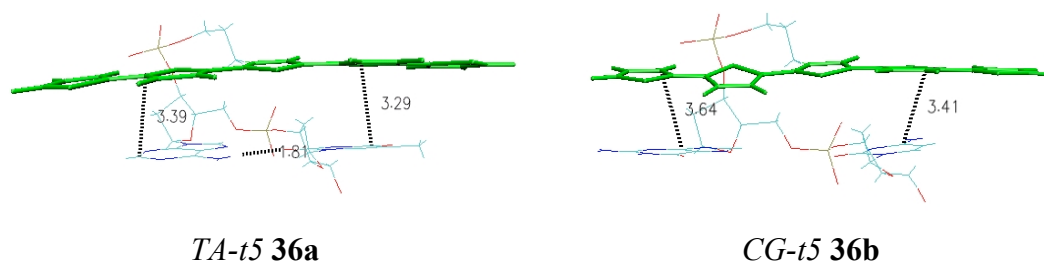

TA-t5 **36a**   *CG-t5* **36b**

Figure 6.12 *Most favoured A form conformations and stacking distances of conjugates 36a,b.*

During the aggregation process the A and B monomeric conformations give rise to different supramolecular systems. In particular for each compound three dimeric aggregates C, D and F (Figure 6.13) were investigated. The free energies of all types of aggregates were calculated using the equation $\Delta G_{298} = E\ (MM) - RTlnQ$, where E is the energy and Q the partition function.

C   D   E

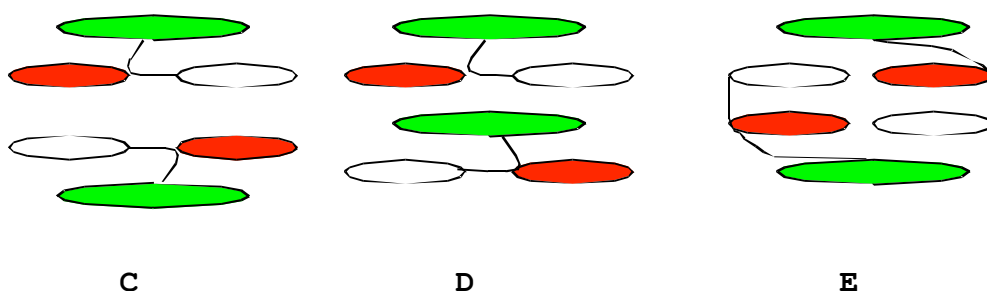**Figure 6.13** *Sketch of the C, D and E dimeric aggregates investigated for conjugates 36a and 36b. Green= t5, red= Adenosine in 36a (Guanosine in 36b), white= Thymidine in 36a (Cytidine in 36b).*

The energetically favored dimeric aggregates were dimer C, for conjugate **36a**, deriving from the aggregation of two monomers in the A form, while for conjugate **36b** the most stable aggregate was found the form E, resulting from the interaction between two monomers in B form (Figure 6.14). In latter case the intermolecular base pairings between the self complementary nucleobases C and G, leading to the formation of three H–bonds for each base pair, provides to a substantial difference (-26.14 KJmol^{-1}) in stabilization energy between the preferred dimer E and the other studied aggregates. For conjugate **36a**, the difference between the most stable dimeric conformation C and the less stable E resulted only of -6.6 KJmol^{-1}, therefore a deeper study of trimeric aggregates structure was needed.
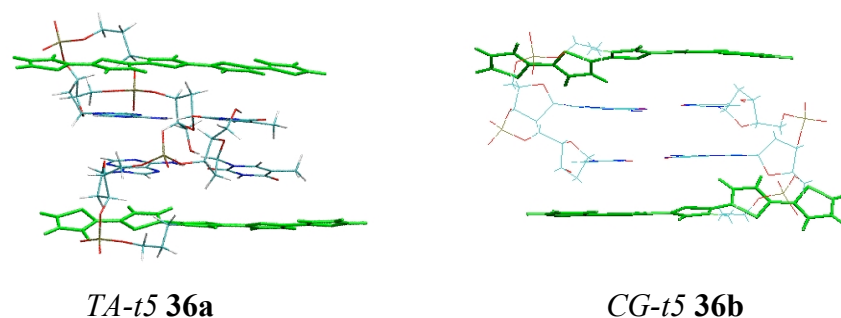

TA-t5 **36a**   *CG-t5* **36b**

Figure 6.41 *Most stable dimers of conjugates **36a** (dimer C) and **36b** (dimer E).*

Figure 6.15 displays the geometry of the favored trimeric aggregate of **36a** together with the corresponding top view showing the relative orientation of the *t5* moieties
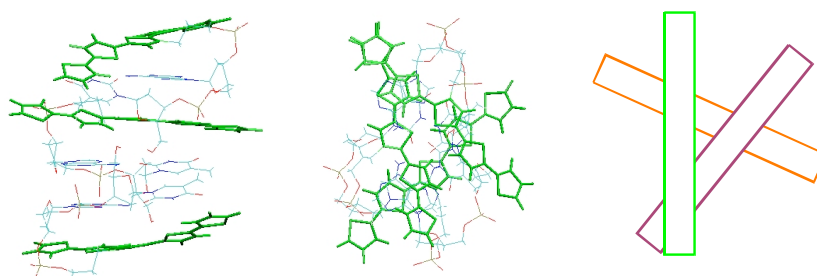

Figure 6.15 *Most stable trimer of conjugates **36a** and corresponding top views showing the relative orientation of the t5 backbones.*

The calculations show that the formation of the favored trimer for compound **36a** is driven by the stacking interactions between the nucleobases of the first monomer and those of the second monomer. Starting from the third one the aggregation process is directed by the intermolecular stacking between the quinquethiophene moiety of a monomer and nucleobases of another molecule. Since the trimer shown in Fig. 6.5 is more stable of only -14 KJmol^{-1} than the other trimeric aggregate studied, is reasonable to suppose that the optimized trimeric conformation for **36a** could be not the only one present in solution as well in solid state.

As shown in Figure 6.15, the *t5* moieties within the trimer are rotated with respect to each other by an angle of about 90 degrees (first and second monomers, red and violet in the sketch) and about 30 degrees (second and third monomers, violet and green in the sketch, fig. 9).

6.3 Conclusions

In summary, we have demonstrated that binding a self-complementary dinucleotide at the beta inner position of quinquethiophene lead to a fluorescent and semiconducting biohybrid conjugates with high tendency to aggregation in film trough maximized thienyl-nucleobase π-π stacking intermolecular interactions. As predicted by theoretical calculations the bioconjugate TA-t5 is able to form open dendritic structures, that under controlled deposition conditions, by using Microfluidic lithography (MIMIC), grew radially, filling the entire channel length and covering almost the whole surface.

6.4 Experimental Section

UV-Vis spectroscopy: Absorption spectra were recorded with a Perkin-Elmer Lambda 20 spectrometer in aqueous solution ($5 \cdot 10^{-6}$ M, pH=7.4) and in cast film on quartz (100 μl of 10^{-3} M solution) after solvent evaporation.

CD spectroscopy: CD spectra were recorded with a Spectropolarimeter JASCO J-715, under ambient condition, in aqueous solution (~10^{-5} M, pH=7.4) and in cast film on quartz (100 μl of 10^{-3} M solution) after solvent evaporation.

Fluorescence microscopy: Nikon Eclipse 80i optical microscope was used for optical measurements. The images were recorded with a digital color camera Nikon Digital Sight DS-2Mv. Glass substrate were furnished by Knittel gläser and were previously

washed with Acetone spectroscopic grade (Aldrich). Films were cast from H_2O (~50 μL, c~10^{-4} M) on glass substrates and the solvent was evaporated under saturated atmosphere.

Microfluidic Lithography

Poly(dimethylsiloxane) (PDMS) elastomeric moulds were obtained by a photolithographically structured silicon masters with a micro-channels network of about 28 μm-wide parallel stripes, spaced of about 98 μm, and a depth of 1.7 μm.

The silicon Si (1,0,0) substrates were cleaned, before using, in an ultrasonic bath by acetone and isopropyl-alcohol. In order to achieve better hydrophilic surface properties, favouring the capillary penetration of water solutions inside micro-channels, we performed an O_2 plasma treatment on silicon substrates (time =3s, rf power=50W, pressure=52 mTorr).

The micro-channels, obtained by the conformal contact between the PDMS mould and a silicon substrate, were filled by concentrated acqueous solutions (H_2O milliQ) of quinquethiophene conjugate **36a**. The solution penetrates inside the elastomeric channels by capillary effect, and the PDMS replicas were removed after a complete water evaporation.

Morphology and Optical characterization

The morphology of the molecular self-assembled structure have benne characterized by an optical microscope (*FluoView 1000, Olympus*) with a CCD colour camera and by Atomic Force Microscopy (AFM, *Solver Pro, NT-MDT*) in semi-contact mode.

The photoluminescence (PL) spectra and the reconstruction of the molecular optical emission have been collected by confocal laser scanning microscope (*FluoView 1000, Olympus*), in order to perform a resolved spatial analysis of the optical properties, with a xy-resolution of about 200 μm.

Molecular modeling: The supramolecular assemblies structures were fully optimized using the AMBER* force field. All the molecular mechanics calculations were performed with the MacroModel software package.[10]

Electrical characterization:

Substrates consisted of two interdigitated comb-like gold electrodes deposited onto a layer of silicon dioxide thermally grown on silicon plates. The thickness of the oxide was 1 μm and that of the metal layer was 0.6 μm. The distance between two consecutive

gold fingers (the spacing between the two electrodes) was 20 μm. The active area, calculated from the free space among the gold fingers, was 4.35×10^{-4} cm^2.

36a films were deposited onto the substrates by casting 5 μL of an aqueous solution in order to completely cover the interdigitated area. The concentration of the solution was 25 g/l, leading to films with a thickness higher than that of the electrodes layer. The film thickness, measured with a Tencor Alphastep 200 profilometer, was in the range 1.1 – 1.4 μm. The samples were dried at ambient condition. The electrical characterization was performed, at ambient temperature, under dynamic vacuum (2×10^{-5} mbar). The current-voltage curves were taken by using a Keithley 487 source-picoammeter.

6.5 References.

[1] a) Y. Kanemitsu, K. Suzuki, Y. Masumoto, *Phys. Rev. B* **1994**, *50*, 2301-2305; b) R. S. Becker, J. Seixas de Melo, A. L. Maçanita, F. Elisei, *J. Phys. Chem.* **1996,** *100,* 18683-18695; c) M. Melucci, G. Barbarella, M. Zambianchi, P. Di Pietro, A. Bongini, *J. Org. Chem.* **2004**, *69*, 4821-4828; d) M. Melucci, G. Barbarella, G. Sotgiu, *J. Org. Chem.* **2002**, *67*, 8877-8884.

[2] Y. Xia, G.M. Whitesides, Angew. Chem. Int. Ed. **1998**, 37,550.

[3] R. Kimmich, Chem. Phys, **2002**,284:253,.

[4] D. Myers, Surface, Interface, and Colloids: principles and applications, Wiley-VCH, NY, **1999**

[5] a) J.N. Israelachvili, Intermolecular and Surface Forces. Academic Press, London, **1992**; b) I. Viola et al. Adv. Mater. 17:2935, **2005**. c) I. Viola et al. Adv. Mater. 19:1597, **2007**]

[6] *Y. Xia, G.M. Whitesides, Angew. Chem. Int. Ed.* **1998**, *37*, 550-575.

[7] Dimitrakopoulos, C. D.;. Malenfant, P. R. L. *Adv. Mater.* 2002, 14, 99-117

[8] [M. A. Lampert, P. Mark. *Current Injection in Solids.* Academic Press, New York, 1970.],

[9] a) A. Acocella, A. Venturini, F. Zerbetto, *J. Am. Chem. Soc.* **2004**, *126*, 2362-2367. b) J. Scott, P. A. Weiner, D.A.; Kollman, U. Case. *J. Comput. Chem.* **1990**, *11*, 440–467. c) C. Singh, C. Ghio, G. Alagona, S. Profeta, P. Weiner, *J. Am. Chem. Soc.* **1984**, *106*, 765–784. d) W. Clark Still, A. Tempczyk, R. C. Hawley, T. Hendrickson, *J. Am. Chem. Soc.* **1990**, *112*, 6127–6129.

[10] F. Mohamadi, N. G. J. Richards, W. C. Guida, R. Liskamp, M. Lipton, C. Caufield, G. Chang, T. Hendrickson, W. C. Still. *J. Comput. Chem.* **1990**, *11*, 440-467.

Conclusions

During this PhD thesis, an innovative, heterogeneous Suzuki protocol for the preparation of highly pure oligothiophenes was first been developed.

The new, ecofriendly, procedures work in EtOH/water or isopropanol, under microwave irradiation, and make use of silica- and chitosan-supported Pd complexes. They represent the fist example of heterogeneous synthesis applied to thiophene-based materials. α-β Alkyl substituted oligothiophenes (up to hexamers) and thiophene co-oligomers were prepared in high yield and in short reaction times free from residual metals and with improved film forming properties.[1]

Subsequently, oligothiophene-5-labeled deoxyuridines were synthesized and incorporated into 19-meric oligonucletide sequences. We showed that the oligothiophene-labeled oligonucletide sequences obtained can be used as probes to detect a single nucleotide polymorphism (SNP) in complementary target sequences. In fact, all the probes showed marked variations in emission intensity upon hybridization with a complementary target sequence.[2] The observed variations in emitted light were comparable or even superior to those reported in similar studies, showing that the biohybrids can potentially be useful to develop biosensors for the detection of DNA mismatches.

Finally, water-soluble, photoluminescent and electroactive dinucleotide-hybrid derivatives of quaterthiophene[3] and quinquethiophene[4] were synthesized. By means of a combination of spectroscopy and microscopy techniques, electrical characterizations, microfluidic measurements and theoretical calculations, we were able to demonstrate that the self-assembly modalities of the biohybrids in thin film are driven by the interplay of intra and intermolecular interactions in which the π-stacking between the oligothiophene and nucleotide bases plays a major role.

---

[1] S. Alesi, F. Di Maria, M. Melucci, D. J. Macquarrie, R. Luque, G. Barbarella *Green Chem.***, 2008**, DOI: 10.1039/b718776a

[2] M. L. Capobianco, A. Cazzato, S. Alesi, G. Barbarella *Bioconjugate Chem.* **2008**, *19*, 171–177.

[3] S. Alesi, G. Brancolini, M.Melucci, M. L. Capobianco, A. Venturini, N. Camaioni, G. Barbarella *Chem. Eur. J.* **2008**, *14*, 513 – 521.

[4] S. Alesi, M.Melucci, I. Viola, G. Brancolini, M. L. Capobianco, A. Venturini, N. Camaioni, G. Gigli, G. Barbarella, *manuscript in preparation.*